

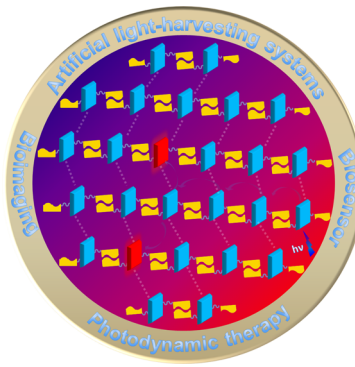
Biological Applications of Supramolecular Assemblies Designed for Excitation Energy Transfer

Hui-Qing Peng,[†] Li-Ya Niu,^{†,‡} Yu-Zhe Chen,[†] Li-Zhu Wu,[†] Chen-Ho Tung,^{*,†,§} and Qing-Zheng Yang^{*,†,‡}

[†]Key Laboratory of Photochemical Conversion and Optoelectronic Materials, Technical Institute of Physics and Chemistry, Chinese Academy of Sciences, Beijing 100190, People's Republic of China

[‡]Key Laboratory of Radiopharmaceuticals, Ministry of Education, College of Chemistry, Beijing Normal University, Beijing 100875, People's Republic of China

[§]Collaborative Innovation Center of Functionalized Probes for Chemical Imaging in Universities of Shandong, Shandong Normal University, Jinan 250014, People's Republic of China



CONTENTS

1. Introduction	7502
1.1. Energy Transfer Processes and Their Mechanisms	7503
1.1.1. Fluorescence Resonance Energy Transfer	7503
1.1.2. Electron Exchange	7503
1.2. Self-Assemblies for Energy Transfer	7504
2. Artificial Light-Harvesting Systems	7504
2.1. Multiporphyrin Arrays for Light Harvesting	7505
2.2. Low Molecular Weight Gels for Light Harvesting	7507
2.3. Biomaterials for Light Harvesting	7507
2.3.1. Proteins for Light Harvesting	7507
2.3.2. DNA as a Scaffold	7509
2.4. Organic–Inorganic Hybrid Materials for Light Harvesting	7511
2.5. Other Scaffolds for Light Harvesting	7513
3. Bioimaging	7515
3.1. Multicolor Imaging	7516
3.2. NIR Imaging	7518
3.3. Stimuli-Responsive Bioimaging	7519
3.3.1. Photoresponsive Imaging	7519
3.3.2. pH-Responsive Imaging	7522
3.4. Upconversion Luminescence Bioimaging	7523
4. Biosensor	7525
4.1. Ratiometric Biosensing	7525
4.2. Upconversion Luminescence Biosensing	7526
4.3. Biosensing by Signal Amplification	7527
5. Photodynamic Therapy	7528
5.1. Photodynamic Therapy Based on Single-Photon Excitation	7529
5.2. Photodynamic Therapy Based on Multi-photon Excitation	7530
5.2.1. Photodynamic Therapy Based on Two-Photon Excitation	7530
5.2.2. Photodynamic Therapy Based on Up-conversion Nanoparticles	7532
6. Conclusion	7534
Author Information	7534
Corresponding Authors	7534
Notes	7534
Biographies	7534
Acknowledgments	7535
References	7535

1. INTRODUCTION

Absorption of light by a molecule (donor, D) generates an excited state, which may subsequently transfer the excitation to another chromophore (acceptor, A) in the vicinity. Such excitation energy transfer (EET) is an essential process for a chromophore. It plays a crucial role in photosynthesis,¹ where the energy of photons absorbed by antenna chromophores flows to the reaction center by highly efficient excitation energy transfer.² Excitation energy transfer between chromophores is routinely exploited for tuning the photophysics of luminescent systems and generating excited states of molecules which are difficult to be obtained by direct photoirradiation (e.g., singlet oxygen). Excitation energy transfer plays a key role in certain luminescent materials,³ light-emitting devices,⁴ fluorescent probes,⁵ and solar cells,⁶ among others. Supramolecular assemblies of spatially well-organized chromophores can facilitate excitation energy transfer and enable a variety of applications. In this review, we will analyze a subset of such potential applications in biochemistry, physiology, and medicine. Although this review may feature some supramolecular assemblies that have been discussed in other reviews, we will focus on strategies reported for assembling donors/

Special Issue: 2015 Supramolecular Chemistry

Received: December 17, 2014

Published: June 4, 2015

acceptors and the functional aspects of such assemblies for biological applications with the hope that this may disclose the structure–function relationship of supramolecular assemblies and inform the future development.

1.1. Energy Transfer Processes and Their Mechanisms

Three types of spin-allowed excitation energy-transfer processes are recognized: singlet–singlet energy transfer (SSET), triplet–triplet energy transfer (TTET), and triplet–triplet annihilation (TTA). During SSET an electronically excited singlet donor produces an electronically excited singlet acceptor, i.e., ${}^1\text{D}^* + {}^1\text{A} \rightarrow {}^1\text{D} + {}^1\text{A}^*$. Likewise, the TTET produces triplet species from a triplet excited donor: ${}^3\text{D}^* + {}^1\text{A} \rightarrow {}^1\text{D} + {}^3\text{A}^*$. In TTA two triplets are converted into singlets: ${}^3\text{D}^* + {}^3\text{A} \rightarrow {}^1\text{D} + {}^1\text{A}^*$.

In any of these processes the donor and acceptor can exchange energy by fluorescence (or Förster) resonance energy transfer (FRET), by electron exchange, or both.⁷

1.1.1. Fluorescence Resonance Energy Transfer. FRET is an electrostatically mediated energy transfer,⁸ whereby long-distance dipole–dipole interactions between the fluorescent donor and the fluorescent or nonfluorescent acceptor decrease the emission intensity of the former by transferring the energy to the latter.

According to the Förster theory, the rate of energy transfer, $K_{\text{T}(r)}$, is

$$K_{\text{T}(r)} = \frac{1}{\tau_D} \left(\frac{r_0}{r} \right)^6$$

where τ_D is the fluorescent lifetime of the donor in the absence of an acceptor, r is the distance between the donor and the acceptor, and r_0 is the distance between the donor and the acceptor for which energy-transfer efficiency $\Phi_{\text{ET}} = 50\%$. At distance $r = r_0$, the FRET rate equals the decay rate of the donor ($1/\tau_D$). r_0 is calculated as

$$r_0 = 9.78 \times 10^3 [k^2 n^{-4} Q_D J(\lambda)]^{1/6} (\text{in } \text{\AA})$$

where k^2 describes the transition dipole orientation (and equals $2/3$ for a random distribution of interacting dipoles), n is the refractive index of the medium, Q_D is the quantum yield of the donor fluorescence in the absence of an acceptor, and $J(\lambda)$ is the integral of the normalized spectral overlap between the donor emission and the acceptor absorption

$$J(\lambda) = \int_0^\infty F_D(\lambda) \epsilon_A(\lambda) \lambda^4 \, d\lambda$$

where λ is the wavelength of light (nm), $\epsilon_A(\lambda)$ is the molar absorptivity of the acceptor at that wavelength ($\text{M}^{-1} \text{cm}^{-1}$), and $F_D(\lambda)$ is the donor fluorescence spectrum normalized so that

$$1 = \int_0^\infty F_D(\lambda) \, d\lambda$$

Another key parameter that determines the practical utility of FRET is the energy-transfer efficiency, Φ_{ET} , or the fraction of the absorbed energy that is transferred to the acceptor. Experimentally, it is measured as a ratio either of the fluorescence intensities or of the fluorescence lifetimes of the donor in the absence and presence of the acceptor (F_D and F_{DA} or τ_D and τ_{DA} , respectively)

$$\Phi_{\text{ET}} = 1 - \frac{F_{\text{DA}}}{F_D} = 1 - \frac{\tau_{\text{DA}}}{\tau_D}$$

Because FRET is based on the interaction between randomly fluctuating dipoles, Φ_{ET} decays rapidly with distance between the donor and the acceptor

$$\Phi_{\text{ET}} = \frac{1}{1 + \left(\frac{r}{r_0} \right)^6}$$

This strong distance dependence makes FRET especially useful as a spectroscopic ruler to measure the separation of chromophores, particularly for biomolecules whose dimensions (10–100 Å) are of the right magnitude to give observable FRET.⁹ This application of FRET has been reviewed extensively elsewhere.¹⁰

1.1.2. Electron Exchange. Electron exchange, also called Dexter interaction, is the short-range (<10 Å) mechanism of energy transfer involving transfer of an electron from the LUMO of electronically excited D^* to the LUMO of A simultaneously with the movement of an electron between the HOMOs of A to D^* .¹¹ The rate of exchange energy transfer, K_{Dexter} , was shown by Dexter to follow the equation

$$K_{\text{Dexter}} = \frac{2\pi}{\hbar} K J(\lambda) \exp\left(-\frac{-2r_{\text{DA}}}{L}\right)$$

where K is an empirical factor related to specific orbital interactions, $J(\lambda)$ is the integral of normalized spectral overlap of the donor emission and acceptor absorption, r_{DA} is donor–acceptor separation, and L is the sum of the van der Waals radii of the donor and acceptor.

Like FRET, the energy-transfer rate for the electron exchange mechanism depends on spectral overlap, but it decays with donor–acceptor separation exponentially rather than as r^{-6} . As a result, Dexter interactions are limited to short distances (<10 Å).

The name “energy transfer” is generally reserved for flows of excitation to low-energy traps, which occurs when the donor and acceptor are chemically distinct. In contrast, energy migration described an isoenergetic transfer of energy between two molecules of the same compound, one of which is electronically excited.^{12,13} Energy migration allows energy to flow over large distances before being transferred to a distinct acceptor chromophore. The models of energy transfer discussed above also apply to energy migration. Energy migration plays a vital role in the light-harvesting system of photosynthesis,^{2a,14} chemical sensing by signal amplification,¹⁵ and solar cells with high energy capture efficiency.^{6b}

1.2. Self-Assemblies for Energy Transfer

Spatial organization of chromophores is of crucial importance in governing energy-transfer processes and hence the performance of devices that exploit such energy flows. Studying EET processes in systems with the donor and acceptor connected by covalent bonds has provided most of the fundamental advances in this field.^{14,16} However, with the evolution of energy-transfer systems toward increasingly large, sophisticated donor–acceptor assemblies, the reliance on covalent linking becomes increasingly untenable.¹⁷ Noncovalent interactions, including van der Waals, hydrophobic, π – π , dipole, and metal ligation, may provide limitless possibilities to construct self-assembled architectures for various applications without time-consuming synthesis.¹⁸ Indeed, nature relies to a large extent on such noncovalent interactions to perform a variety of sophisticated biological functions. The best-known examples include protein

folding from a polypeptide to a well-defined three-dimensional tertiary structure via multiple noncovalent interactions or the formation of the DNA double helix by complementary pairing of nucleotides by hydrogen bonding.¹⁹ In this context, investigation of the photoinduced energy transfer between donor and acceptor chromophores assembled via noncovalent interactions has attracted increasing interest recently.

Over the years, significant progress in designing versatile supramolecular assemblies for energy transfer as well as their various applications has been reported.²⁰ For instance, inspired by the natural light-harvesting system, scientists prepared self-assemblies with a large number of donors involved for energy collection to improve the efficiency of solar cells.⁶ Partial energy transfer through controlled self-assembly of donor and acceptor molecules has been exploited to fabricate white-light-emitting organic materials.²¹ Reported biological applications of self-assemblies capable of energy transfer include multicolor bioimaging, biosensing, and photodynamic therapy.²² Supramolecular assemblies manifesting efficient energy transfer were reviewed according to the nature of the scaffolds bearing donors and acceptors (notable examples are dendrimers²³ and DNA²⁴), the type of noncovalent interactions underlying self-assembly,²⁵ or the material that such self-assembly yielded (e.g., organogel^{26,27}). However, biological applications of such assemblies, which is an area that has seen an explosion in activity over the past decade, have not yet been reviewed. This review is intended to remedy the situation by describing briefly but critically all reported applications of energy-transducing supramolecular assemblies in functional biomimicry (particularly in context of light harvesting), bioimaging and biosensing, and photodynamic therapy.

2. ARTIFICIAL LIGHT-HARVESTING SYSTEMS

Nature relies heavily on supramolecular assemblies. Among the most impressive is the light-harvesting complex of the photosynthetic centers of bacteria and plants, in which the initial steps of photosynthesis occur. In light-harvesting complex, the chromophores are held in place by the surrounding proteins via noncovalent interactions.²⁸ As soon as one of these chromophores absorbs light, the excitation energy migrates from one chromophore molecule to another unidirectionally until the energy is funneled to the reaction center, where long-lived charge separation occurs. The energy transfer is generally thought to occur by the singlet–singlet FRET mechanism. In addition to the important role for understanding photosynthesis, biomimetic self-assemblies displaying efficient energy transfer from multiple chromophores to individual acceptors may be of potential significance to luminescent materials, photocatalysts, solar cells, optical sensors, etc.^{2e} Accordingly, recent decades have seen a surge of the use of self-assembly to prepare energy-transfer systems that mimic the natural light-harvesting systems.^{1g,29}

The energy-transfer efficiency and “antenna effect” are widely used empirical parameters to evaluate light-harvesting ability.³⁰ The energy-transfer efficiency quantifies changes of donor emission intensity in the presence of different concentrations of the acceptor, and the antenna effect describes changes of the acceptor emission parameters in different concentrations of the donor.³¹ The calculations of energy-transfer efficiency are described in section 1.1.1. The antenna effect under certain concentrations of donor and acceptor equals the ratio of the emission intensity of the acceptor upon excitation of the donor, $I_{\text{AF}\lambda(\text{D})}$, to that of the direct excitation of the acceptor, $I_{\text{AF}\lambda(\text{A})}$

$$\text{antenna effect} = \frac{I_{\text{AF}\lambda(\text{D})}}{I_{\text{AF}\lambda(\text{A})}}$$

Combination of the two parameters (Φ_{ET} and antenna effect) makes evaluation of the light-harvesting system straightforward and general. Promising candidates for artificial light harvesting should transfer excited energy with ~100% efficiency and have an antenna effect over 10. To achieve these parameters, the chromophores need to have proper spatial organization (favorable spacing and orientation) and distinct spectroscopic properties. The former is key to minimizing energy loss (for example, by avoiding self-quenching), and the latter is required to form so-called energy gradients that facilitate the energy flow from antennas to energy sinks.³² In the following, artificial supramolecular light-harvesting systems constructed from multiporphyrin arrays, low molecular weight gels, biomaterials, organic–inorganic hybrid materials, and other scaffolds exploiting a variety of construction strategies are reviewed.

2.1. Multiporphyrin Arrays for Light Harvesting

Porphyrins are ideal chromophores for artificial light harvesting because they are structurally similar to photosynthetic pigments and have advantageous photophysical properties, such as photostability, visible-light absorption,³³ long-lived excited states, rapid excitation energy exchange,³⁴ and high molar extinction coefficients, which can be easily tuned by metal coordination.³⁵ Metalloporphyrin-based supramolecular constructs, typically built by exploiting coordination between the central metal ions and the nitrogen-containing ligands, are among the most popular artificial light-harvesting molecular assemblies.^{36,37}

Aida and co-workers in 2004 reviewed multiporphyrin arrays, including the pioneering work by the groups of Sanders and Hunter.^{23a} Later, Osuka and Kim reviewed cyclic porphyrin arrays as models of the photosynthetic light-harvesting antenna complexes.³⁸ Here, we will highlight the remarkable progress of the field in the past decade. In 2003 Kobuke and co-workers reported the first example of a cyclic hexamer prepared by connecting slipped-cofacial dimer units via coordination from the imidazolyl arm to the central Zn ion (Figure 1a).³⁹ The overall structure, porphyrin–porphyrin separation, and relative orientation of the chromophores in this system closely resemble those of the light-harvesting complexes in photosynthetic bacteria.

Building on Kobuke’s work, in 2004 Osuka and Kim successfully addressed one of the main challenges for molecular

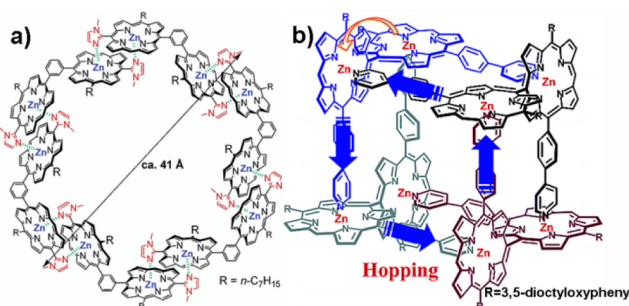


Figure 1. (a) Structural model for a cyclic hexamer. Reprinted with permission from ref 39. Copyright 2003 American Chemical Society. (b) Porphyrin boxes constructed by homochiral self-sorting assembly. Reprinted with permission from ref 40. Copyright 2004 American Chemical Society.

design of photosynthetic model systems: the precise spatial control of chromophore arrangement, which is a key parameter in determining excitation energy transfer, by developing a rigid self-assembled porphyrin “box” (Figure 1b).⁴⁰ In addition to simultaneous eight-point cooperative coordination, which improves the driving force of self-assembly, the box formation rigidifies the perpendicular conformation of meso–meso-linked diporphyrin, fixing the spatial separation between porphyrins. This feature enabled the demonstration and careful studies of self-sorting of chiral precursors to chiral porphyrin boxes, which hitherto had been rarely considered. The unique structural aspects of the box yielded important clues for understanding exciton coupling between noncovalently linked neighboring porphyrin rings. Thanks to the fast energy migration rate, the porphyrin boxes served as platforms for very efficient energy migration processes.

Herz and co-workers⁴¹ reported an impressive supramolecular mimic of the light-harvesting system comprising two supramolecular antenna complexes of free-base porphyrin dimers as an energy donor and 12-porphyrin nanoring (c-P12) as the energy acceptor (Figure 2). The efficient energy transfer

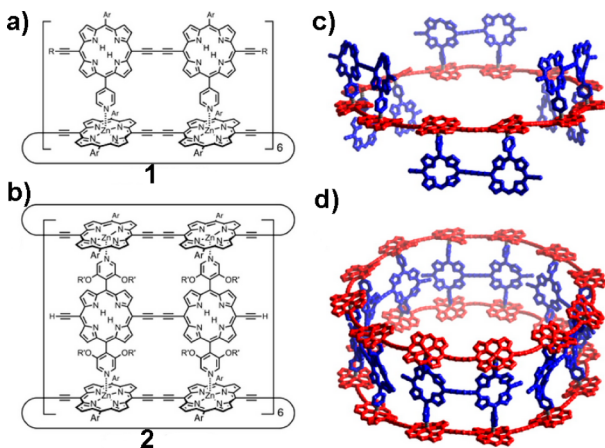


Figure 2. (a, b) Chemical structures and (c, d) structural models of **1** (top) and **2** (bottom). Ar = 3,5-bis(triethylsilyl)phenyl, R = triethylsilyl, R' = dodecyl. Adapted with permission from ref 41. Copyright 2014 American Chemical Society.

was first verified by steady state emission titration experiments. As dimers were added to c-P12, the photoluminescence spectra showed effective quenching of dimer emission until metal–ligand coordination was saturated (Figure 3). When pyridine as a competing ligand was added, the dimer emission recovered. The energy-transfer rates were $(1.25 \text{ ps})^{-1}$ and $(0.65 \text{ ps})^{-1}$ for **1** and **2**, respectively, which is comparable to those in the natural light-harvesting systems. The rate difference between the two complexes indicated the contributions of uni- and bidirectional energy funneling.

The main disadvantage of multiporphyrin arrays reported to date is their fairly narrow absorption windows, arising from the use of only a very limited range of porphyrinoid macrocycles. Consequently, the fraction of solar light that these light-harvesting systems can collect remains modest.

2.2. Low Molecular Weight Gels for Light Harvesting

Gels formed by reversible noncovalent interactions of small molecules (so-called low molecular weight gelators) are one type of media to facilitate energy-transfer processes by combining appropriate energy donors and energy acceptors

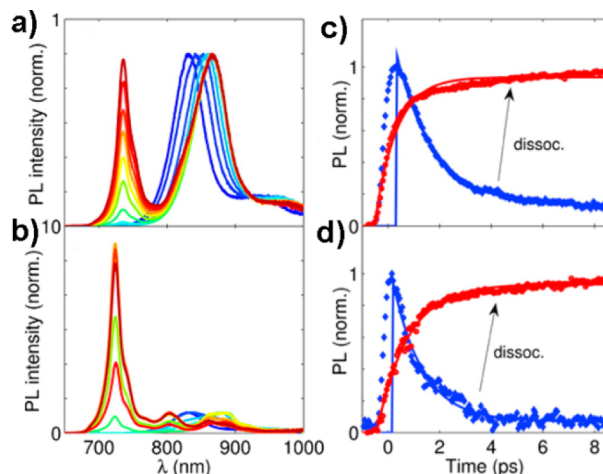


Figure 3. (a, b) Steady state emission titrations of a 12-porphyrin nanoring with free-base porphyrin dimers, **1** and **2**, respectively ($\lambda_{\text{ex}} = 450 \text{ nm}$). (c, d) Comparison of time-resolved photoluminescence dynamics for dimer emission in associated (blue) and dissociated (red) state for **1** (c) and **2** (d). Reprinted with permission from ref 41. Copyright 2014 American Chemical Society.

in different molar ratios.^{21d,42} Several groups have demonstrated and reviewed various organogels^{27,43} and hydrogels⁴⁴ for excitation energy transfer. In the following, we highlight examples of chromophore-based gels for artificial light harvesting.

Ajayaghosh and co-workers studied gelation-assisted light harvesting by self-assembling oligo(phenylenevinylene)s (OPVs).^{17b,45} In their study, Rhodamine B (**5**) as the energy acceptor was mixed with OPV derivatives (**3** or **4**) (Figure 4a) in a mixture of cyclohexane and chloroform (16:1) to fabricate a gel.⁴⁶ The amplified emission of the energy acceptor upon indirect excitation of donor **4** indicated efficient energy hopping from the donor to the acceptor by FRET (Figure 4b).

Later the same group extended this work to compounds **6** (donor) and **7** (acceptor) to study the effect of acceptor concentration on light harvesting. In gel, excitation of **6** in the presence of 0–2 mol % of **7** resulted in a gradual decrease in the emission of the former with an increase in the emission of the latter. However, gels of **6** with 2–20 mol % of **7** showed a gradual red shift of the emission toward the aggregate state of **7**, indicating that the aggregates with a narrow HOMO–LUMO gap served as the energy acceptor. Such results suggested that both isolated molecules of **7** and its aggregates served as energy acceptor to yield different emission colors under excitation of the donor (Figure 5).⁴⁷

In 2007, Ajayaghosh et al. constructed another OPV-based light-harvesting gel with a semiconducting molecular wire **11** as an energy acceptor (Figure 6)⁴⁸ to illustrate the importance of gelation for efficient energy transfer. The energy-transfer efficiency of OPV **8** gel with a very low concentration of **11** (1.53 mol % of **8**) reached 95% as calculated from the fluorescence-quenching data. For weakly gelling OPV **9** and nongelling OPV **10**, the energy-transfer efficiencies were very low, probably due to the limited exciton migration over long intermolecular distances. Interestingly, since heating a gel turns it into solution, increasing the temperature tunes the emission of the supramolecular gel from red to white to blue.

In contrast to the linearly stacked OPV systems, the didecyl derivative of anthracene **12** (Figure 7) assembles into triads that pack head-to-tail in layers and wrap around a central axis to

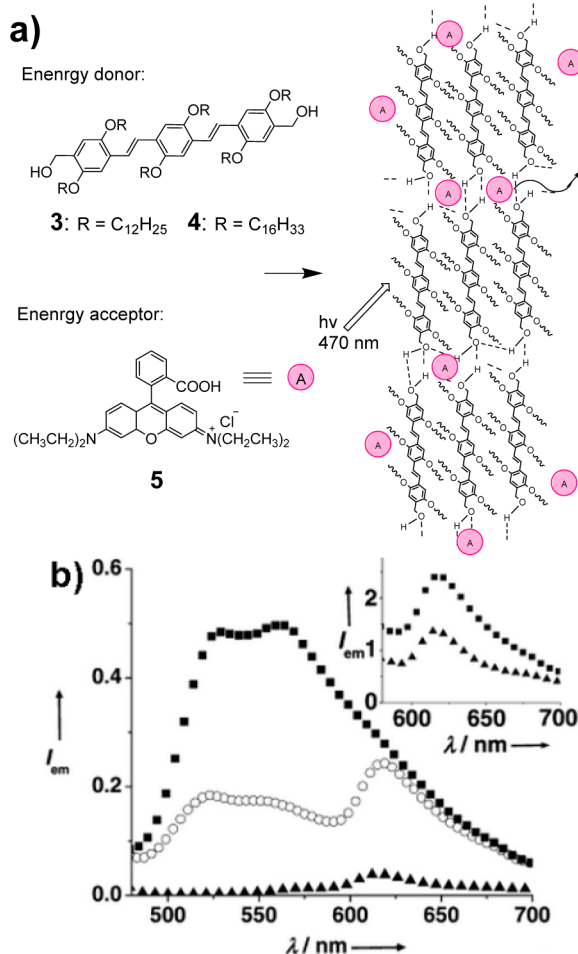


Figure 4. (a) Probable self-assembly of Rhodamine B (**5**) dispersed in OPV (**3** or **4**) gel. (b) (■) Fluorescence of **4**, (○) fluorescence of **4** + **5** at an excitation wavelength of 470 nm, and (▲) direct excitation of **5** at 535 nm. (Inset) Emission of **5** on indirect excitation (■) at 470 nm and direct excitation (▲) at 535 nm illustrating the emission amplification. Reprinted with permission from ref 46. Copyright 2002 Wiley-VCH Verlag GmbH & Co. KGaA, Weinheim.

form fibers.⁴⁹ Guerzo and Desvergne et al. doped gels of donor **12** with 2,3-*n*-dialkoxytetracene (DnOT) acceptors, including three 2,3-disubstituted (**13**, **14**, and **15**) and one 5,12-disubstituted (**16**) tetracenes (Figure 7)⁵⁰ and found that the energy-transfer efficiency decreased in the order **13** = **14** > **15**, with **16** not affecting the emission of **12** at all. This trend probably reflects the capacity of the substituted tetracenes to replace **12** in the triads. The smallest members of the series, **13** and **14**, being closest in size to **12** may be able to arrange themselves parallel with the donor, which increases k^2 , thus maximizing dipole–dipole interactions and hence the energy-transfer efficiency. In gels containing 1.0 mol % of **13**, emission of **12** was quenched almost entirely and emission of **13** dominated. A comparison of the emission quantum yields of isolated **14** with that of **14** in gels of **12** suggested that out of 100 deexcitations of **12** 54 occurred by energy transfer to the acceptor. Fifty-four effective donors per acceptor is very high and greatly surpasses those derived from other organogels. This value may be increased by improving the spatial ordering of **12** in the gels to offer multiple pathways for exciton migration and energy transfer as opposed to a single linear path expected from stacked gelator systems.

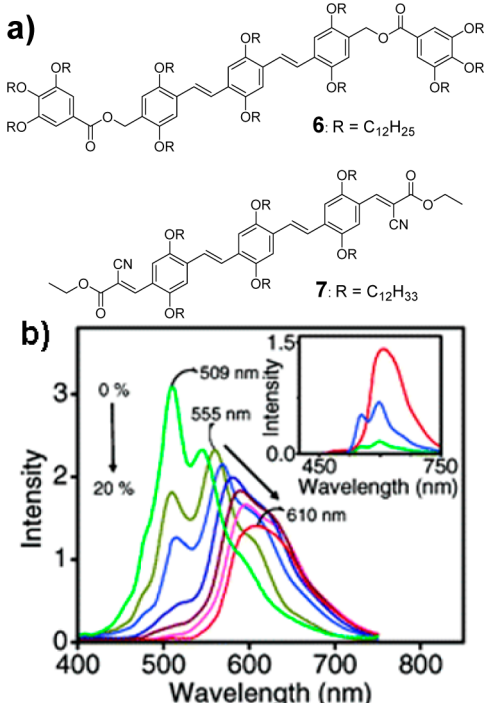


Figure 5. (a) Chemical structures of donor **6** and acceptor **7**. (b) Fluorescence emission of **6** on addition of different amounts of **7** (0–20 mol %). (Inset) Comparison of FRET emission with 20 mol % of **7** excited at donor absorption (red), upon direct excitation of **7** in the absence of **6** excited at acceptor (blue), and at donor absorption (green). Reprinted with permission from ref 47. Copyright 2006 American Chemical Society.

The Shinkai group fabricated a visible-light-harvesting organogel from cholesterol-perylene derivatives (Figure 8, 17–20)⁵¹ These cleverly designed molecules combine the easy tunability of the optical properties of perylene with gelating capacity of cholesterol. Fluorescence measurements indicated that light energy efficiently transferred from **17** to **20** using **18** and **19** as intermediate chromophores.

The use of water, a nontoxic cheap solvent, in preparation of hydrogels makes them advantageous over organogels for fabricating artificial light-harvesting systems.⁵² A notable example of light-harvesting hydrogels includes those by Kimizuka and Nakashima, prepared by self-assembly of glutamate amphiphiles as receptors (**21**) and anionic fluorophores as energy donor (**22**) and acceptor (**23**) (Figure 9).⁵³ The bundling and cross-linking of the resulting nanofibers by electrostatic and van der Waals interactions facilitated efficient energy transfer by reducing intermolecular distances. Another example is a light-harvesting bicomponent hydrogel of Nandi et al.⁵⁴ prepared by combining in water a 1:1 (mol) mixture of 6,7-dimethoxy-2,4[1H,3H]-quinazolininedione (**24**) and melamine (**25**) with riboflavin (**26**) at 0.25–1.25 mol % (relative to **24**) (Figure 10). The energy-transfer efficiency depended on the ratio of **24** to **26**, reaching 82.8% at 1.25 mol % **26**. The authors observed FRET emission through a wide range of temperature and pH.

Generally, gels formed from low molecular weight gelators have played a significant role in mimicking light-harvesting scaffolds by incorporating a large number of chromophores. In fibers of coassembled gels donors and acceptors are present in close proximity, facilitating energy transfer. The π – π stacked

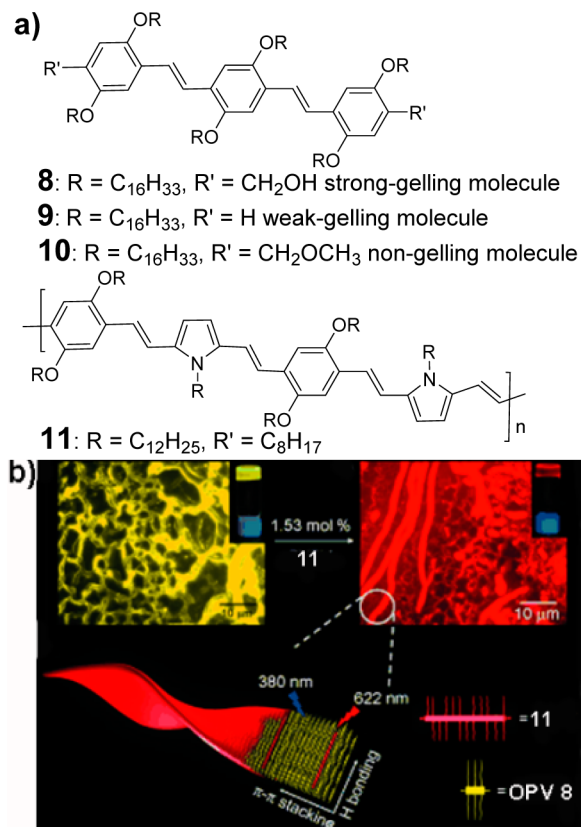


Figure 6. (a) Chemical structures of OPV derivatives 8–10 and 11. (b) Schematic representation of the light-harvesting process in 11-encapsulated OPV 8 gel. Adapted with permission from ref 48. Copyright 2007 Wiley-VCH Verlag GmbH & Co. KGaA, Weinheim.

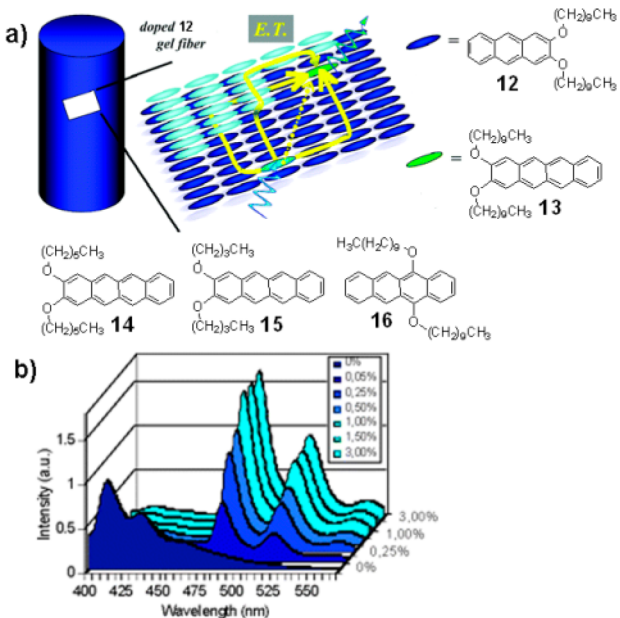


Figure 7. (a) Schematic representation of an acceptor-doped gel fiber. (b) Emission spectra of the DMSO gel of 12 (λ_{ex} = 384 nm) doped with increasing proportions of 13. Adapted with permission from ref 50. Copyright 2005 American Chemical Society.

systems also enforce the parallel orientation of the dipoles of the donor and acceptor chromophores, which is optimal for

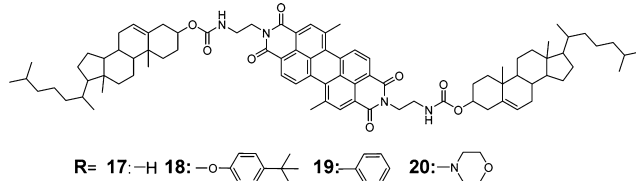


Figure 8. Chemical structures of cholesterol-perylene derivatives 17–20.

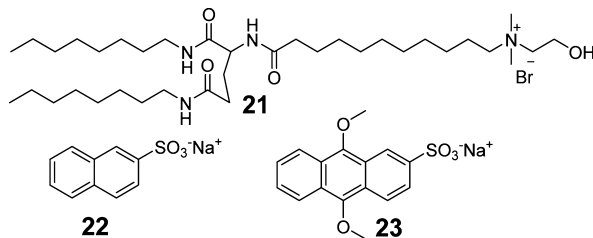


Figure 9. Chemical structures of self-assembling receptor (21), donor (22), and acceptor (23).

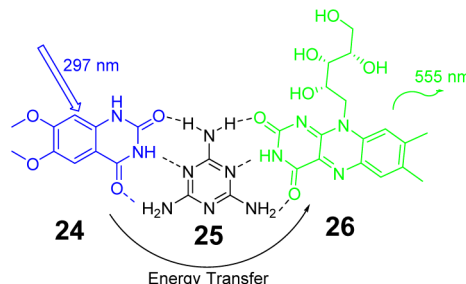


Figure 10. Supramolecular complex of 24, 25, and 26.

resonant energy transfer. However, compared with the spatial organization of the individual chromophores in the photosynthetic center, the known gels appear to pack donors and acceptors more densely, which partially reduces the efficiency of energy transfer by self-quenching and/or excimer formation. Another distinct disadvantage of gels for light harvesting is that the molecular arrangement of the donor in gels is usually disturbed by the incorporation of inappropriate molecular structure as energy acceptor, interfering with the stability of self-assembled gels, and decreased the efficiency of the energy transfer.

2.3. Biomaterials for Light Harvesting

Recent studies demonstrated the utility of biological materials, including proteins and DNA, as templates to guide nanoscale organization of covalently or electrostatically bound pigments.⁵⁵ Impressive progress has been achieved in controlling the distribution and orientation of the chromophores in such hybrid biomaterials, which is the key in achieving highly efficient light harvesting.⁵⁶

2.3.1. Proteins for Light Harvesting. Scaffolds based on tobacco mosaic virus coat protein (TMVCP) and filamentous bacteriophage M13 coat protein have been widely used in constructing light-harvesting systems, because these proteins (i) permit many chromophores of different types to be integrated for light collection over a broad spectral range and (ii) enforce rigid organization of closely spaced chromophores for optimal energy transfer without energy loss by contact quenching.

In 2007, Francis et al. constructed self-assembled light-harvesting systems from a synthetically modified TMVP.^{30a} Compounds **27**, **28**, and **29** were selected as the primary donor, the intermediate donor, and the acceptor, respectively (Figure 11), whose maleimide moieties reacted with the cysteine

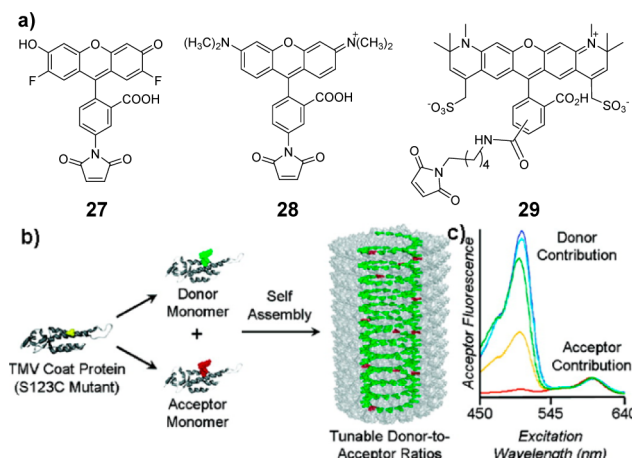


Figure 11. (a) Chemical structures of primary donor **27**, intermediate donor **28**, and acceptor **29**. (b) Self-assembly of modified TMVP into disk and rod structures. (c) Fluorescence excitation spectra from monitoring the fluorescence of acceptor **29** at 650 nm and normalizing at the maximum excitation wavelength of **29** at 597 nm. Reprinted with permission from ref 30a. Copyright 2007 American Chemical Society.

residues of TMVP to yield TMVP–chromophore conjugates. In a suitable buffer these conjugates assembled into stacks of disks or into rods. Fluorescence excitation measurements on the rods assemblies with different molar ratios of **27** (donor) to **29** (acceptor), indicating that donor-to-donor energy migration allowed at least 20 donor chromophores to funnel energy to a single acceptor. The energy transfer from **27** to **29** occurred in 187 ps and energy migration between donors in 70 ps, as derived from picoseconds time-resolved fluorescence and global lifetime analysis (Figure 12a).⁵⁷ The maximum observed antenna effect was 11 at the ratio of 1 acceptor per 101

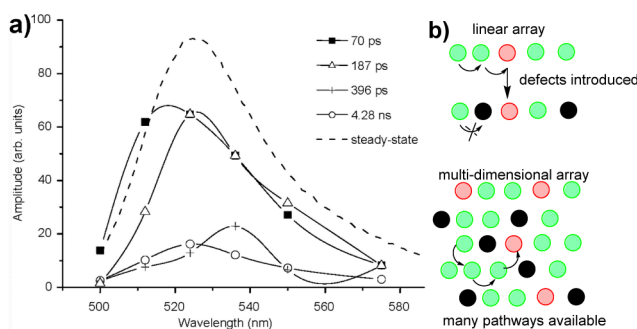


Figure 12. (a) Lifetime analysis indicated distinct decay components in the donor **27** emission band at the 100:1 donor **27** to acceptor **29** rod system. Reprinted with permission from ref 57. Copyright 2008 American Chemical Society. (b) A few defect sites (black) can block energy transfer from donors (green) to acceptors (red) in disk or linear arrays (top) but not in the rods or multidimensional systems, where multiple transfer pathways allow defect sites to be circumvented (bottom). Adapted with permission from ref 58. Copyright 2010 American Chemical Society.

donor molecules. However, the energy-transfer efficiency was only 34–47%. Adding chromophore **28** as the intermediate donor increased the efficiency of these rod assemblies to 90%. In 2010 the same group explained the dramatically more efficient energy transfer in rods compared to disks⁵⁸ by postulating the existence of multiple energy migration pathways in rods (Figure 12b). The results provided a useful benchmark for synthetic arrays based on self-assembling protein scaffolds.

Majima and Endo et al.⁵⁹ reported mimics of the light-harvesting complex using TMVP modified with Zn–porphyrin donor **30** and free-base porphyrin acceptor **31** (Figure 13).

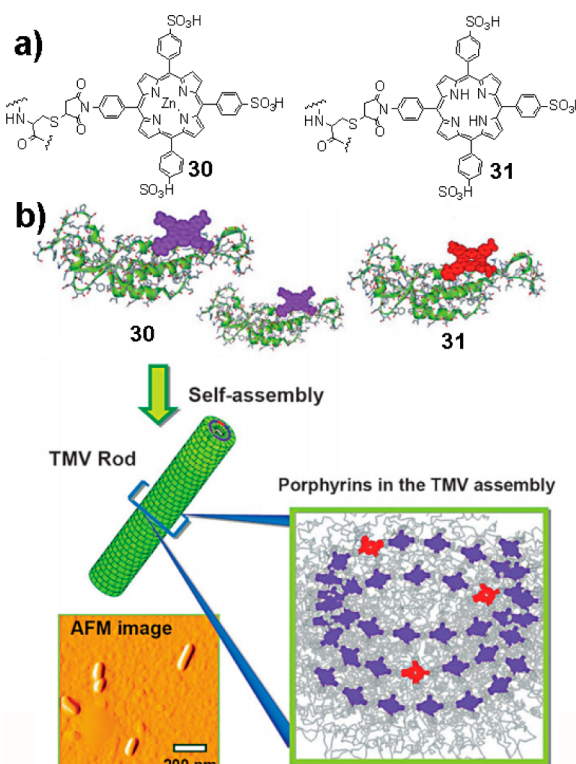


Figure 13. (a) Energy donor **30** and acceptor **31**. (b) Formation of light-harvesting arrays from porphyrin-modified TMVP. Adapted with permission from ref 59. Copyright 2007 Wiley-VCH Verlag GmbH & Co. KGaA, Weinheim.

Steady state fluorescence measurements and time-resolved fluorescence spectroscopy showed light harvesting both in double-layered disks and in multilayered rods with energy-transfer rates from **30** to **31** of 3.1×10^9 and 6.4×10^9 s⁻¹, respectively. These values are close to the theoretical rate of $3\text{--}6 \times 10^9$ s⁻¹ between porphyrins separated by 1.7–2.0 nm, which is the expected distance between side-by-side porphyrins in the TMVP assembly. The good agreement between the measured and the predicted rates indicates that the chromophores bound to TMVP are arranged into a well-defined three-dimensional scaffold.

Belcher et al. showed that a single α -helical coat protein of M13 bearing Zn porphyrins assembled into a light-harvesting antenna (Figure 14a).⁶⁰ The close distances between the primary amines on the viral surface allowed energy transfer between neighboring Zn porphyrins in these assemblies as evidenced by the faster decay of the excited state of **32**–M13 compared to free **32** (Figure 14b). Fluorescence quenching was ascribed to Dexter electronic coupling, which formed energy

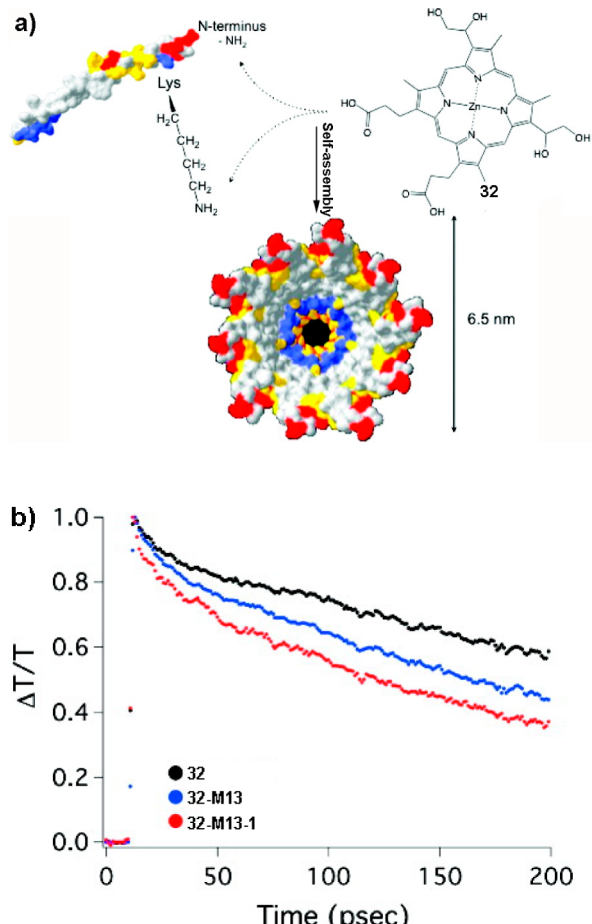


Figure 14. (a) Carboxylic groups of Zn-porphyrin 32 bind to the primary amines of M13 coat proteins. (b) Transient absorption change of 406 nm (the Soret band) of free 32 and 32–M13 complex. 32–M13-1 has a higher surface concentration of porphyrins than 32–M13. Adapted with permission from ref 60. Copyright 2010 American Chemical Society.

trap sites.⁶¹ While a detailed description of the structure and photophysics of these M13-based light-harvesting systems is lacking, they illustrate the potential of M13 viruses, particularly when coupled with the developments in genetic engineering, for accurate positioning of chromophores in molecular-scale devices for manipulating light energy.

Scolaro and Angelini's groups demonstrated light-harvesting systems⁶² based on cationic porphyrins electrostatically bound to the surfaces of M13 viruses. The fluorescence intensity of porphyrins on irradiation at the absorption maximum of the tryptophan residues was much higher than those observed on direct excitation of porphyrins at longer wavelengths. Moreover, the fluorescence excitation spectra of the porphyrins showed an intense band centered at about 280 nm, assigned to tryptophan residue absorption. These results indicated that tryptophan residues of M13 served as antenna chromophores, contributing significantly to the intense fluorescence of the porphyrins.

MacPhee et al. exploited the tendency of certain polypeptides to readily assemble into stable and morphologically regular multimolecular fibrils by nonspecific hydrogen-bonding interactions^{63,55c,64} to create a series of unique light-harvesting systems (Figure 15).⁶⁵ This peptide aggregation placed the long-lived donor and high-quantum-yield acceptor bound to

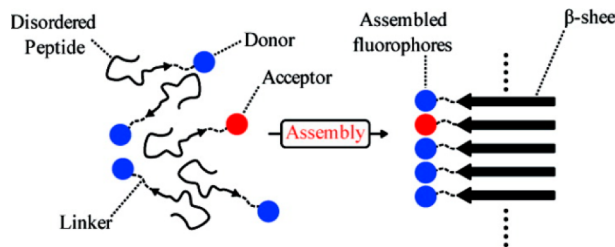


Figure 15. Light-harvesting fiber formed by self-assembly of donor- and acceptor-labeled peptides. Reprinted with permission from ref 65. Copyright 2009 American Chemical Society.

the peptides in close proximity, facilitating efficient energy transfer, which resulted in intensive acceptor emission. Importantly, in this work the average donor/acceptor separation was controlled by mixing labeled and unlabeled peptides, which may comprise an additional general control parameter in optimization of energy-transfer efficiencies in artificial light harvesting.

2.3.2. DNA as a Scaffold. Although a protein's capacity to support 3-dimensional organization of multiple chromophores has enabled the design of several impressive multichromophore artificial light-harvesting antennas, proteins offer only approximate control over the interchromophore distances and orientations. In this respect, DNA scaffolds offer considerable advantages.⁶⁶ In 2009, Kumar and co-workers reported the first examples of light-harvesting units based on a quaternary supramolecular complex⁶⁷ of the Hoechst 33258 energy donor, which has a moderate affinity for DNA, and the Coumarin 540A acceptor, which has a high affinity for bovine serum albumin (cBSA), DNA, and cBSA, which served as scaffolds (Figure 16a). Singlet–singlet energy transfer from the donor to

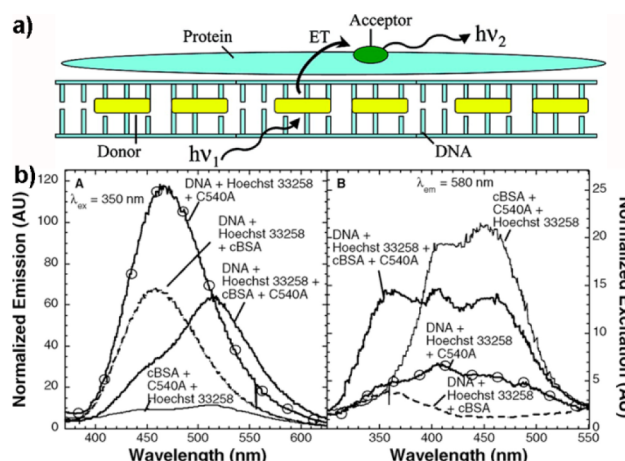


Figure 16. (a) Schematic representation of energy transfer in the donor-DNA/acceptor-protein quaternary complex. Emission (A) and excitation (B) spectra of samples with different components. Reprinted with permission from ref 67. Copyright 2009 American Chemical Society.

the acceptor in the quaternary complex was confirmed by fluorescence studies. No energy transfer between Hoechst 33258 and Coumarin 540A was observed in the absence of either DNA or cBSA, strongly indicating that a supramolecular complex was required to bring the donor and the acceptor within the Förster distance (Figure 16b). This study illustrates

opportunities for applications of DNA in mimicking natural light-harvesting systems.

In 2011, Liu's group demonstrated the assembly of a series of structurally well-defined artificial light-harvesting triads, where three distinct chromophore arrays were used as the primary donor (33), the intermediate donor (34), and the acceptor (35).^{30b} Dye-modified oligonucleotides at selected positions coassembled with DNA to afford multiple arrays of chromophores with controlled interchromophore distances (Figure 17). Efficient, stepwise FRET from the primary donors

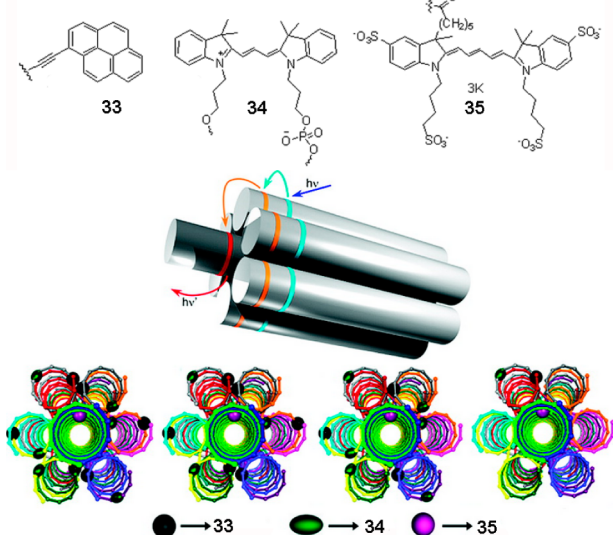


Figure 17. Chemical structures of the primary donor (33), intermediate donor (34), and acceptor (35), and a schematic representation of the self-assembled nanoscaffold containing these three distinct arrays of chromophores. Reprinted with permission from ref 30b. Copyright 2011 American Chemical Society.

to the acceptors through the intermediate donor in each triad was demonstrated by steady state and time-resolved fluorescence spectroscopy. The dependence of the energy-transfer efficiency and antenna effect on the ratio of the primary to the intermediate donors was ascribed to the importance of multiple energy-transfer pathways for energy funneling to the acceptor (Table 1). The measured FRET efficiencies were smaller than the expected values (based on the Förster distances), possibly because of the unfavorable transition dipole orientation (k^2) of the dyes. The number of possible orientations of dyes was restricted by their relatively rigid attachment to the DNA, thus reducing the value of k^2 below 2/3. These detailed studies

Table 1. Measured FRET Efficiency and Antenna Effect for Each Sample Containing Different Molar Ratios of the Three Chromophores^a

sample	FRET efficiency	antenna effect 1(%)	antenna effect 2 (%)
6:6:1	90	85	93
6:3:1	30	43	39
3:6:1	90	47	89
1:1:1	70	16	16

^aAdapted with permission from ref 30b. Copyright 2011 American Chemical Society. Antenna effects 1 and 2 are obtained by comparing the emission of 35 by excitation at 33 or 34 to the emission of 35 by direct excitation.

demonstrated the potential of DNA-based scaffolds to control the key factors (i.e., the distance between chromophores and their relative orientations) governing the light-harvesting efficiency and also provided a guideline for the future design of artificial light-harvesting systems.

Albinsson et al.⁶⁸ presented artificial, self-assembled, light-harvesting complexes consisting of DNA scaffolds, intercalated donor dyes 36, and porphyrin acceptor 37 anchored to a lipid bilayer (Figure 18). Unsatisfied with the antenna effect, AE, to

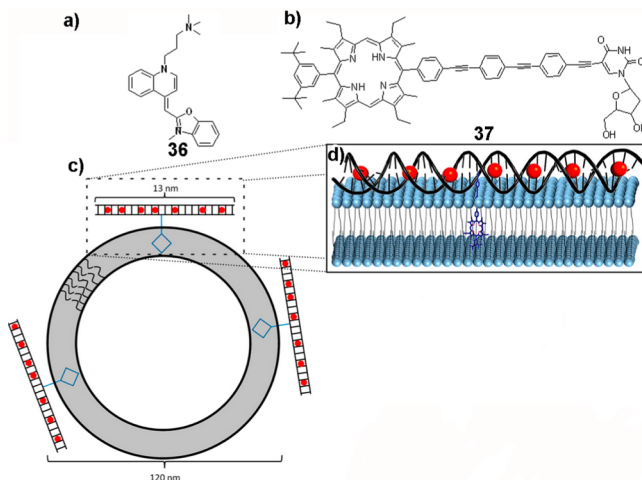


Figure 18. (a) Energy donor 36. (b) Energy acceptor 37. (c) Schematic representation of the 36–DNA–37 system bound to lipid vesicles. (d) Close up showing a single DNA–37 construct with seven intercalated molecules of 36, bound to a vesicle bilayer via porphyrin. Adapted with permission from ref 68. Copyright 2013 American Chemical Society.

quantify the light-harvesting ability, the authors introduced an alternative measure, the effective molar extinction coefficient of the acceptor, ϵ_{eff} , defined as the product of AE and the molar extinction coefficient of the acceptor, $\text{AE} \times \epsilon_A$. The authors argued that ϵ_{eff} allows for a less biased comparison of light-harvesting abilities of various donor/acceptor combinations, particularly for acceptors with modest ϵ_A . In their study, the effective absorption coefficient reached $260\,000\text{ M}^{-1}\text{ cm}^{-1}$ at a donor-to-acceptor ratio of 20:1 vs $22\,000\text{ M}^{-1}\text{ cm}^{-1}$ for the extinction coefficient of porphyrin acceptor 37, corresponding to an antenna effect of 12. Both the time-resolved fluorescence measurements and the simulations of energy transfer revealed a substantial contribution of donor–donor energy migration to the funneling of excitation energy to the porphyrin acceptor (Figure 19).

Häner and Garo described a DNA-assisted formation of a light-harvesting complex which involved stacks of phenanthrenes as the energy donor in the center of a DNA duplex, which efficiently transfer energy to a phenanthrene–pyrene exciplex at one end of the phenanthrene stack (Figure 20). The number of photons emitted by the exciplexes was proportional to the number of phenanthrenes, implying energy transfer.⁶⁹

The Schenning group reported a new type of DNA-template assembly, made of a chiral single strand of oligothymine terminated by a modified cyanine dye 39 as energy acceptor.^{70,71} The strand served as a template to which complementary diaminopurine moieties bearing donor naphthalenes hydrogen bonded (38) to yield a one-dimensional supramolecular “wire” (Figure 21). The well-defined positions of the

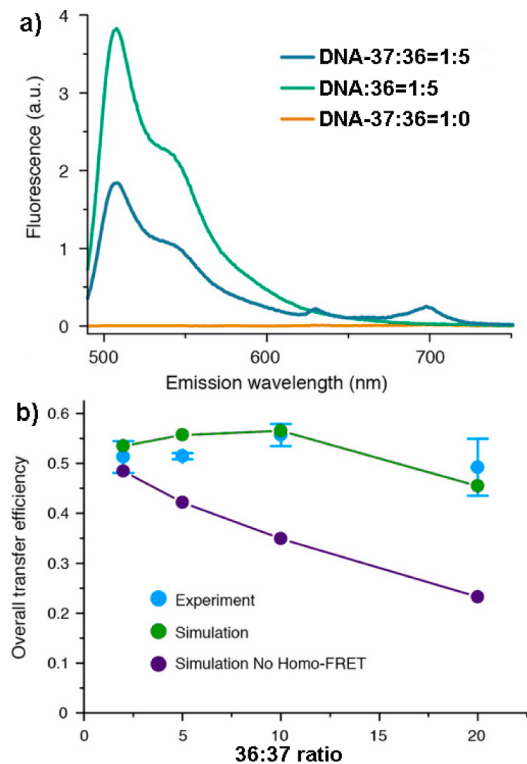


Figure 19. (a) Fluorescence spectra of the DNA–37 and DNA with different molar ratios of 36. (b) Overall transfer efficiency as a function of 36:37 mixing ratio for experimental and simulated data. Experimental data and simulated data with homo-FRET are in close agreement, indicating the effect of energy migration on overall transfer efficiency. Adapted with permission from ref 68. Copyright 2013 American Chemical Society.

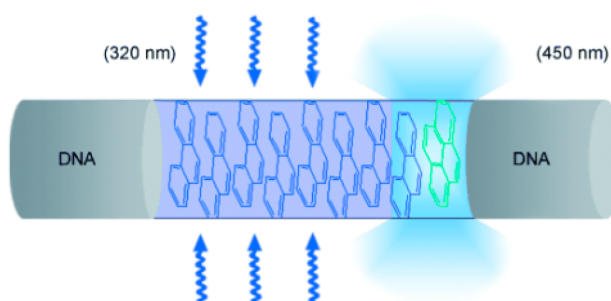


Figure 20. Illustration of a DNA-embedded, light-harvesting antenna composed of π -stacked phenanthrenes (purple block) and a fluorescent phenanthrene–pyrene exciplex (blue). Reprinted with permission from ref 69. Copyright 2012 Wiley-VCH Verlag GmbH & Co. KGaA, Weinheim.

chromophores in the helical stack facilitated efficient energy hopping. The tunable length of the stack offered an opportunity to achieve an ideal system for light harvesting.

The Qu group demonstrated light harvesting in nanoparticles formed upon mixing of guanosine 5'-monophosphate (GMP), energy donor thioflavin T, energy acceptor thiazole orange, and Eu(NO₃)₃.⁷² The role of metal coordination in the assembly of the nanoparticles was proposed on the basis of a shift in the IR bands of the phosphate group and the nucleobase moiety of GMP after addition of Er³⁺. Light harvesting was claimed on the basis of amplified emission of acceptor. In an extension of this work,⁷³ they obtained right-handed helical nanofibers by

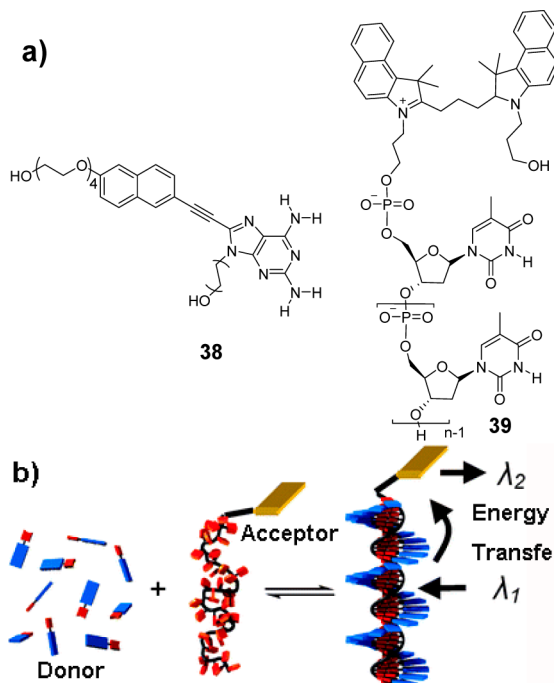


Figure 21. (a) Chemical structures of donor 38 and acceptor 39. (b) Schematic representation of the DNA-templated self-assembly and energy-transfer process. Adapted with permission from ref 71. Copyright 2011 The Royal Society of Chemistry.

Sr²⁺-templated self-assembly of GMP. In addition to chromophores thioflavin T and thiazole orange, pyronin Y was encapsulated in the fibers as the final acceptor for two-step FRET. These reports demonstrate the simplicity and lower cost of light-harvesting materials derived from biomolecules other than DNA.⁷⁴

2.4. Organic–Inorganic Hybrid Materials for Light Harvesting

Although impressive results have been obtained with proteins, DNA, and other expensive biomolecules, their cost may hamper their scale up and widespread applications in artificial light-harvesting system. Recently, organic–inorganic hybrid materials attracted considerable attention for their low costs and excellent mechanical properties, which are required for device applications. Inagaki and co-workers achieved light harvesting with a periodic mesoporous organosilica (PMO), which represents a new class of hybrid organic–inorganic porous material with mesochannels.⁷⁵ These PMOs were obtained by surfactant-assisted supramolecular assembly of organic-bridged alkoxysilanes (R'O)₃Si–R–Si(OR')₃ (R = organic groups, R' = CH₃, C₂H₅), which resulted in organic groups covalently embedded within the framework at high density. This configuration could potentially be exploited to promote the transfer of excitation energy from framework donors to acceptors in the mesochannels (Figure 22).

In the study of Inagaki and co-workers, R = biphenyl was chosen as the donor and coumarin dye **40** as the acceptor doped in mesochannels. Efficient energy transfer between biphenyl and **40** was demonstrated by measurements of the fluorescence quantum yield and fluorescence decay kinetics (Figure 23). The quenching rate of biphenyl emission is close to 100% at low **40** concentrations of 0.8 mol %, indicating that 125 biphenyl groups in the biphenyl–PMO are funneled to a

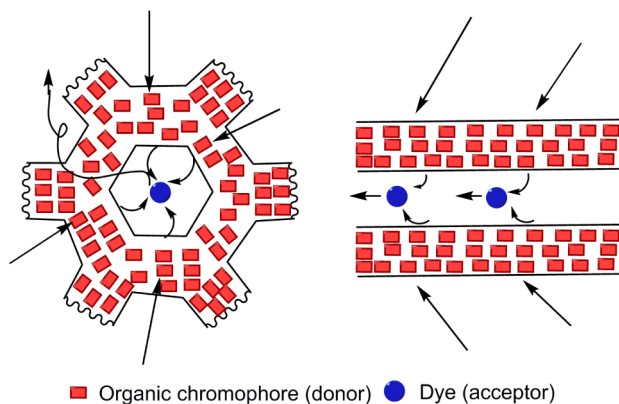


Figure 22. Schematic representation of energy transfer from organic chromophores in the PMO framework to dyes in the mesochannels of PMO. Adapted with permission from ref 75. Copyright 2009 Wiley-VCH Verlag GmbH & Co. KGaA, Weinheim.

single-molecule **40** and demonstrating the advantage of PMO as a light-harvesting scaffold. In addition to the above particle morphologies, films of biphenyl-PMOs exhibited efficient energy transfer. Later, the same group synthesized visible-light absorptive acridone-bridged PMO powder for light harvesting since biphenyl-PMOs have the limitation of absorbing only UV light (<300 nm), which may hamper their practical applications.⁷⁶ Recently, enhanced fluorescence detection of metal ions was realized using these PMOs,⁷⁷ opening up opportunities for exploiting such materials in applications of dedicated fluorescence chemosensors.

Clays are another class of layered silicate materials. George's and Takagi's group reported in 2011 two clay/dye composites for mimicking a light-harvesting system. George et al. chose amino-group-functionalized organoclays for the design of hybrid clay materials, since the functional amino groups can be exploited for noncovalent attachment of chromophore molecules whereas protonation of such groups in water would result in repulsion between the layers, making this clay

easily exfoliable.⁷⁸ Potassium tetracarboxylates of coronene (**41**, CS) and perylene (**42**, PS) were chosen as the energy donor and acceptor, respectively (Figure 24a), so that the negatively

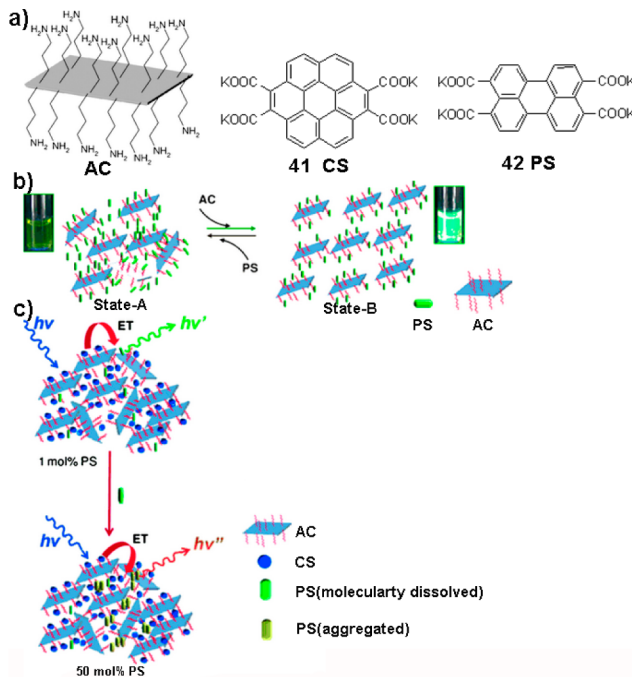


Figure 24. (a) Chemical structures of a single layer of aminoclay (AC), energy donor (**41** CS), and energy acceptor (**42** PS). (b) Schematic representation of different states of AC-42 hybrids in solution. (c) Schematic representation of the self-assemblies and energy transfer in clay-dye hybrid gels. Adapted with permission from ref 78. Copyright 2011 Wiley-VCH Verlag GmbH & Co. KGaA, Weinheim.

charged carboxylate groups of these dyes would interact electrostatically with the positively charged aminoclay in

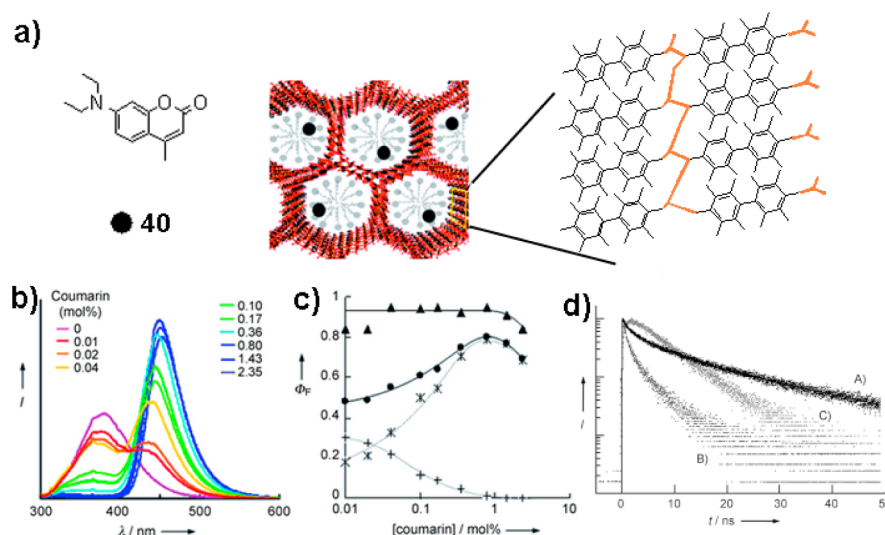


Figure 23. (a) Schematic representation of coumarin **40**/biphenyl-PMO. Orange lines represent alkoxy silanes. (b) Fluorescence spectra for **40**/biphenyl-PMO powders with 0–2.35 mol % **40** ($\lambda_{\text{ex}} = 270$ nm). (c) Fluorescence quantum yield (Φ_F) of **40**/biphenyl-PMO under excitation at 270 nm (●) and 380 nm (▲) vs concentration of **40**. (+ and *) Contribution of biphenyl and **40** components to Φ_F (270 nm). (d) Fluorescence decay profiles of biphenyl-PMO powder monitored at 370 nm (A) and **40**/biphenyl-PMO powder (0.66 mol %) monitored at 370 (B) and 500 nm (C) ($\lambda_{\text{ex}} = 266$ nm). Adapted with permission from ref 75. Copyright 2009 Wiley-VCH Verlag GmbH & Co. KGaA, Weinheim.

water. Interestingly, the authors designed two different states by tuning the concentration ratio of clay and dye: state A is a solution containing clustering of clay hybrids, and state B is a solution containing exfoliable clay sheets with a lower density of dye molecules (Figures 24b and 25a). In particular, increasing

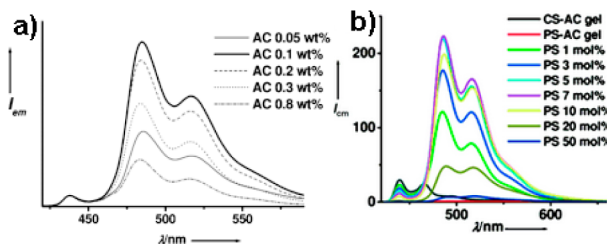


Figure 25. (a) Normalized emission spectra at the maximum of donor emission with increasing amounts of AC keeping the concentration and composition of the donor and acceptor chromophores constant ($\lambda_{\text{ex}} = 350 \text{ nm}$). Dyes with 0.1 wt % of AC correspond to state A and dyes with 0.8 wt % of AC corresponds to state B. (b) Emission spectra from energy transfer in hybrid gels ($\lambda_{\text{ex}} = 350 \text{ nm}$). Reprinted with permission from ref 78. Copyright 2011 Wiley-VCH Verlag GmbH & Co. KGaA, Weinheim.

the concentration of the dyes and the clay in water while keeping their ratio similar to that of state A yielded highly stable transparent hydrogels. The efficiency of energy transfer from **41** to **42** (**41** containing 10 mol % of **42** at $1 \times 10^{-4} \text{ M}$) in state A was higher than in state B, suggesting the absence of interclay excitation energy transfer. In clay gels containing **41** and **42**, less loading of **42** resulted in amplified green emission from the gels. However, increasing **42** concentration ($>10 \text{ mol } \%$ of **41**) decreased and shifted the emission bathochromically because of the interaction between molecules of **42** (Figure 25b). These fluorescence changes hold promise for application as stimuli-responsive supramolecular systems and sensors.

The artificial light-harvesting system based on organoclay–dye hybrids presented by George et al. manifested good energy-transfer efficiency. However, the self-quenching of the chromophores due to their stacking at high dye loadings may cause energy losses. Takagi et al. successfully addressed this problem with unique clay/porphyrin complexes in which the porphyrin molecules adsorb on the clay surface without aggregation even at high dye loadings (Figure 26).⁷⁹ The formation of these hybrids was rationalized by size matching of distances between the charged sites in the porphyrin molecule with the distances between anionic sites on the clay surface.⁸⁰ The steady state and time-resolved fluorescence measurements indicated an energy-transfer efficiency approaching 100%.

To improve the photostability and widen spectral windows for light collecting, Nabiev and Gonorov et al. developed hybrid materials in which fluorescent quantum dots (QD) collected light and transferred energy to the complex of photosynthetic reaction centers (RC)⁸¹ from *Rb sphaeroides*. The RC electrostatically bound QDs (QD570 or QD530) that strongly absorb light and strongly photoluminesce at a wavelength matching the RC pigments (Figure 27a). In the QD–RC complex the emission of QD was quenched and their excited state lifetime significantly shortened (Figure 27b and 27c), while the RC luminescence at 910 nm was significantly enhanced, suggesting efficient QD → RC FRET (Figure 27d). This study represents the first example of efficient transfer of excitation energy harvested by nanoparticles to a complex biological photosynthetic system.

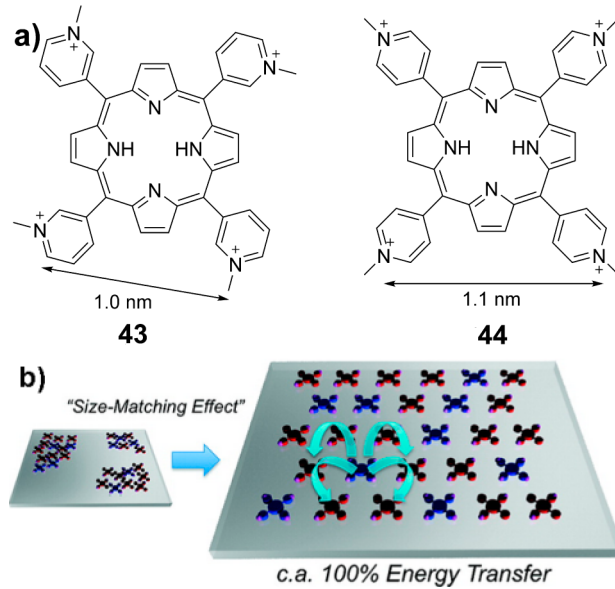


Figure 26. (a) Chemical structures of porphyrins **43** (donor) and **44** (acceptor) for quantitative energy transfer in clay/porphyrin complex. (b) Schematic representation of quantitative energy transfer by controlled assembly of **43** and **44** on the clay surface. Reprinted with permission from ref 79. Copyright 2011 American Chemical Society.

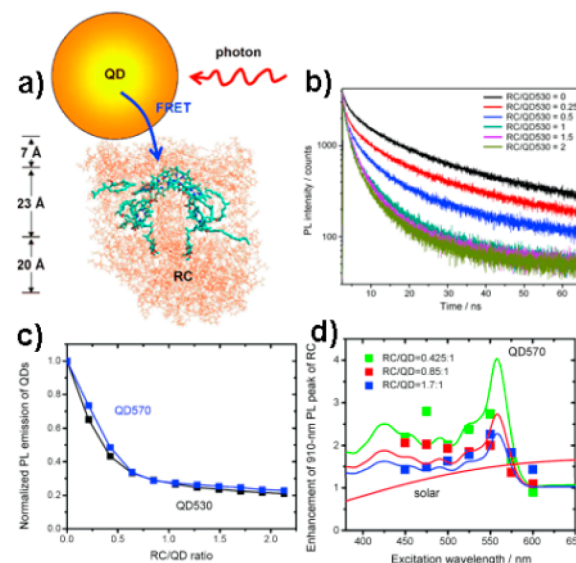


Figure 27. (a) Schematic representation of light-harvesting energy transfer from quantum dots (QD) to reaction centers (RC). (b) Quenching of the QD emission vs the RC/QD molar ratio ($\lambda_{\text{ex}} = 450 \text{ nm}$). (c) Fluorescence decay curves for QD570-RC complexes measured in the spectral region of QD emission at different RC/QD molar ratios. (d) Enhancement of photoluminescence from the RC at 910 nm vs excitation wavelength. Reprinted with permission from ref 81. Copyright 2010 Wiley-VCH Verlag GmbH & Co. KGaA, Weinheim.

2.5. Other Scaffolds for Light Harvesting

Self-assembly of a chromophore-derived macromolecule is another promising strategy for artificial light harvesting. Dendrimers in particular have been widely used due to their well-defined tree-like structures, providing predetermined sites for grafting chromophores.⁸² However, undesired molecular

interactions such as self-quenching and excimer formation increase in severity for dendrimers of high generations, decreasing the energy-transfer efficiency.

In 2009, Li and co-workers developed a self-assembly approach that avoids undesired chromophore interactions in dendrimers.⁸³ Water-soluble dendrimers G0–G3 were synthesized with peripheral naphthyl groups as antenna chromophores, which showed intensive self-quenching and excimer formation in buffer solution, resulting in extra energy dissipation (Figure 28). Consequently, the efficiency of energy

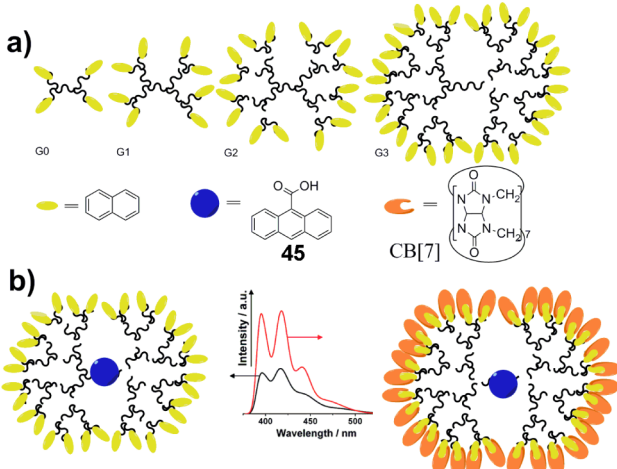


Figure 28. (a) Zeroth- to third-generation G0–G3 dendrimers with 4, 8, and 32 terminal naphthyl groups. (b) Light-harvesting process in dendritic systems with or without Cucurbit[7]uril CB[7]. Adapted with permission from ref 83. Copyright 2009 American Chemical Society.

transfer from naphthyl to the 9-anthracenecarboxylic acid acceptor (**45**) was very low. Adding cucurbit[7]uril to such solutions increased the energy-transfer efficiency to 70% for the second-generation and to 100% for the third-generation dendrimers thanks to formation of naphthyl/CB guest–host complexes due to the high affinity of naphthyls for the hydrophobic cavity of cucurbituril.

Because the synthesis of monodispersed dendrimers with a large number of antenna chromophores is time consuming and challenging, Yang et al. prepared a highly efficient antenna system based on multifunctional surface-cross-linked micelles (SCMs) (Figure 29).⁸⁴ The micellization supplied a large number of sites for binding donors and/or acceptors without tedious synthesis.⁸⁵ As a result, up to 50 of 9,10-bis (4-methylphenyl)anthracene (**46**) were localized on each cationic SCM. Excitingly, in the highly crowded **46**-SCMs, neither self-quenching nor excimer formation was significant, which may result from the nonplanarity of the **46**, the relatively rigid linkages connecting **46** to SCMs, and electrostatic repulsion among **46**-SCMs.

Anionic Eosin Y disodium salt (**47**) was chosen as the energy acceptor, which assembled spontaneously on the surface of the positively charged **46**-SCM by electrostatic interactions. Addition of **47** to **46**-SCMs lowered donor emission at 430 nm while enhancing acceptor emission at 550 nm (Figure 30a), indicating the occurrence of the energy transfer. The excitation spectrum of the acceptor was nearly identical to the absorption spectrum of **46**-SCM, demonstrating that the donor contributed directly to the acceptor emission (Figure 30b). The

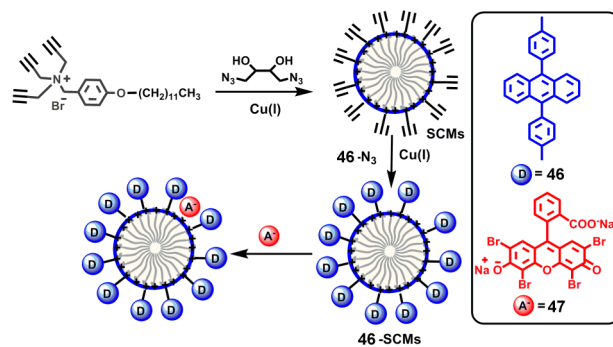


Figure 29. Preparation of donor-functionalized surface-cross-linked micelles and construction of a light-harvesting system by assembly of Eosin Y disodium salt (**47**) through electrostatic interactions. D and A represent donor and acceptor, respectively. Adapted with permission from ref 84. Copyright 2012 Wiley-VCH Verlag GmbH & Co. KGaA, Weinheim.

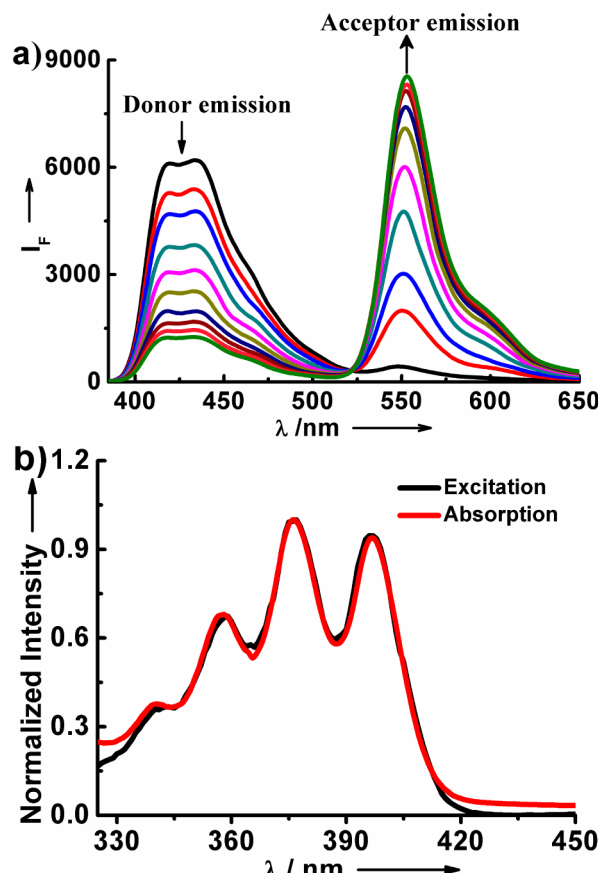


Figure 30. (a) Fluorescence spectra of **46**-SCMs in THF with different concentrations of **47** ($\lambda_{\text{ex}} = 375$ nm). (b) Normalized excitation spectrum of **47**/**46**-SCMs ($\lambda_{\text{em}} = 550$ nm, black trace), and absorption spectrum of **46**-SCMs (red trace). Reprinted with permission from ref 84. Copyright 2012 Wiley-VCH Verlag GmbH & Co. KGaA, Weinheim.

photophysical studies indicated that energy migration played an important role for efficient energy transfer. This highly efficient light-harvesting system built of inexpensive starting materials and with simple chemistry could provide a new direction for the construction of supramolecular light-harvesting systems.

The self-complementary 2-ureido-4[1H]-pyrimidinone (UPy) quadruple H-bonding motif developed by Meijer has

been used for self-assembly for energy-transfer systems.⁸⁶ For example, three chromophores with emission spectra in the red, green, and blue region were functionalized with UPy groups at both ends to fabricate white emissive materials at a certain mixing ratio by utilizing partial energy transfer.^{21a} The modularity of the UPy-based supramolecular polymers makes it very promising for incorporating various energy donors and acceptors. However, the comparatively large separation of the adjacent chromophores linked by terminal UPy groups seems to reduce intrachain exciton migration, thus decreasing the overall transfer efficiency.⁸⁷

In 2014, Yang and co-workers reported the first example of nanospheres of quadruply hydrogen-bonded supramolecular polymers that were stable in water (Figure 31).^{30c} The efficient

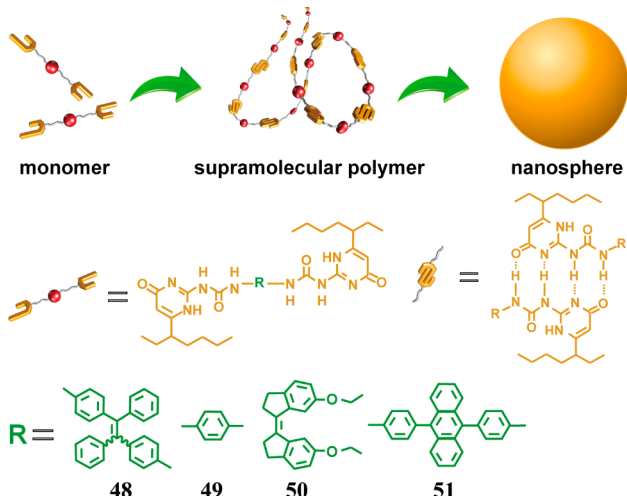


Figure 31. Schematic representation of the assembly of hydrogen-bonded supramolecular polymers from monomers **48–51** with different functional groups to water-dispersible nanospheres. Reprinted with permission of ref 30c. Copyright 2014 The Royal Society of Chemistry.

miniemulsion-based preparation opens up new opportunities for wide applications of UPy-based supramolecular polymers in situations where stability in water is important, such as biomaterials and optoelectronic materials. They used this novel material to construct brightly fluorescent light-harvesting nanospheres from supramolecular copolymers containing an energy donor and an acceptor (Figure 32). The energy funneling from the donor to the acceptor molecules was confirmed by steady state and time-resolved fluorescence spectroscopy. In addition, the amplification of acceptor emission indicated a remarkable antenna effect, which further proved the high light-harvesting ability of the nanospheres. It was suggested that such three-dimensional architectures would provide more energy-accepting sites than one-dimensional polymers for trapping the excitation energy.

Häner and co-workers described an artificial light-harvesting system based on linear polymers, which are formed from the assembly of short amphiphilic oligomers **53** and **54** in water (Figure 33).⁸⁸ Oligomer **53** has three phosphodiester-linked phenanthrene units as donors, while **54** is composed of an additional, terminal pyrene building block as acceptor. Fluorescence of polymers containing exclusively oligomer **53** was extremely weak. However, as minute amounts of pyrene-containing oligomer **54** were added to these polymers, the fluorescence quantum yield increased drastically. On the basis

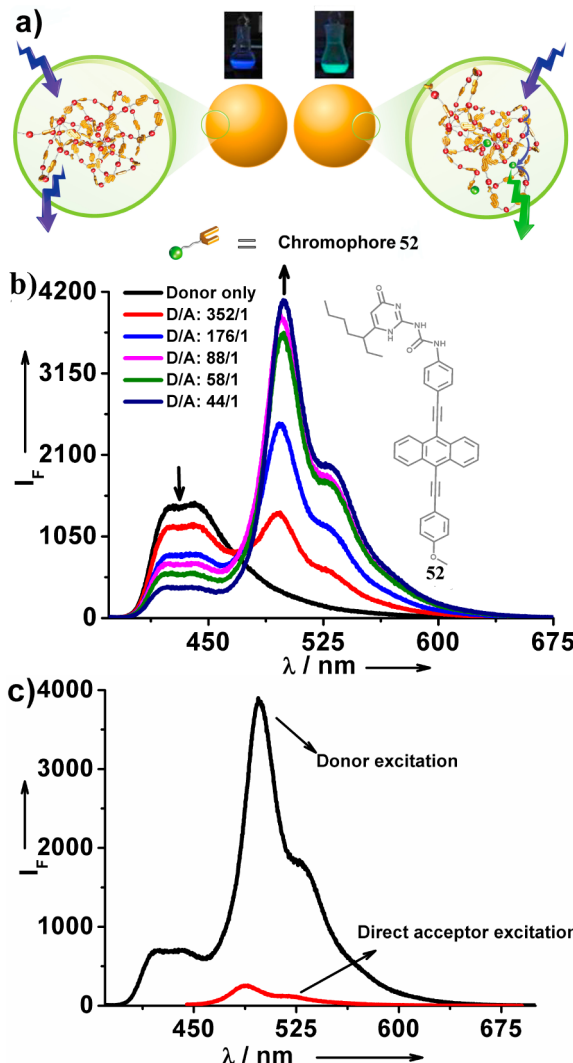


Figure 32. (a) Schematic representation of energy transfer among chromophores densely organized in nanospheres. (Left) Nanospheres prepared from supramolecular polymers of monomer **51**. (Right) Nanospheres prepared from supramolecular copolymers of 88:1 of **51** to **52**; (inset) photographs of dispersions of the nanospheres in water under UV light ($\lambda_{\text{ex}} = 365 \text{ nm}$). (b) Fluorescence spectra of the nanospheres dispersed in water with different molar ratios of the donor and acceptor ($\lambda_{\text{ex}} = 375 \text{ nm}$). (c) Antenna effect for nanospheres with a 88:1 molar ratio of the donor to the acceptor. Black and red lines are spectra from the donor excitation (375 nm) and from excitation of the acceptor directly (445 nm).^{30c} Reprinted with permission of ref 30c. Copyright 2014 The Royal Society of Chemistry.

of the dependence of the fluorescence quantum yield of these polymers on the fraction of pyrenes, the authors guesstimated that the excitation energy was transferred $\sim 150 \text{ nm}$ along the polymer backbone until being trapped by an acceptor molecule. This means that more than 400 donor molecules between one phenanthrene and one pyrene in the polymer participated in energy transfer. Such a long energy-transfer distance cannot be explained by classical FRET or Dexter mechanisms and require a new concept.⁸⁹

3. BIOIMAGING

Fluorescence imaging has become a powerful tool in many fields of science and technology because it enables the

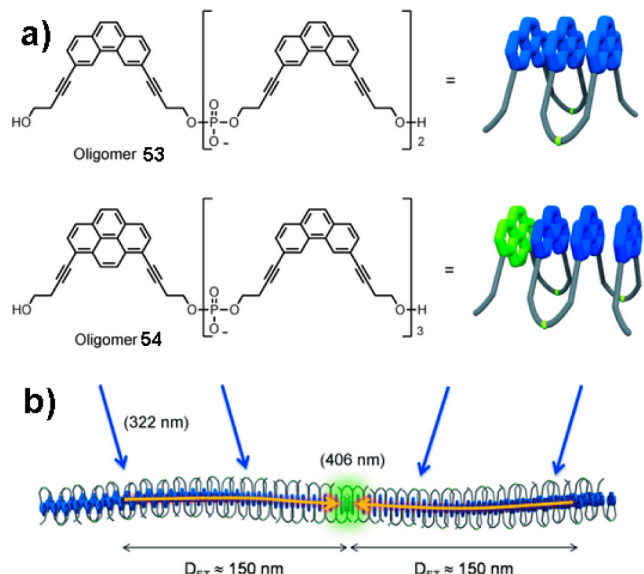


Figure 33. (a) Chemical structures and model representations of oligomers 53 and 54. (b) Illustration of light-harvesting polymer. Adapted with permission from ref 88. Copyright 2014 Wiley-VCH Verlag GmbH & Co. KGaA, Weinheim.

visualization of morphological details of cells for studies of fundamental physiological processes.⁹⁰ Fluorescent nanoparticles formed by self-assembly of small organic molecules or polymers are ideal for intracellular targeting due to their good biocompatibility, easy surface functionalization, and small sizes and have been used extensively for bioimaging.⁹¹

Nanoparticles capable of FRET can be monitored ratio-metrically to minimize background interference and enhance spatiotemporal resolution of imaging. In small molecule FRET systems, the fluorescent donor and acceptor are typically linked covalently, which means that FRET parameters, such as energy-transfer efficiency or absorption or emission wavelength, can only be altered by changing either or both fluorophores, which often requires complex synthesis.⁹² In contrast, self-assembled structures allow facile modulation of, for example, the average spatial distance between the donor and the acceptor by adjusting donor/acceptor ratios during preparation, controlling the functionalization density and position.⁹³

3.1. Multicolor Imaging

In order to monitor multiple biological events simultaneously multicolor imaging is needed. However, individual fluorophores rarely show distinct emission maxima under single-wavelength excitation. Nanoparticles assembled from fluorescent materials have been explored for multicolor applications. These particles encapsulated more than two different but complementary fluorophores. FRET cascades were used to tune emission signals by changing the nature of the fluorophores, their ratios, and total concentrations, thus enabling simultaneous imaging of the nanoparticles at different wavelengths using the same excitation source.⁹⁴

Law and co-workers reported a series of polymeric nanoparticles for multicolor imaging.⁹⁵ The particles contained four carbocyanine fluorophores 55–58 to engender emissions ranging from visible to near-IR. These nanoparticles were <100 nm in diameter and brighter than commercial quantum dots. The hydrophobic fluorophores were confined in close proximity to enable sequential energy transfer (Figure 34).

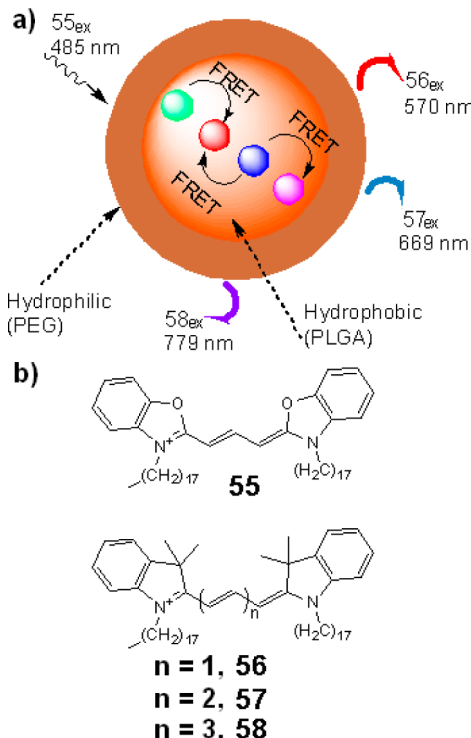


Figure 34. (a) Schematic illustration of the multicolor imaging platform. (b) Chemical structures of 55–58. Adapted with permission from ref 95. Copyright 2013 Wiley-VCH Verlag GmbH & Co. KGaA, Weinheim.

The optical properties of the particles were fine tuned by using different combinations, ratios, and concentrations of the fluorophores. By conjugating specific targeting ligands to the particle surfaces, the nanoparticles were shown to target cancer cells.

Conjugated polymers have attracted great interest for cell imaging. They are brightly fluorescence, photostable, and largely nontoxic.⁹⁶ These advantageous properties are retained when amphiphilic conjugated polymers and oligomers self-assemble into spherical particles or micellar structures. The fluorescence emission wavelength is easily tuned by varying the chemical structure of the π -conjugated building blocks and by using mixed systems capable of energy transfer.⁹⁷

The Schenning group reported the preparation of a set of π -conjugated amphiphilic fluorene oligomers that self-assembled in water into fluorescent particles.⁹⁸ The fluorene oligomers 59–62 consist of two fluorene units connected by an aromatic linker unit with different electron-accepting capacity, resulting in their emission spectra varying from blue, to green, to yellow, to red, thus covering the entire visible range (Figure 35). The emission colors could be tuned by mixing different molar ratios of oligomers 59–62 when partial energy transfer occurred. Subsequently, they extended their method to the preparation of functionalized fluorescent nanoparticles by self-assembly of prefunctionalized π -conjugated oligomers.⁹⁹ The surface properties of these nanoparticles and their binding to dye-labeled target molecules were measured by FRET. This method provides a novel approach to multitarget bioimaging and biosensing.

To be useful fluorophores used for multicolor monitoring must possess narrow emissions. The Chiu group reported multicolor semiconducting polymer dots (Pdots) with narrow

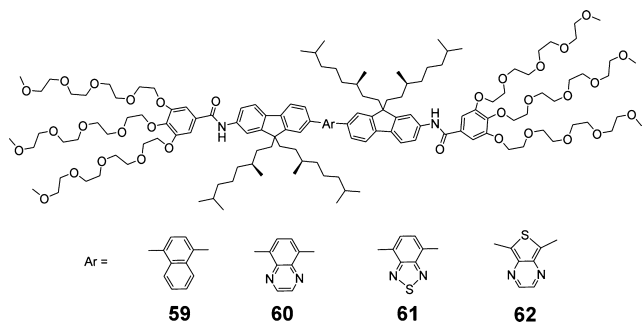


Figure 35. Chemical structures of fluorene oligomers 59–62.

emissions.¹⁰⁰ Different boron dipyrromethene (BODIPY) units with sharp fluorescence peaks and high quantum yields were incorporated into a polymer backbone for the preparation of multicolor Pdots by the nanoprecipitation method. The fwhm values of the fluorescent peaks of these Pdots were 40–55 nm or 1.5–2 times narrower than those of conventional semiconducting polymer dots, probably because of efficient energy transfer among the chromophores within individual particles (Figure 36). The emission color was tuned by modifying the BODIPY core, and bioconjugation tests demonstrated the specific cellular targeting ability of these nanoparticles.

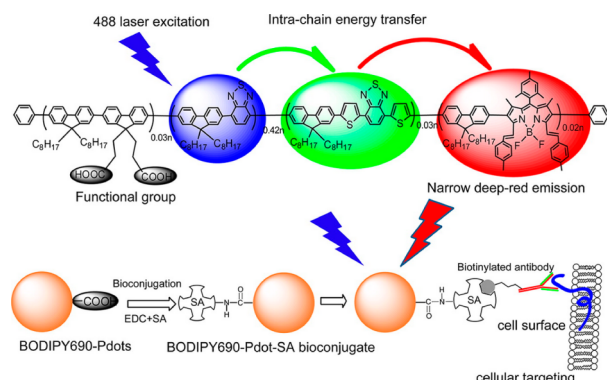


Figure 36. Schematic illustration of the narrow emissive multicolor semiconducting polymer and bioconjugates for specific cellular targeting. Reprinted with permission from ref 100. Copyright 2013 American Chemical Society.

Bacteria and biological macromolecules (e.g., DNA and protein) have been used as templates to construct complex structures by electrostatic interactions with cationic conjugated polymers. Wang and co-workers developed multicolor microfibers by self-assembly of bacteria and conjugated polymer nanoparticles.¹⁰¹ The conjugated polymer nanoparticles were prepared from four conjugated polymers with emissions in the blue, green, yellow, and red. The resulting nanoparticles bound to the outer-surface membrane of *Escherichia coli* (*E. coli*) cells through electrostatic and hydrophobic interactions, which kept the nanoparticles in close proximity to allow efficient interparticle FRET and further achieve large Stokes shifts up to 170 nm. The FRET efficiency was tuned by varying the molar ratios of the conjugated polymer nanoparticles, thus adjusting emissions of the FRET-mediated microconstructs and regulating multicolor fluorescence. These multicolor microconstructs were successfully applied for cell imaging and optical barcoding.

The Wang group also reported multicolor microfibers¹⁰² from coassembly of cationic conjugated polymers with different color emissions, negatively charged DNA, and positively charged histone proteins. Multicolor emissions with large Stokes shifts were obtained by FRET among cationic conjugated polymers under a single-excitation wavelength. To detect the biocompatibility of fibers, they encapsulated GFP-coded *E. coli* BL21 cells into the microfibers. The successful expression of GFP proteins in fibers indicated the biological activity of cells. Thus, these multicolored fibers show great potential in bioimaging and biomedical applications.

The Wang group reported multicolor conjugated polymer nanoparticles for bioimaging and detection of tumor cells^{22c} prepared by self-assembly of four conjugated polymers 63–66 (with blue, green, yellow, and red emissions) and poly(styrene-co-maleic anhydride) (PSMA) by hydrophobic interactions. Upon excitation at 360 nm, the polymers that emit at shorter wavelengths were anticipated to act as the donor for longer wavelength-emissive acceptors by interchain multistep FRET. The efficiency of chain-to-chain FRET was regulated by varying the mixing ratio of the polymers, yielding multicolor emission over the entire visible emission range under one excitation wavelength (Figure 37). They constructed a detection ensemble for binding one tumor cell to two conjugated

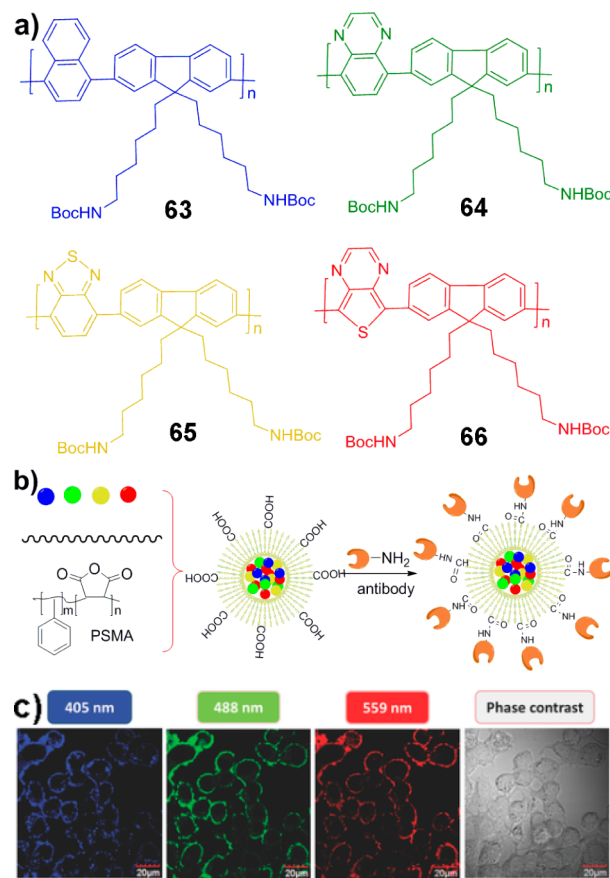


Figure 37. (a) Chemical structures of conjugated polymers 63–66. (b) Preparation of multicolor conjugated polymer nanoparticles and their modification with an antibody. (c) Multichannel fluorescence images of MCF-7 cells with the conjugated polymer nanoparticles. Excitation wavelengths are shown on top of each image. Adapted with permission from ref 22c. Copyright 2014 Wiley-VCH Verlag GmbH & Co. KGaA, Weinheim.

polymer nanoparticles labeled with different antibodies. In comparison to single-antibody recognition, higher specificity for tumor cell detection was achieved by the double-antibody recognition approach.

3.2. NIR Imaging

Optical imaging is restricted by the penetration depth and achievable resolution. Tissue components (such as hemoglobin) absorb visible light, limiting penetration of visible light. Visible light also causes excessive autofluorescence from naturally occurring endogenous fluorophores, such as collagens, porphyrins, and flavins. Other tissue components (e.g., water and lipids) are optically transparent from the visible to the NIR but absorb light in the IR. Consequently, absorbance and autofluorescence of the human tissue are minimal in the 650–900 nm range, where the penetration depth is greatest.¹⁰³ Direct employment of NIR dyes in bioimaging is still challenging because (1) the large conjugation systems of NIR dyes decrease their quantum yield of fluorescence, increase their hydrophobicity, and induce their self-aggregation in aqueous solution, which dramatically reduces the brightness of NIR dyes, and (2) most NIR dyes have small Stokes shift, which can cause interference between the excitation light and the resulting fluorescence signals. Self-aggregation can be eliminated by dispersing NIR dyes within inert nanoparticles. Conjugated polymer nanoparticles provide the ideal matrix for entrapping NIR dyes: efficient energy transfer from the excited conjugated polymer matrix to the doped dyes results in large Stokes shifts and enhances fluorescence signals by taking advantage of the light-harvesting ability of conjugated polymers.

Semiconducting polymer dots (Pdots) are highly fluorescent, but most emit in the visible range. Doping organic NIR dyes into such Pdots can overcome this limitation while taking advantage of the large extinction coefficients of Pdots and facile energy migration along conjugated polymer backbones.¹⁰⁴ The Chiu group prepared a NIR polymer dot by doping NIR dye **68** into particles of poly(9,9-diocetylfluorene-co-benzothiadiazole) (**67**) formed by a nanoscale precipitation technique (Figure 38).¹⁰⁵ Coassembly of **67** with an amphiphilic polymer (**69**) produced Pdots with a hydrophilic surface, whose COOH groups enabled bioconjugation of biomolecules. The **68**-doped nanoparticles exhibited 40 times stronger fluorescence in aqueous solution over the equivalent amount of free dye **68**.

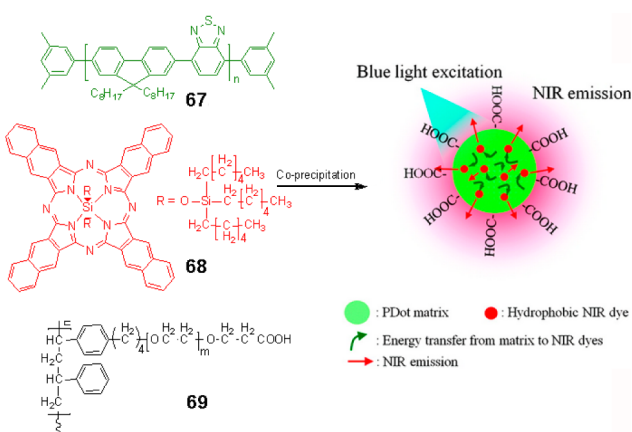


Figure 38. Preparation of the NIR dye-doped Pdots, and schematic illustration of the energy transfer from matrix to NIR dyes. Adapted with permission from ref 105. Copyright 2011 American Chemical Society.

excited in THF. The dramatic brightness enhancement was attributed to the excellent light-harvesting ability of **67** and the efficient energy transfer from **67** to NIR dye **68**.

In another example, they prepared water-dispersible multi-component Pdots by assembly of four polymers with different emission wavelengths.¹⁰⁶ By optimizing cascade energy transfer in these polymer nanoparticles, the emissions of the first three polymers were quenched so that the Pdots exhibited bright fluorescence (quantum yield = 0.32) at 710 nm with large Stokes shifts (up to 330 nm) and narrow emission bands (fwhm = 44 nm). Single-particle fluorescence imaging showed that under identical conditions these NIR nanoparticles were more than three times brighter than the commercially available quantum dots (Qdot705) of comparable sizes. In addition, the cellular targeting was successfully performed with the NIR-emitting Pdots bioconjugated to streptavidins.

Another strategy of overcoming the limited penetration depth of light in human tissue is based on self-luminescing hybrid probes which exploit bioluminescence resonance energy transfer (BRET).¹⁰⁷ A self-luminescing protein (such as *R. reniformis* luciferase) emits light without external excitation, which often causes strong background autofluorescence of human tissue. The Rao group developed self-luminescing NIR nanoparticles by integrating BRET and FRET in an energy-transfer relay (Figure 39).¹⁰⁸ The nanoparticles were prepared by nanoprecipitation of a poly(phenylenevinylene) derivative (**70**) and NIR dye **68** as the emitters and a polystyrene/PEG copolymer (**69**) as the matrix, followed by conjugation with a bioluminescent eight-mutation variant of Luc8 and RGD peptides. Efficient BRET occurred from Luc8 to **70** and from **70** to NIR dye **68**. After injection of the nanoparticles to the U87MG tumor xenograft mouse model, strong bioluminescence emission was observed in the U87MG tumor with little signal from other tissues. The nanoparticles allowed simultaneous fluorescence and bioluminescence imaging. NIR fluorescence was observed in the liver, and it was much weaker than the bioluminescence signal, indicating that bioluminescence imaging of tumors provided much higher sensitivity than fluorescence imaging.

Conventional fluorophores encapsulated in nanoparticles tend to aggregate by strong hydrophobic and $\pi-\pi$ stacking interactions, leading to reduced fluorescence, the phenomenon known as aggregation-caused quenching (ACQ). This disadvantage is overcome by using aggregation-induced emission (AIE) luminogens, which show bright fluorescence when aggregated.¹⁰⁹ Consequently, conventional ACQ chromophores can be converted to efficient solid emitters by combining them with AIE luminogens.¹¹⁰ Encapsulation of a suitable fluorescent dye into AIE assemblies often yields nanoparticles with bright luminescence as a result of energy transfer from AIE dyes to doped fluorophores. In a typical example, Jen and co-workers reported the use of three amphiphilic block copolymers to form polymeric micelles for encapsulation of hydrophobic AIE donor–acceptor pairs.¹¹¹ The observed large Stokes shift and amplification of emission were ascribed to efficient energy transfer.

The ACQ phenomenon is even more significant for NIR dyes because their large π -conjugated systems with multiple aromatic rings favor strong $\pi-\pi$ interaction, which quenches the fluorescence.¹¹² The Liu group used conjugated polymers and a NIR AIE luminogen as FRET pairs to create a signal-amplified NIR probe for live-animal imaging and cancer diagnosis.¹¹³ A green-emitting conjugated polymer polyfluor-

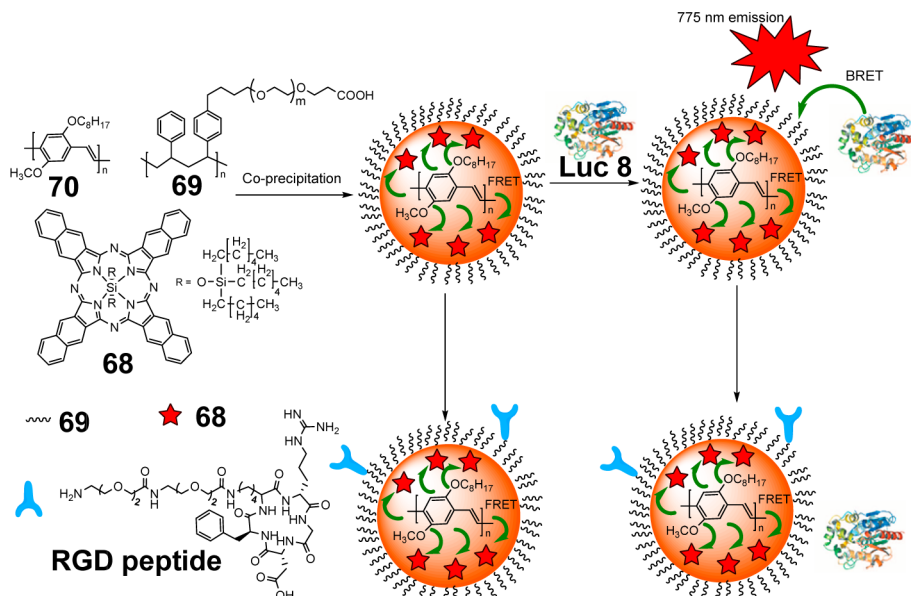


Figure 39. Schematic illustration of self-luminescing BRET-FRET NIR polymer nanoparticles. Adapted with permission from ref 108. Copyright 2012 Nature Publishing Group.

enyldivinylene (PFV) was used as a FRET donor, and bovine serum albumin (BSA) was selected as the polymer matrix due to its biocompatibility. Functionalization of the nanoparticles with arginine-glycine-aspartic acid (RGD) peptide allowed the nanoparticles to be used for specific cancer targeting. The resulting nanoparticles manifested a large Stokes shift of 223 nm and low cytotoxicity. The NIR emission at 660 nm was amplified up to 5.3-fold compared to that from the same amount of the acceptor upon direct excitation.

They also encapsulated an AIE luminogen with red fluorescence (FRET donor 71) and silicon NIR dye 68 (acceptor) in amphiphilic polymer 72 (Figure 40) to obtain nanoparticles manifesting narrow NIR emission ($\text{fwhm} = 20$ nm) and with a large Stokes shift of 275 nm.¹¹⁴ The efficient energy transfer resulted in a 47-fold enhancement of the NIR dye 68 emission intensity. The NIR nanoparticles were utilized in fluorescence imaging in bare mice with excitation at 523 and 704 nm to match the absorption maxima of the donor (510 nm) and the acceptor (760 nm). The fluorescence intensity of the nanoparticles upon excitation at 523 nm was on average 5.2-fold higher than that upon excitation at 704 nm (Figure 41).

3.3. Stimuli-Responsive Bioimaging

FRET efficiency is sensitive to many factors, including the extent of spectral overlap between the fluorescent donor and acceptor and their relative molecular orientation. FRET within assemblies can be modulated by using stimuli-sensitive dyes, whose spectroscopic properties can be facilely switched by external stimuli. Such stimuli-responsive assemblies can exhibit reversible or irreversible changes in their physical properties and/or chemical structures in response to external stimuli, such as light irradiation, pH, and temperature.¹¹⁵

3.3.1. Photoresponsive Imaging. Photochromic compounds interconvert between two isomers with distinct absorption spectra when irradiated at appropriate wavelengths. Azobenzene,¹¹⁶ spiropyran,¹¹⁷ and dithienylethene¹¹⁸ (Figure 42a) are widely used photochromic compounds because of the good reversibility of the photoisomerization, modularity, and

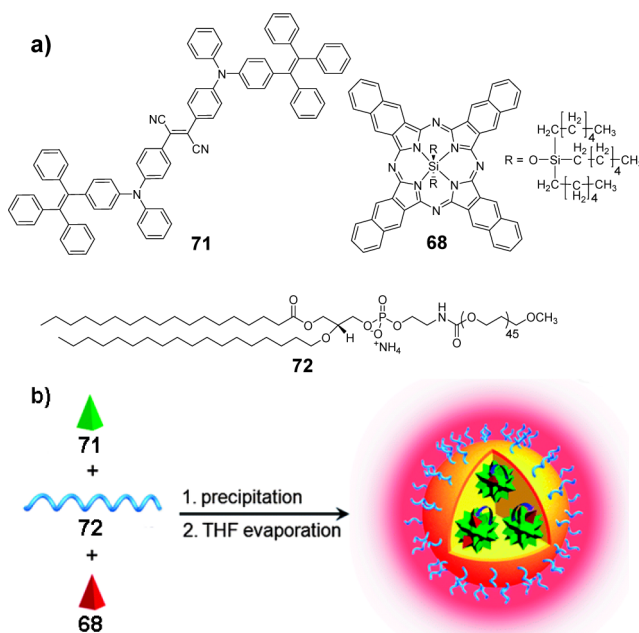


Figure 40. (a) Chemical structures of 71, NIR dye 68, and 72. (b) Schematic illustration of the fabrication of NIR nanoparticles. Adapted with permission from ref 114. Copyright 2013 Wiley-VCH Verlag GmbH & Co. KGaA, Weinheim.

diversity in property regulation, the advantages that have long been exploited in material science.¹¹⁹ If the spectrum of only one isomer overlaps with the emission of a nearby fluorophore functioning as a donor, the pair will exhibit switchable FRET (Figure 42b), a process denoted previously by Jares-Erijman's group as photochromic FRET (pcFRET).¹²⁰ In such systems, the photoinduced and reversible transformations of the photochromic switches effectively modulate the photophysical properties of the fluorophores.¹²¹

Spiropyran (SP) photoisomerizes reversibly between non-fluorescent spiropyran and red-emitting fluorescent merocyanine (MC). Hurst and co-workers reported the synthesis of

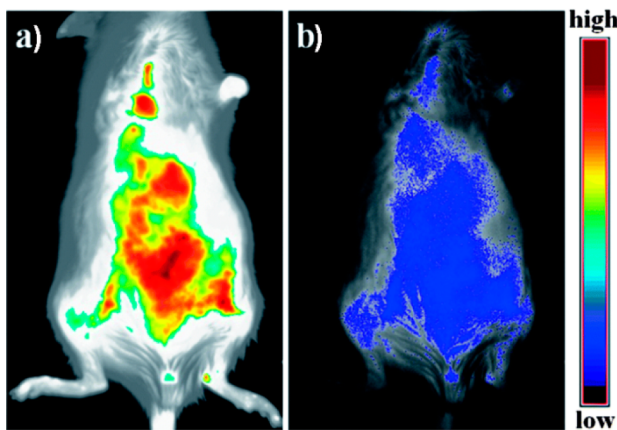


Figure 41. Fluorescence imaging of mice after injection of the NIR nanoparticles upon excitation at (a) 523 and (b) 704 nm. Reprinted with permission from ref 114. Copyright 2013 Wiley-VCH Verlag GmbH & Co. KGaA, Weinheim.

photoinduced fluorogenic polymeric nanoparticles with spirobifluorene moieties covalently attached within the hydrophobic interior (Figure 43).¹²² The fluorogenic process was switched on or off by irradiation at different wavelengths (UV, visible light, or NIR, the last case relying on two-photon absorption). They further integrated the nanoparticles with fluorescent perylenediimides FRET donors **73** and photoinduced SP moieties **74** as acceptors to construct reversibly photo-switchable dual-color fluorescent nanoparticles. The as-prepared nanoparticles had an average diameter of 56 nm with negatively charged carboxyl groups on the surfaces to make them easily dispersible in water and stable in biological buffers. When SP **74** was in the colorless ring-closed form, the fluorophores **73** located in the hydrophobic core fluoresced intensely green. Under UV irradiation, SP converted to its colored ring-opened MC form (**75**), whose absorption overlaps with emission of **73**, enabling FRET from **73** to **75** and resulting in a strong red emission. FRET was switched off under visible-light irradiation, recovering green emission. The switching was repeated many times without any photobleaching or apparent “fatigue effects”, an important advantage attributed to the protection by the polymer shell. The nanoparticles were

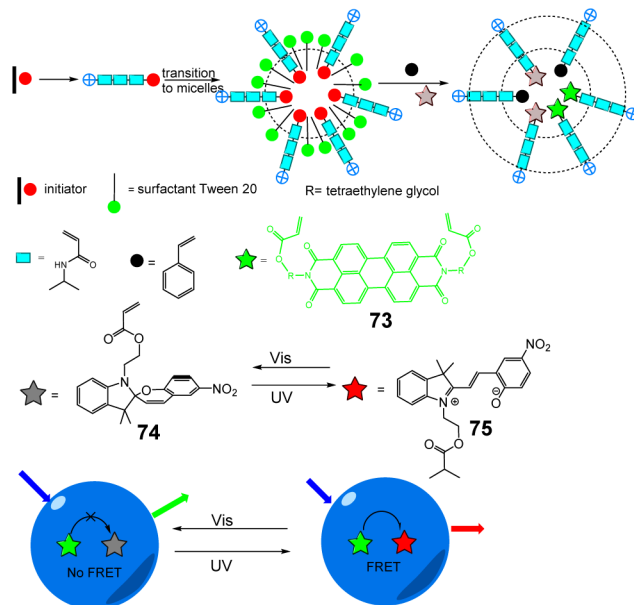


Figure 43. Schematic illustration of the fabrication of SP-embedded polymeric nanoparticles, and proposed modulation of emissions upon UV-vis irradiation. Adapted with permission from ref 122. Copyright 2007 American Chemical Society.

successfully delivered into human embryonic kidney (HEK-293) cells, and their green or red emissions were detected, suggesting that such high-contrast, dual-color fluorescent nanoparticles are suited for tracking and labeling components in complex biological systems.

Raymo and co-workers reported a supramolecular strategy for constructing photoswitchable fluorescent assemblies¹²³ by improving their previously reported photoswitchable fluorescent dyad consisting of a boron dipyrromethene (BODIPY) fluorophore covalently connected to a spirobifluorene photochrome. The previous molecular system manifested slow switching rates and poor fatigue resistance, and multiple and tedious synthetic steps were required to make the components hydrophilic.¹²⁴ Amphiphilic copolymer (**80**) was free of these limitations and formed micelles in water (Figure 44). These micelles captured mixtures of BODIPY dyes (**78** or **79**) and

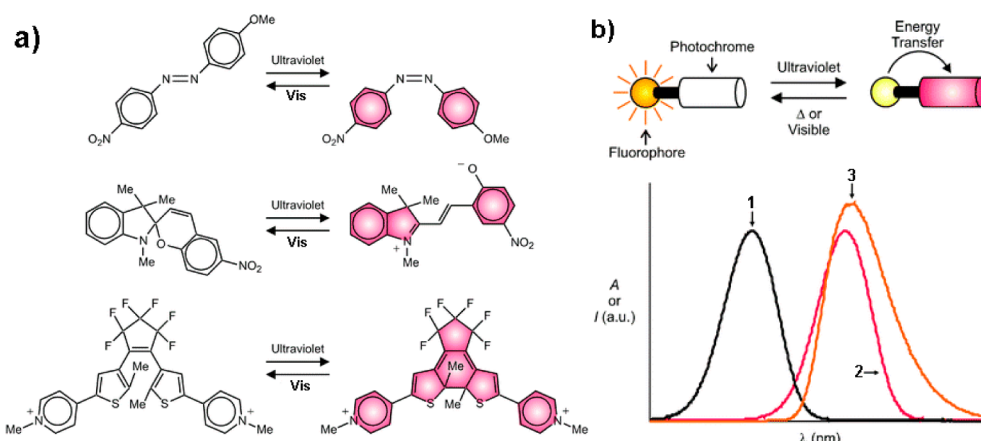


Figure 42. (a) Photoinduced reversible interconversion of some commonly used photochromic (PC) compounds. (b) Schematic mechanism of fluorescence modulation of pcFRET. Photoinduced reversible interconversion of PC compounds results in a bathochromic shift of their absorption from 1 to 2, which overlap well with fluorophore emission 3. Adapted with permission from ref 121. Copyright 2009 The Royal Society of Chemistry.

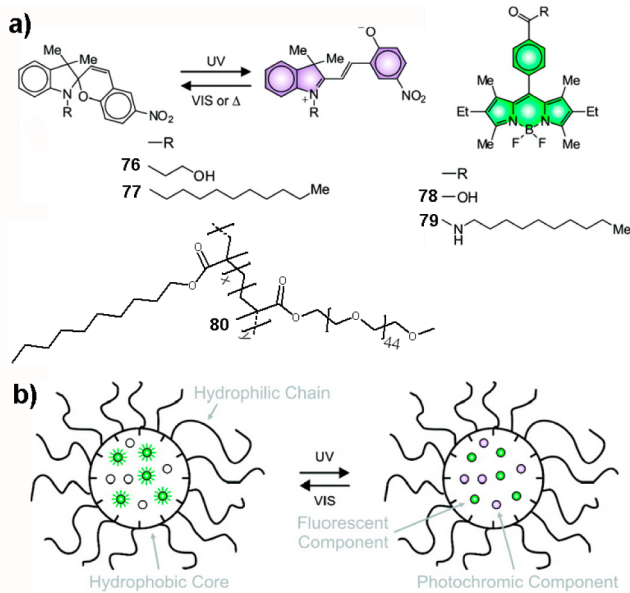


Figure 44. (a) Photoinduced reversible transformation of spiroxans into merocyanines, and structures of BODIPY derivatives. (b) Schematic representation of photoswitchable fluorescent assemblies. Adapted with permission from ref 123. Copyright 2010 American Chemical Society.

spiroxan photochromes (76 or 77). The supramolecular structures buried the more hydrophobic guests 77 and 79 within the hydrophobic interior, which shielded them from water, and lead to fast switching kinetics and good photostability. Within these supramolecular structures, photoinduced reversible transformation of SP 77 to MC 77 activated the energy transfer from BODIPY 79 to MC 77, thus quenching fluorescence of BODIPY as demonstrated by confocal microscopy in Chinese hamster ovarian (CHO) cells. It is noteworthy that MC at room temperature will revert to SP quite quickly, and the impact of this kinetics will limit its application to some extent.

Dithienylethenes reversibly interconvert between a colorless ring-open isomer and a colored ring-closed one when exposed to UV or visible light. Kim and co-workers reported dendritic nanoclusters with high on–off contrast for fluorescence imaging.¹²⁵ Cy3 (81) modified polyamidoamine (PAMAM) dendrimers were oligomerized to form nanoclusters using diarylethene (82) as a cross-linker, which interconverted between ring-closed and -opened isomers by alternate irradiation with UV and visible light to reversibly quench the fluorescence of 81 (Figure 45). The formation of such a porous nanocluster was sought to distribute 82 and 81 uniformly throughout both the interior and the exterior of the nanostructure, leading to efficient FRET. Moreover, reversible photoswitching for up to 10 cycles was achieved in living zebrafish. The same group also reported the reversible fluorescence photoswitching in living cells based on silica nanoparticles.¹²⁶

Kim and Park et al. constructed closely integrated binary nanoparticles of a cyanovinylene-backboned conjugated polymer (cvCP) and a bisthienylethene derivative (Figure 46).¹²⁷ The π -conjugated polymer showed bright solid-state fluorescence, which was turned on and off by photochromic switching through FRET. The dense physical assembly allowed for facile integration of solid-state NIR fluorescence and photochromism

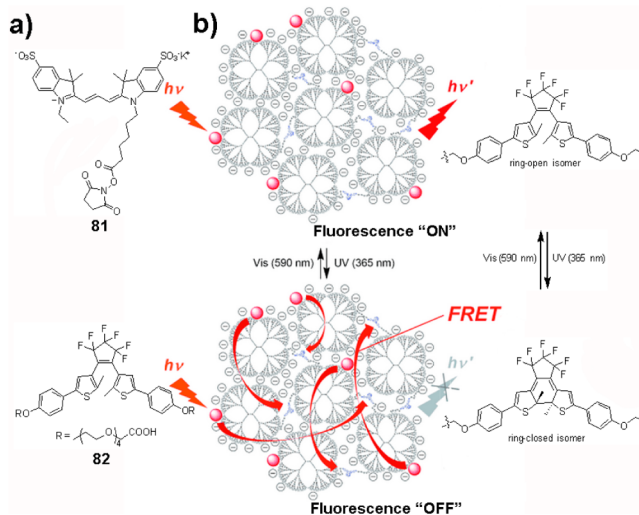


Figure 45. (a) Chemical structures of 81 and diarylethene 82. (b) “ON” and “OFF” fluorescence tuned by photoswitchable diarylethenes on dye-cross-linked dendritic nanoclusters. Reprinted with permission from ref 125. Copyright 2012 Wiley-VCH Verlag GmbH & Co. KGaA, Weinheim.

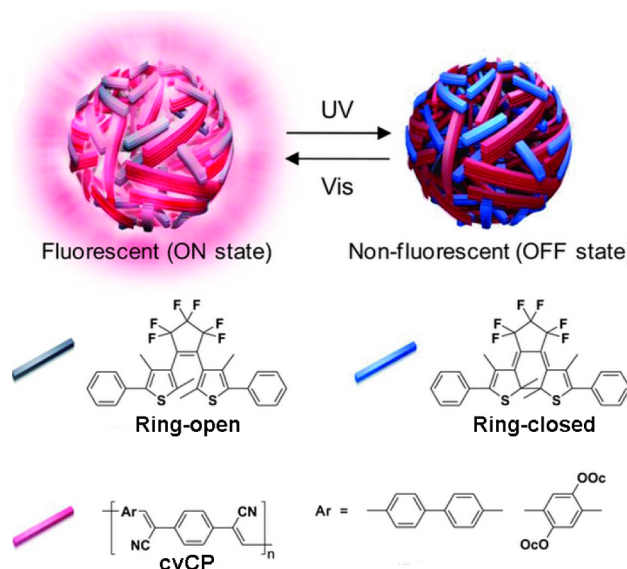


Figure 46. Schematic representation of cvCP/bisthienylethene-integrated nanoparticles and their photoswitching process tuned by UV-vis light illumination. Reprinted with permission from ref 127. Copyright 2013 Wiley-VCH Verlag GmbH & Co. KGaA, Weinheim.

in a nanoparticle to accomplish *in vivo* photoswitching and imaging in mouse models.

Quantum dots (QDs) have uniquely suitable properties for biological imaging: they have high brightness and photostability, broad excitation, and narrow emission.¹²⁸ Moreover, well-established surface chemistries enable the convenient assembly of acceptors around the surface of QDs which serve as the donor.¹²⁹ Borrowing a strategy from the Parak laboratory¹³⁰ for transferring hydrophobically capped nanocrystals from organic to aqueous solution by wrapping them into an amphiphilic polymer, photochromic diheteroaryleneethenes were covalently linked to an amphiphilic polymer that self-assembled with the lipophilic chains surrounding commercial hydrophobic core–shell CdSe/ZnS QDs (Figure 47).¹³¹

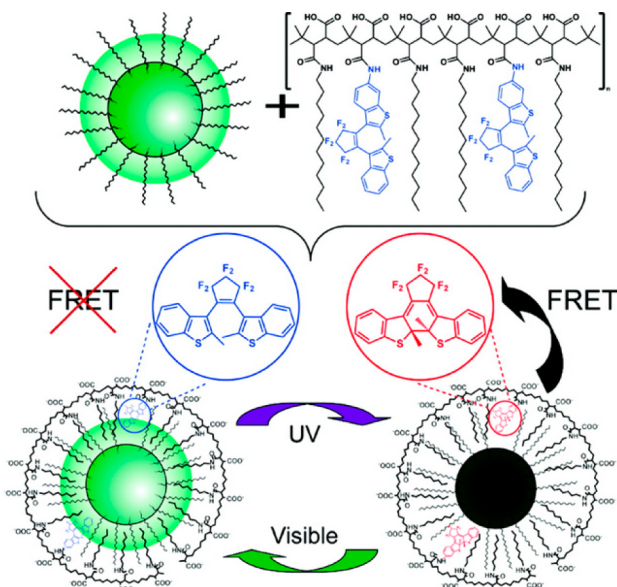


Figure 47. Schematic illustration of the photoswitchable QDs. QDs were coated with an amphiphilic photochromic polymer. Fluorescence of the QD was modulated by the photoconversion of diheteroarylethenes with UV or visible light. Reprinted with permission from ref 131. Copyright 2011 American Chemical Society.

Under UV irradiation, diheteroarylethenes converted to a closed state, and the emission of the QDs was quenched by FRET; the emission recovered when the particles were exposed to visible light, which switched the dithienylethenes to an open state and blocked FRET. These photochromic QDs retained the desirable properties of the original QDs and allowed the emission to be switched on and off by light. Later they used this architecture to create biocompatible photoswitchable QDs with a secondary dye acting as an internal standard for dual-color, ratiometric sensing and imaging.¹³²

In another example, QDs were used as a template for the preparation of an amphiphilic fluorescent photomodulatable polymer bearing covalently bound donor, Lucifer Yellow (LY), and acceptors, diheteroarylethenes.¹³³ In an aqueous medium, the polymer formed polymersomes of ~75 nm in diameter. The QD template reduced the diameter of the nanoparticle to 20 nm and created a dual-color fluorescent nanoparticle (emissive at 525 and 635 nm) with the QD serving as an internal standard while retaining the single excitation wavelength. The QD template increased the polymer density and efficiency of diheteroarylethene photoconversion. As a result, the LY emission monitored by both steady state and time-resolved fluorescence was modulated to a greater extent than polymersomes without QD template due to their different FRET efficiency to diheteroarylethenes.

Branda and co-workers reported a novel water-dispersible nanoassembly using upconverting nanoparticles wrapped in an amphiphilic polymer shell, in which photoresponsive dithienylethenes were trapped.¹³⁴ Both the upconverting nanoparticle and photoresponsive dithienylethenes resided within the “inner” shell, which created a local hydrophobic environment, ensuring that photochemistry was not affected when the particles were dispersed in water. Upon irradiation at 980 nm, these wrapped nanoparticles exhibited green (504–568 nm) and red emissions (627–684 nm). Both emissions overlapped with the absorption band of the ring-closed dithienylethenes

isomer. Irradiation with UV-vis light altered the structure of dithienylethenes and reversibly switched on/off the fluorescence due to modulated FRET processes.

3.3.2. pH-Responsive Imaging. pH represents an important physiological parameter that directly affects many processes. Consequently, pH triggers are extensively studied stimuli, biologically relevant in at least two contexts: (1) pathological (e.g., tumor) tissues and (2) acidic intracellular compartments (e.g., endocytic vesicles).

Gao and co-workers reported a series of tunable, pH-responsive micellar nanoparticles based on supramolecular self-assembly of ionizable block copolymers (Figure 48).¹³⁵ They

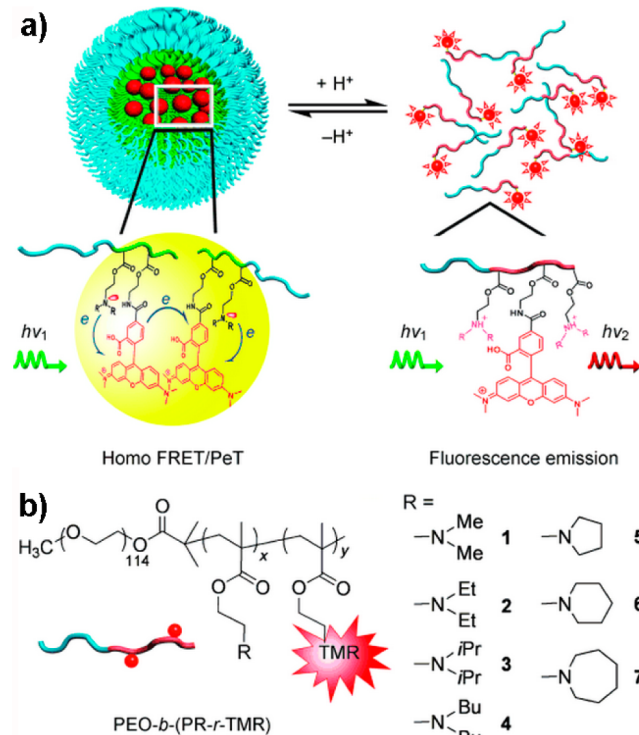


Figure 48. (a) Schematic design of pH-sensitive nanoparticles. (b) Structures of the PEO-*b*-(PR-*r*-TMR) copolymers in the dialkyl and cyclic series. Reprinted with permission from ref 135. Copyright 2010 Wiley-VCH Verlag GmbH & Co. KGaA, Weinheim.

synthesized two series of block copolymers (PEO-*b*-PR) by atom-transfer radical polymerization of dialkyl or cyclic tertiary amine moieties with poly(ethylene oxide) (PEO) segments. Tetramethylrhodamine (TMR), a pH-insensitive dye, was used as a model fluorophore. At pH > pK_a of the amine groups, PR segments self-assembled into the hydrophobic cores of micelles, thus leading to the aggregation of the fluorophores and quenching of fluorescence by homo-FRET and photoinduced electron transfer (PET) from the tertiary amines to TMR. At pH < pK_a of the amine groups, protonated and positively charged PR segments induced micelle disassembly and a dramatic increase in fluorescence emission. The nanoparticles incubated with human H2009 lung cancer cells were selectively activated in acidic compartments, including early endosomes (pH 5.9–6.2) and lysosomes (pH 5.0–5.5). Gao and co-workers extended this work to multicolored pH-tunable fluorescent nanoparticles using commonly available pH-insensitive dyes with emission from green to near IR and demonstrated complete switching of their fluorescence within

0.25 pH windows, which is much narrower than small molecular pH sensors.¹³⁶

Würthner and co-workers reported precise control of the assembly of a series of perylenebisimide with different ratios of hydrophobic and hydrophilic segments.¹³⁷ A mixture of wedge-shaped amphiphile **83** bearing a hydrophobic hexylester chain at one end and a hydrophilic triethylene glycol chain at the other end and dumbbell-shaped **84** formed bilayer vesicles (Figure 49), which were photopolymerized using the terminal

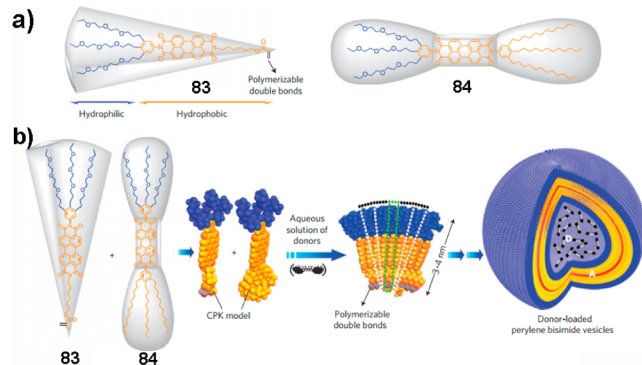


Figure 49. (a) Chemical structures of **83** and **84**. (b) Schematic illustration of the formation of donor (D)-loaded perylenebisimide vesicles in aqueous solution. Adapted with permission from ref 138. Copyright 2009 Nature Publishing Group.

double bonds in the hydrophobic side chains.¹³⁸ This photopolymerization preserved the original structure and size of the vesicles and improved their stability. When the vesicles were prepared in the presence of acid-sensitive bis-pyrene triamine (Figure 50), it became trapped in the aqueous inner compartment, turning the particles after photopolymerization into a fluorescent FRET-based pH sensor that was stable over the entire aqueous pH range. At low pH, electrostatic forces between the protonated amine groups of the donor (**85**) constrained bispyrene in the open conformation (Figure 50a). Upon excitation at 363 nm, the pyrene monomers emitted at 370–420 nm, which does not overlap with the absorption of perylene diimide. At high pH bispyrene adopts a closed conformation (**86**) to maximize $\pi-\pi$ interactions between the pyrene moieties. The green emission of this stacked conformation overlaps with the perylene diimide absorption, thus allowing energy transfer. It provided ultrasensitive pH information on their aqueous environment with fluorescence color changes covering the whole visible light range (Figure 50b). At pH 9.0 these water-soluble donor-loaded perylene diimide particles exhibited exceptional white fluorescence.

Given the complexity of microenvironments in certain bioapplications, it is highly desirable to combine multiple external stimuli-triggered systems to maximize the temporal spatial imaging resolution. Liu et al. constructed the first system capable of reversible three-state switching of multicolor fluorescence emission (green, yellow, orange, and red) by modulating two independent FRET processes with external stimuli (pH, temperature, and light) (Figure 51).¹³⁹ The system consisted of a donor **91** and two acceptors: pH-switchable rhodamine **87** and photoresponsive spiropyran fluorophore **89**, which were attached to thermoresponsive PS-PNIPAM diblock copolymer chains. The fluorescence emissions of rhodamine and spiropyran is switched on and off by changing pH and by light irradiation (UV-vis), respectively.

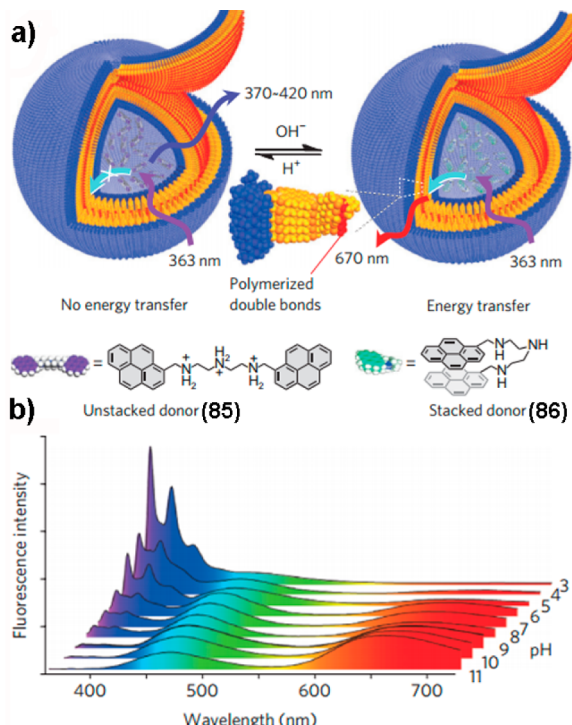


Figure 50. (a) Schematic illustration of the donor-loaded polymerized vesicles with pH-tunable energy transfer. (b) Fluorescence spectra of donor-loaded polymerized vesicles in aqueous solution at pH 3.0–11.0. Reprinted with permission from ref 138. Copyright 2009 Nature Publishing Group.

Moreover, the efficiency of FRET from **91** to ring-opened rhodamine **88** below pH 6 depended on temperature due to the thermally induced collapse of the micellar coronas, which affected the separation between FRET pairs of **91** and **88**.

3.4. Upconversion Luminescence Bioimaging

Upconversion luminescence (UCL) is a unique process whereby low-energy (long wavelength) photons are converted into higher energy (shorter wavelength) photons by a series of energy-transfer processes.¹⁴⁰ Two main upconversion processes are recognized: multiphoton upconversion and triplet-triplet annihilation-based upconversion (TTA-based upconversion). UCL under NIR excitation offers unique advantages for photoluminescent bioimaging applications, including little accompanying autofluorescence, large tissue penetration depth, and minimal photodamage of the samples.¹⁴¹ Bioimaging applications of multiphoton upconversion were reviewed recently.¹⁴² In this section, we will focus on TTA-based upconversion luminescence imaging.

In TTA-based upconversion energy is transferred from a sensitizer molecule to an emitter by triplet-triplet energy transfer (TTET), and then two triplet emitters come together to form one emitter in an excited singlet state and the other in the ground state by triplet-triplet annihilation (TTA).¹⁴³ The excited singlet state species emits a photon of higher energy than that of the exciting photon (Figure 52). As compared to multiphoton upconversion which requires excitation with high power density ($\sim\text{MW cm}^{-2}$), TTA-based upconversion can be achieved by excitation with incoherent light of low power density ($\sim\text{mW cm}^{-2}$). In addition, the excitation and emission wavelengths are tunable by selecting different donor/acceptor couples.

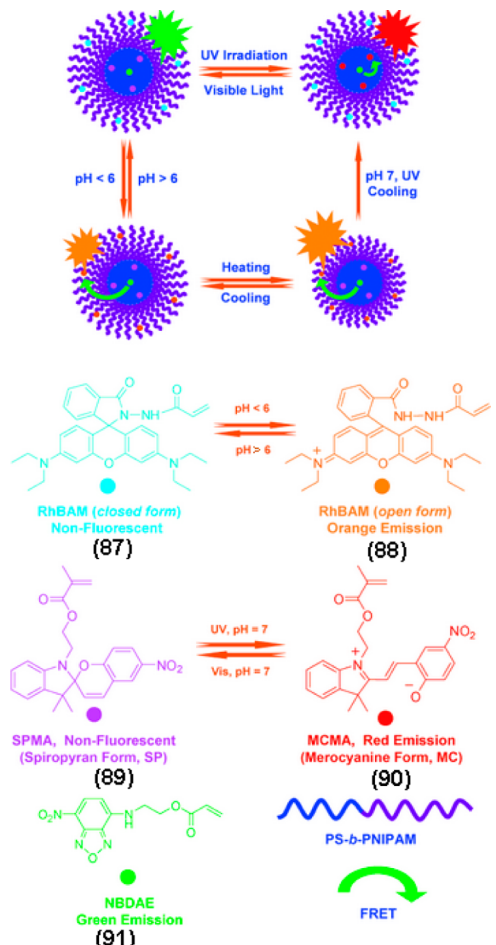


Figure 51. Schematic illustration of a three-state switchable multicolor fluorescent which allows its independent FRET processes to be modulated with different external stimuli. Adapted with permission from ref 139. Copyright 2010 Wiley-VCH Verlag GmbH & Co. KGaA, Weinheim.

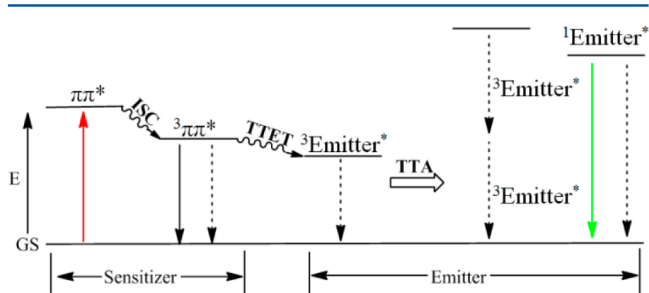


Figure 52. Energy level diagram illustrating the TTA-based upconversion process, wherein ISC is intersystem crossing.

Li et al. were first to fabricate water-soluble upconversion luminescent nanoparticles (TTA-UCNP) for bioimaging by physisorption of a sensitizer PdOEP and an emitter DPA onto silica nanoparticles (Figure 53) using a direct micelle-assisted method with surfactant F127.¹⁴⁴ The resulting particles contained a sensitizer-to-emitter molar ratio of 1:14. The particles irradiated at 532 nm to selectively excite PdOEP luminescence at 433 nm, which is the emission wavelength of DPA excited directly at 375 nm. These blue-emissive nanoparticles manifested an upconversion quantum yield of 4.5% and were successfully used to label living cells and for

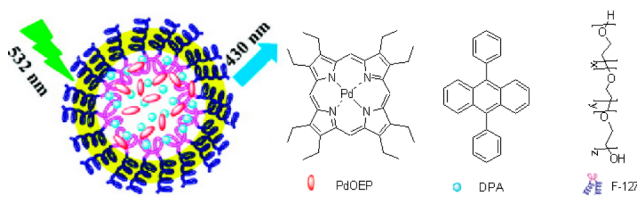


Figure 53. Schematic representation of upconversion luminescence of TTA-UCNP, and chemical structures of sensitizer PdOEP, emitter DPA, and surfactant F127. Reprinted with permission from ref 145. Copyright 2012 American Chemical Society.

lymph node imaging in a living mouse under a low power density excitation of 8.5 mW cm^{-2} .

The modest upconversion quantum yield in the above example was due to immobilization of the chromophores on silica nanoparticles, which suppressed diffusional encounters of triplet pairs needed for efficient triplet–triplet energy transfer and triplet–triplet annihilation. To address this issue, in 2013 the Li group developed a method in which sensitizer and emitter were encapsulated into an emulsion of nanosized oil-in-water droplets (Figure 54).¹⁴⁵ In their study, a bovine serum

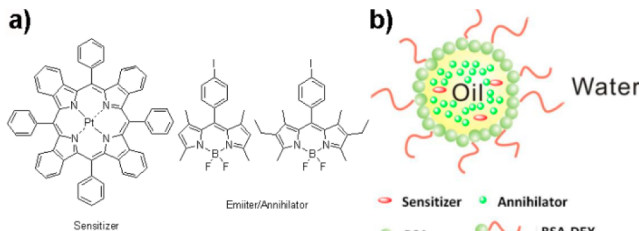


Figure 54. (a) Chemical structures of sensitizer PtTPBP and emitters BDP-G and BDP-Y. (b) Schematic representation of upconversion luminescence of TTA-based nanocapsules. Reprinted with permission from ref 145. Copyright 2013 American Chemical Society.

albumin (BSA)-dextran conjugate was dissolved in deionized water, and soybean oil containing a sensitizer (PtTPBP) and an emitter (BDP-G or BDP-Y) in a 1:100 molar ratio was added to it. A stable emulsion formed with BSA and dextran acting as a hydrophobic and hydrophilic part of a surfactant to stabilize the emulsion against coalescing and flocculating. The upconversion quantum yield reached 1.7% and 4.8% for BDP-G and BDP-Y emitters, respectively, in contrast to the <0.1% value for these BODIPY emitters in SiO_2 particles coated by a conventional method. These new TTA-based upconversion materials were successfully applied to lymph node imaging, giving excellent signal-to-noise ratios (>10) under excitation of power density as low as 12.5 mW cm^{-2} .

Bioimaging based on TTA upconversion luminescence is still in its infancy probably due to (1) the limited choice of sensitizer/emitter pairs for UCL that completely excludes NIR dyes and (2) low upconversion quantum yields, which produce fluorescence that is too faint for bioimaging. In future research, design of new sensitizer/emitter pairs, especially pairs capable of NIR excitation, may significantly increase the role of upconversion luminescence in bioimaging. Moreover, supramolecular assemblies of sensitizer/emitter pairs with high triplet energy-transfer efficiency remain highly desirable.

4. BIOSENSOR

4.1. Ratiometric Biosensing

For many fluorescent probes, the concentration of the analyte is derived from changes in the intensity of a single emission band of the sensor. This intensity, however, is often susceptible to interference from environmental factors that are not related to the concentration of the analyte, such as pH, temperature, and solvent polarity. Consequently, the use of single-wavelength sensors under complex biological conditions can be problematic. Ratiometric sensing relies on measurements of the ratio of intensities of two emission bands at different wavelengths, which can be made far less sensitive to interference than single-wavelength detection.¹⁴⁶

FRET-based ratiometric sensors have been widely employed both as small molecules and as nanoparticles. In the presence of target analytes, FRET can be modulated by varying the optical properties of the FRET pairs or their separation, leading to the ratiometric sensing.

Wolfbeis and co-workers reported a ratiometric fluorescent nanogel for pH measurements in the physiological range from 6 to 8.¹⁴⁷ The nanogels were prepared from biocompatible polyurethane loaded with the pH indicator bromothymol blue and two standard fluorophores, coumarin 6 and Nile Red. The pH value was derived from the ratio of emission intensities of coumarin 6 at 520 nm and Nile Red at 620 nm upon irradiation of the gel at 440 nm corresponding to coumarin 6 excitation. At pH below 6, bromothymol blue is yellow with an absorption maximum at around 435 nm, absorbing the green emission of coumarin 6, and Nile Red emission at 620 nm is observed due to the partial energy transfer from coumarin 6 to Nile Red. At pH above 8, bromothymol blue is blue with an absorption maximum at 628 nm, which absorbs most of the red fluorescence of Nile Red, leaving the green emission of coumarin 6 to be observed (Figure 55a). This illustrates how

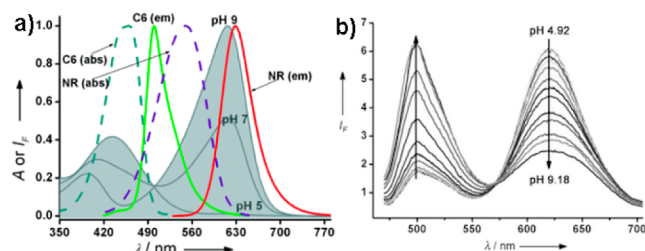


Figure 55. (a) pH-dependent absorption spectra of bromothymol blue (BTB) in aqueous solution at pH 5.0, 7.0, and 9.0 (gray curves), and absorption and emission spectra of coumarin 6 (C6) and Nile Red (NR) in ethanol. (b) Fluorescence spectra of nanogels at different pH values under excitation of 450 nm. Reprinted with permission from ref 147. Copyright 2010 Wiley-VCH Verlag GmbH & Co. KGaA, Weinheim.

energy transfer altered by changes in the absorption of bromothymol blue at different pH results in large changes in relative emission ratios (Figure 55b). This smart design is likely to find many uses in intracellular biosensing.

McNeill et al. developed a ratiometric oxygen sensor based on conjugated polymer nanoparticles.¹⁴⁸ The nanoparticles were prepared by assembly of conjugated polymers, poly-fluorene derivatives poly(9,9-dihexylfluorene) (PDHF) and poly(9,9-diethylfluorene) (PFO), with an oxygen-sensitive phosphorescent dye platinum(II) octaethylporphine (PtOEP).

Efficient energy transfer from conjugated polymers to PtOEP took place under irradiation, greatly enhancing phosphorescence emission. The small particle size, bright phosphorescence, and low cytotoxicity of the nanoparticles allowed ratiometric O₂ sensing in living cells by monitoring the ratio of the emission intensities of conjugated polymers and of PtOEP.

Rao and co-workers¹⁴⁹ reported dual-color nanoparticles for imaging of reactive oxygen and nitrogen species (RONs) in inflammatory microenvironments in living mice. The semiconducting polymer nanoparticles (SPN) were prepared by nanoprecipitation of **94** as NIR-emissive polymer and **92** and **93** as the matrix polymers, followed by attaching carboxy-terminated NIR dye **95** to the surface amino groups by carbodiimide-activated coupling (Figure 56a). Upon excitation

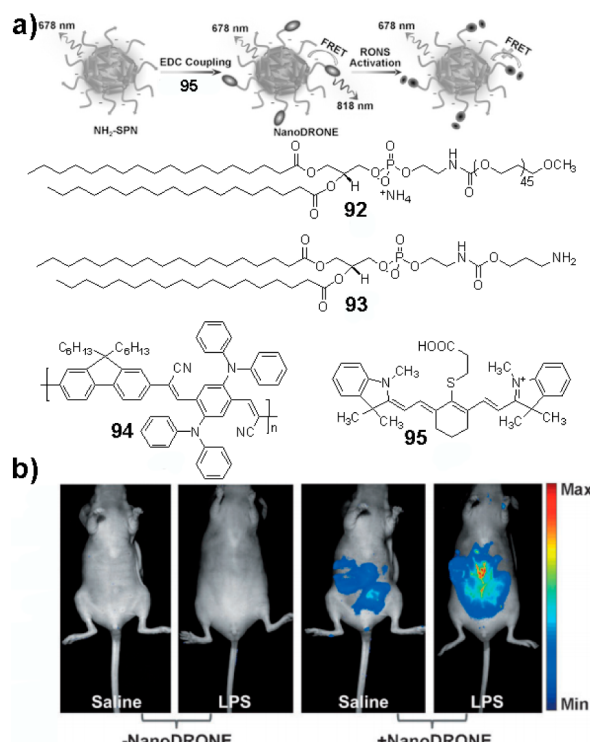


Figure 56. (a) Preparation of the dual-color nanoparticles and ratiometric sensing of RONs by FRET. (b) In vivo imaging of RONs with as-prepared nanoparticles (NanoDRONE) in a lipopolysaccharide (LPS)-induced acute peritonitis mouse model. Saline and LPS were administered by intraperitoneal (i.p.) injection, followed 4 h later by i.p. administration of the nanoparticles. Images were acquired before and 30 min after particle administration. Adapted with permission from ref 149. Copyright 2013 Wiley-VCH Verlag GmbH & Co. KGaA, Weinheim.

of **94**, the nanoparticles exhibited two emission peaks at 678 and 818 nm, the latter due to FRET from **94** to **95**. Upon gradual addition of RONs, the emission peak at 678 nm increased while that at 818 nm decreased simultaneously, due to oxidative degradation of **95** by RONs. The nanoparticles showed specific RON detection in living mice. The lipopolysaccharide (LPS) injection would elicit the elevated production of RONs. LPS-treated mice showed 2.7 times higher fluorescence than saline-treated mice (Figure 56b).

Wu et al. reported polymeric nanoparticles for FRET-based ratiometric chemosensing of Hg²⁺ in water.¹⁵⁰ The nanoparticles were prepared by miniemulsion polymerization of methyl methacrylate (MMA) and acrylic acid (AA). A

hydrophobic dye nitrobenzoxadiazolyl (NBD, FRET donor) was embedded into the hydrophobic core of nanoparticles. A spirolactam rhodamine derivative (**96**, as the acceptor) was covalently linked onto the particle surface. Hg^{2+} in an aqueous dispersion of the nanoparticles induced ring opening of rhodamine's spirolactam, thus enabling FRET (Figure 57). The large Stokes shift (>170 nm) minimized the contribution of excitation backscattering to fluorescence intensity, leading to the detection limit of 100 nM (20 ppb).

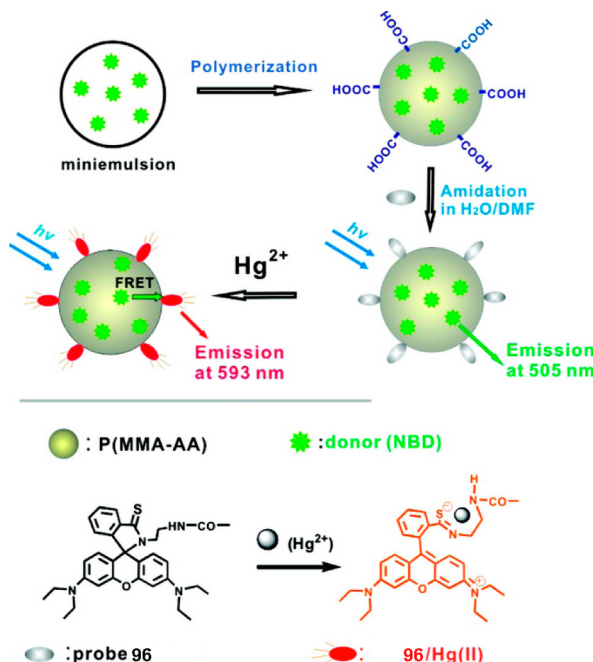


Figure 57. Preparation of the polymeric nanoparticle as a ratiometric fluorescent sensor for Hg^{2+} . Adapted with permission from ref 150. Copyright 2011 American Chemical Society.

The Chiu group reported a fluorescent nanoparticle for ratiometric sensing of temperature.¹⁵¹ Temperature-sensitive Rhodamine B (RhB) was conjugated to an amino-terminated amphiphilic polystyrene (PS) to form PS–RhB, which was assembled into Pdots with a semiconducting polymer by nanoprecipitation. The good overlap of the emission band of the semiconducting polymer around 540 nm with the absorption of RhB and the close proximity of RhB and the polymer matrix facilitated efficient energy transfer. The ratio of fluorescence intensities at 573 and 510 nm changed linearly with temperature at 10–70 °C. The Pdot–RhB was used to measure intracellular temperature in living HeLa cells.

4.2. Upconversion Luminescence Biosensing

Lanthanide-doped upconversion nanoparticles have attracted great attention for visualizing living cells and animals.^{141,152} Such particles, however, typically lack recognition units. In order to achieve sensing function, a common strategy is to combine the upconversion nanoparticles with other chromophores that have recognition sites. At the same time, the chromophores can also serve as an energy acceptor for luminescence resonance energy transfer (LRET). In general, analytes capable of reaction with the acceptor would quench the emission of the upconversion nanoparticles, leading to ratiometric sensing.

Li and co-workers reported an upconversion nanoparticle coated with an iridium(III) complex as a ratiometric luminescence probe for highly selective detection of cyanide.¹⁵³ The upconverting nanocrystals were coated with hydrophobic oleic acid (OA) and a CN⁻ responsive chromophoric complex **97** (Figure 58). Upon addition of CN⁻, the green upconversion

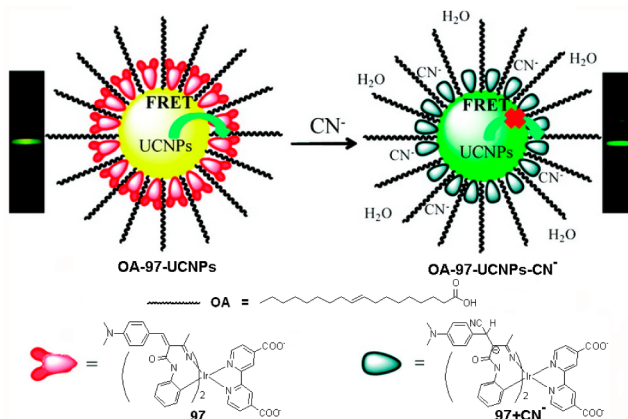


Figure 58. Schematic illustration of the proposed mechanism of recognition of CN⁻ by iridium(III) complex-coated upconversion nanoparticles based on FRET. Adapted with permission from ref 153. Copyright 2011 American Chemical Society.

luminescence (UCL) was enhanced, which was attributed to the inhibition of energy transfer from the nanoparticle to **97**. By taking upconversion luminescence at 800 nm as the internal standard, the concentration of CN⁻ was derived from the ratio of UCL emissions at 540 to 800 nm (I_{540}/I_{800}) with high sensitivity (detection limit of 0.18 μM). The upconversion nanoparticles were used as a ratiometric UCL probe for monitoring intracellular CN⁻ in living HeLa cells.

Li and co-workers reported the fabrication of dye-modified upconversion nanoparticles for luminescence bioimaging of methylmercury in vivo.¹⁵⁴ The hydrophobic dye **98** and amphiphilic polymer P-PEG were physisorbed onto the surface of hydrophobic upconversion nanoparticles by hydrophobic interactions to obtain water-dispersible three-layer nanoparticles. The addition of MeHg⁺ shifted the absorption from 670 nm of **98** to 845 nm of dye **99**. The two absorption bands at 845 and 670 nm matched the upconversion luminescence (UCL) emissions of ${}^3\text{H}_4 \rightarrow {}^3\text{H}_6$ transition ($\lambda_{\text{UCL}} = 800 \text{ nm}$) of Tm³⁺ and ${}^4\text{F}_{9/2} \rightarrow {}^4\text{I}_{15/2}$ transition ($\lambda_{\text{UCL}} = 660 \text{ nm}$) of Er³⁺, respectively. Under excitation at 980 nm, in the presence of MeHg⁺, the UCL emission intensities at 660 and 800 nm increased and decreased, respectively, due to the LRET from the UCNPs to **99** (Figure 59). It was noted that no significant change in the UCL intensity at 534–560 nm was observed, which was used as the reference. The detection limits using $\text{UCL}_{660 \text{ nm}}/\text{UCL}_{540 \text{ nm}}$, $\text{UCL}_{800 \text{ nm}}/\text{UCL}_{540 \text{ nm}}$, and $\text{UCL}_{660 \text{ nm}}/\text{UCL}_{800 \text{ nm}}$ ratios of intensities were 0.58, 0.25, and 0.18 ppb, respectively. These nanoassemblies were used to detect MeHg⁺ in living cells (Figure 60) and in small animals.

Chu and co-workers reported a phospholipid-modified nanosystem for upconversion fluorescence bioimaging of phospholipase D (PLD) activity.¹⁵⁵ The water-dispersible nanoprobe was synthesized by self-assembly of a phospholipid monolayer composed of a PEG-modified phospholipid and a Rhodamine B (RhB)-labeled phospholipid onto the surface of hydrophobic upconversion nanoparticles. Upon excitation at

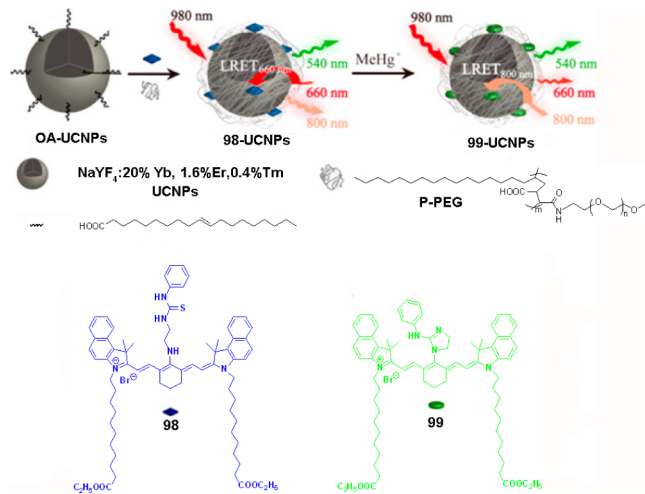


Figure 59. Synthesis of dye-modified upconversion nanoparticles, and mechanism of sensing of MeHg^+ by monitoring the change in upconversion luminescence emission via LRET process. Adapted with permission from ref 154. Copyright 2013 American Chemical Society.

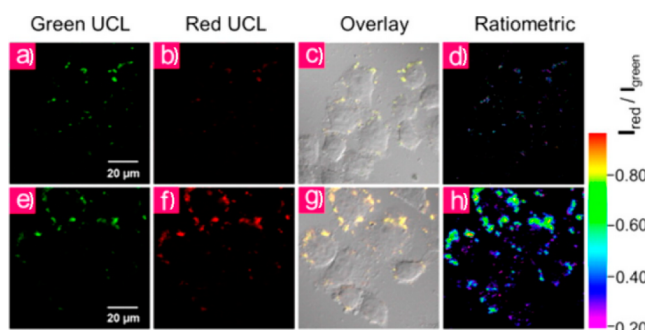


Figure 60. (a–d) UCL images of living HeLa cells incubated with the upconversion nanoparticles (0.05 mg mL^{-1}) for 2 h at 37°C : (a) green channel image at 500 – 560 nm ; (b) red channel image at 600 – 700 nm ; (c) overlay of bright-field, green, and red UCL images; (d) ratiometric UCL images with ratio of red to green channels. (e–h) UCL images of living HeLa cells incubated with $50 \mu\text{M}$ MeHg^+ -pretreated upconversion nanoparticles (0.05 mg mL^{-1}) for 2 h at 37°C : (e) emission was collected by green channel at 500 – 560 nm and (f) red channel at 600 – 700 nm ; (g) overlay of bright-field, green, and red UCL imageries; (h) ratiometric UCL images with ratio of red to green channels. Reprinted with permission from ref 154. Copyright 2013 American Chemical Society.

980 nm, the UCL emission at 540 nm was quenched by RhB by FRET and only the UCL emission at 655 nm was observed. Hydrolysis of the phosphodiester bond by the phospholipase released RhB from the UCNPs surface, thus eliminating FRET and increasing the emission at 540 nm. The loss of RhB did not change UCL emission at 655 nm, which was used as the internal standard for the ratiometric detection of the PLD activity in living cells.

Zhu and co-workers reported supramolecular upconversion nanoparticles for the detection of Fe^{3+} (Figure 61) based on dye **100** sequestered in γ -cyclodextrin (CD).¹⁵⁶ CD with a hydrophilic outer surface and a lipophilic cavity was conjugated to the surface of the oleic acid (OA)-bearing upconversion nanoparticles as a host–guest complex. Due to its hydrophobicity and size, CD served as a pocket to protect **100** from photobleaching and photodegradation. Under excitation at 980 nm, two emission bands of the upconversion nanoparticles

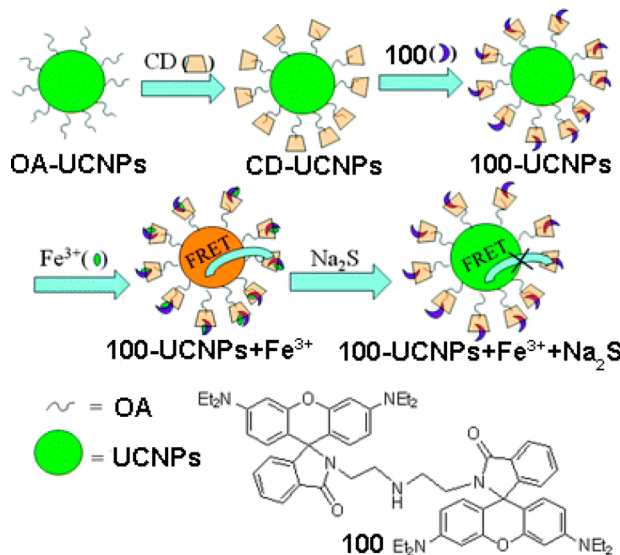


Figure 61. Synthesis of supramolecular upconversion nanoparticles and detection mechanism of Fe^{3+} . Adapted with permission from ref 156. Copyright 2013 The Royal Society of Chemistry.

centered at 542 and 646 nm were observed. Because the emission at 542 nm overlaps with the absorption of $100-\text{Fe}^{3+}$ complex, addition of Fe^{3+} to these nanoparticle/CD assemblies suppressed their green emission by partial FRET-mediated quenching. The red emission was unaffected and served as a reference for ratiometric detection of Fe^{3+} . Moreover, the feasibility of the nanoparticle for clinical applications was investigated using real serum samples.

4.3. Biosensing by Signal Amplification

As discussed in section 2, antennae chromophores absorb light and transfer the harvested energy to the reaction center or another acceptor, which often requires energy migration among chromophores. Achieving such energy migration in self-assembled nanostructures is crucial for designing biosensors capable of signal amplification. In conventional fluorescent sensors, the recognition event changes the fluorescence properties of a single receptor molecule. In the assemblies with multiple fluorophores, complexation/reaction of the analytes to a single binding site can change the photophysical properties not only of the dye immediately connected to the binding site but also of several neighboring dyes by changing energy-transfer/migration processes. Such signal amplification increases the sensitivity of the receptor.

In 1995, the Swager group reported a model study of amplified fluorescent sensing based on a conjugated polymer.¹⁵⁷ A conjugated polymer is a highly efficient medium for energy migration, where excitons move easily along the π -conjugated backbone and collect at energy sinks. When a quencher is bound to one of the repeat units in conjugated polymers, the quencher molecule is sufficient to trap almost all of the excited energy along whole backbone, leading to amplified emission quenching.⁹⁶ In 1999, the Whitten group reported a greater than million-fold amplification of fluorescence quenching of anionic conjugated polymers. Conjugated polymer-based amplifying sensing has been studied extensively for the detection of diverse analytes, including metal ions, DNA/RNA, proteins, and bacteria. Sensors based on conjugated polymers with amplifying fluorescent signal were reviewed by Swager et al. in 2000¹⁵⁸ and 2007.^{15b} Conjugated

polymers also serve as excellent energy donors in FRET-based sensing. They have high extinction coefficients stemming from their delocalized backbone, and most emit light efficiently. Excitons generated by photoexcitation can migrate throughout the entire backbone, allowing for efficient FRET and amplified fluorescence with the resultant enhancement in the signal-to-noise ratios. Numerous examples of using fluorescent conjugated polymers as optical platforms for sensitive detection of targets ranging from small chemical species to biomacromolecules have been reported as reviewed recently.¹⁵⁹

The concept of signal amplification in the field of biosensors was adapted to other systems such as dendrimers¹⁶⁰ and polymeric nanoparticles.¹⁶¹ Among various strategies, dye-doped silica nanoparticles are a very successful material for the amplification of the fluorescence signal. Tonellato and co-workers constructed signal-amplified silica nanoparticles with a dansyl unit as a fluorophore and a polyamine chain as an ion receptor.¹⁶² The separate dansyl units on the surface of nanoparticles are close enough to allow energy- and electron-transfer processes. The presence of copper, cobalt, and nickel ions even at nanomolar concentrations induced a strong quenching of the fluorescence. Each ion quenched up to 13 dansyl units, leading to strong signal amplification. This approach provides new perspectives for the design of fluorescent sensors or photonic devices at the nanometric scale.

Montalti and co-workers reported the first example of signal turn-on amplification based on silica nanoparticles.¹⁶³ They grafted a TSQ derivative (a well-known probe for Zn^{2+}) on the surface of silica nanoparticles. The efficient heteroenergy transfer between the uncomplexed units (acting as donors) and the complexed units (acting as acceptors) takes place (Figure 62), leading to a 50% off/on amplified response.

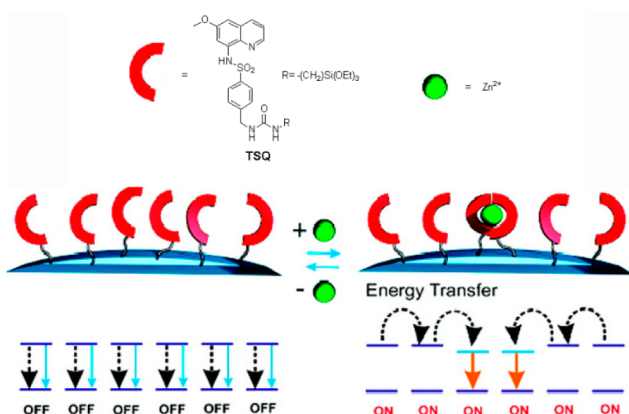


Figure 62. Schematic representation of excited state deactivation processes of TSQ on the surface of silica nanoparticles. At low zinc concentration, TSQ– Zn^{2+} complexes are formed and resulted in the turn-on fluorescence. Reprinted with permission from ref 163. Copyright 2008 American Chemical Society.

Larpent and co-workers reported dual-fluorescent polystyrene nanoparticles with cyclam attached to the surface and two fluorophores, **101** (donor) and **102** (acceptor), embedded within the core (Figure 63).¹⁶⁴ Cascade FRET processes took place from **101** to **102**, followed from the encapsulated dyes to copper complexes as quenchers. The dual-fluorescent nanoparticles possess tunable fluorescence that depends on the doping ratio of the donor to acceptor. With the increasing ratios of donor/acceptor, the fluorescence signal of the acceptor

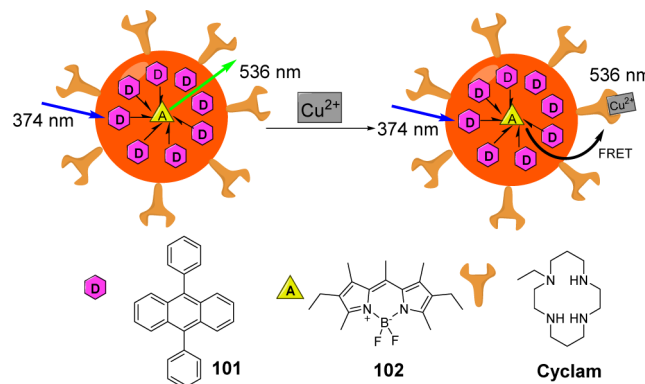


Figure 63. Schematic illustration of the cascade FRET-mediated sensor for Cu^{2+} ions.

was enhanced with a maximum of 9-fold amplification. The fluorescent nanoparticles were used for Cu^{2+} detection over a wide range of concentrations from 20 nM to 8.5 μ M.

Prodi and co-workers reported the synthesis of dye-doped core/shell silica nanoparticles containing a coumarin dye within the silica core and a BODIPY sensor **103** for Cu^+ in the outer shell (Figure 64).¹⁶⁵ The dyes were close enough to the

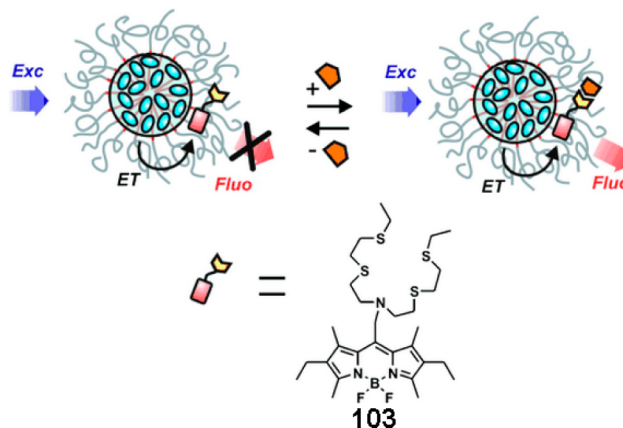


Figure 64. Schematic representation of the proposed sensing mechanism for Cu^+ . Adapted with permission from ref 165. Copyright 2011 Wiley-VCH Verlag GmbH & Co. KGaA, Weinheim.

nanoparticle core to enable energy transfer among the coumarins and to **103**. The efficiency of the energy transfer was modulated by Cu^+ complexation, leading to a ratiometric response and amplification of the fluorescence. A further advantage of this system is the great separation between the excitation and the emission wavelengths that ensures low noise. The strategy was also exploited for sensing Hg^{2+} .¹⁶⁶

5. PHOTODYNAMIC THERAPY

Photodynamic therapy (PDT), a method for destroying unwanted cells and tissue in the treatment of cancer and other diseases, has attracted considerable attention in recent years.¹⁶⁷ It is a noninvasive procedure that relies on the combination of narrow-bandwidth irradiation, photosensitizer (PS) located in the tumor tissues, and oxygen molecules surrounding PS. PDT is initiated when the PS absorbs a photon and generates either free radicals or other cytotoxic reactive oxygen species (ROS) by 1-electron reduction of O_2 or singlet O_2 by triplet–triplet energy transfer. Singlet O_2 is commonly

accepted as the main substance responsible for irreversible destruction of diseased cells and tissues. As a result, efficiency of the PS-mediated generation of singlet oxygen is the primary determinant of the PDT efficiency.

5.1. Photodynamic Therapy Based on Single-Photon Excitation

Porphyrins are the most commonly used PSs for PDT due to their effective singlet-to-triplet intersystem crossing and good biocompatibility. Wang and co-workers utilized a conjugated polymer as light-harvesting antenna to enhance the energy utilization of photosensitzers.¹⁶⁸ They synthesized a water-soluble anionic conjugated polymer (**104**) and cationic porphyrin (**105**) (Figure 65). The electrostatic interaction

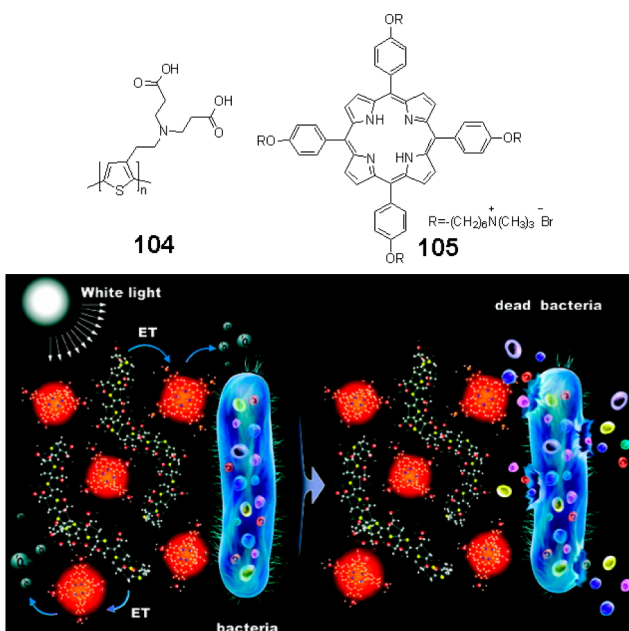


Figure 65. Chemical structures of conjugated polymer **104** and porphyrin **105**, and schematic representation of antibacterial mechanism of **104/105** energy-transfer complex. Reprinted with permission from ref 168. Copyright 2009 American Chemical Society.

drove the formation of a **104/105** complex in which singlet–singlet energy transfer by the Dexter mechanism occurred with an efficiency of up to 96% (Figure 66a). The ${}^1\text{O}_2$ generation capacity of **104/105** complex was quantified by the decrease of the absorption of 9,10-anthracedipropionic acid (ADPA),

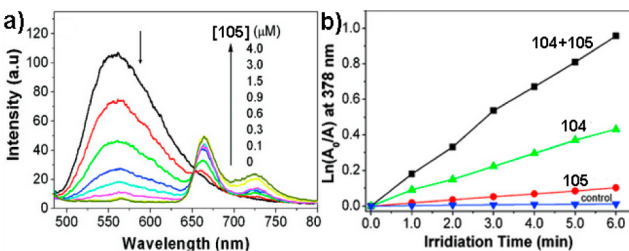


Figure 66. (a) Fluorescence emission spectra of **104** in buffer solution with successive addition of **105**. (b) Change in absorbance at 378 nm vs irradiation time with **104**, **105**, and **104/105** complex ($[104]/[105] = 3.0$) in the presence of ADPA and with **104/105** in the absence of ADPA (control) in a PBS buffer solution. Adapted with permission from ref 168. Copyright 2009 American Chemical Society.

which is converted by ${}^1\text{O}_2$ to endoperoxide. A more noticeable absorption decrease and faster bleaching rate constants of ADPA in the presence of **104/105** complex than of **104** or **105** alone indicated that energy transfer from **104** to **105** enhanced the generation of ${}^1\text{O}_2$ (Figure 66b). As a result, in comparison to porphyrin itself, the **104/105** complex could be irradiated for a shorter time to achieve the same ~70% reduction of bacterial viability.

In another example of using light-harvesting strategy, the same group attached porphyrin derivative covalently to a polythiophene backbone at ~1% molar fraction (Figure 67).¹⁶⁹

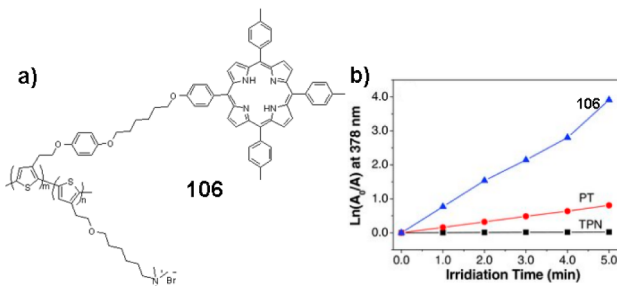


Figure 67. (a) Chemical structure of **106**. (b) Decrease of ADPA absorption at 378 nm vs irradiation time in the presence of cationic porphyrin derivative (TPN), polythiophene (PT), and polymer **106**. Adapted with permission from ref 169. Copyright 2011 Wiley-VCH Verlag GmbH & Co. KGaA, Weinheim.

The resulting polymer **106** assembled to nanoparticles in aqueous solution. These three-dimensional architectures with **106** manifested efficient FRET, resulting in higher ${}^1\text{O}_2$ generation efficiency than with either porphyrin or polythiophene alone. In addition to effective photocytotoxicity of **106** toward cancer cells, emission from polythiophene due to incomplete energy transfer from polythiophene to porphyrin derivative was used for fluorescence imaging, which was exploited to distinguish between living and dead cells, thus offering a new dimension to the function of the PSs in PDT treatment.

Porphyrins with their extended π systems tend to aggregate in aqueous media, which generally cause self-quenching of the excited state and deceases PDT efficiency. One strategy is to modify the porphyrins with four naphthalene–methylpyridinium moieties. Thus, CB[7] as the bulky substituents were noncovalently attached to the porphyrins by strong host–guest interactions between CB[7] and naphthalene–methylpyridinium subgroups. The hydrophilic exterior and large molecular volume of CB[7] suppressed the π stacking caused self-quenching of porphyrins and improved PDT efficiency.¹⁷⁰ In another strategy, Zhang et al. prepared porphyrin-doped perylene nanoparticles (NPs) by the nanoprecipitation method driven by hydrophobic force.¹⁷¹ The perylene NPs not only dispersed and stabilized porphyrin **107** in aqueous environment but also acted as a FRET donor (Figure 68) for the acceptor **107**. The antenna effect in the **107**/perylene energy-transfer system led to a dramatic fluorescence enhancement of **107** compared to **107**-doped polystyrene NPs that lacked an energy donor. Porphyrin **107** also served as photosensitizer for ${}^1\text{O}_2$ generation in PDT. Under identical conditions, **107**-doped perylene NPs caused significantly faster photobleaching of ADPA than **107** nanoparticles without perylene donors. That result confirmed the improvement of ${}^1\text{O}_2$ generation by the

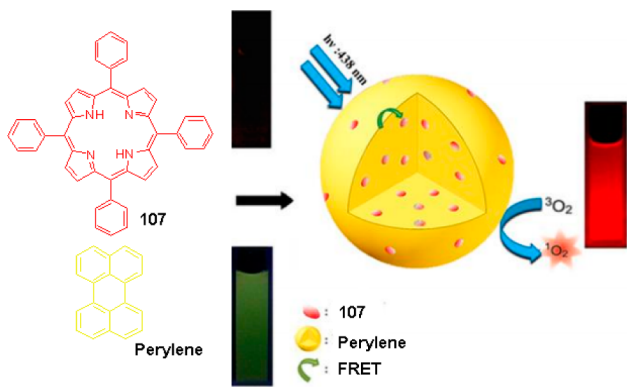


Figure 68. Schematic representation of the photodynamic therapy mechanism using of photosensitizer-doped perylene nanoparticles with FRET and antenna effect. Adapted with permission from ref 171. Copyright 2013 Royal Society of Chemistry.

107/perylene energy-transfer system. In vitro PDT tests showed HeLa cell death with accumulation of target NPs in the cytoplasm upon irradiation. This new FRET–PDT binary system decreased the self-quenching of PSs by utilizing photoactive matrices without complex synthesis.

The Chang group described a self-assembly scaffold for integrating energy donors and PS for efficient FRET and $^1\text{O}_2$ generation by using the tetraphenylporphyrin **108** as the hydrophobic core conjugated with a different number ($n = 1$ – 3) of hydrophilic chromophores **109** to obtain **110**, **111**, and **112** (Figure 69).¹⁷² Above the critical micelle concentration,

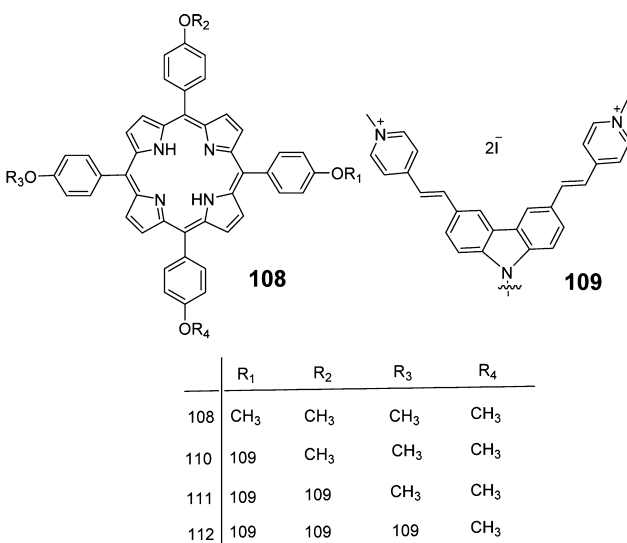


Figure 69. Chemical structures of binary conjugates **110**–**112** composed of **109** as energy donor and porphyrin **108** as energy acceptor. Reprinted with permission from ref 172. Copyright 2011 Elsevier.

the amphiphilic binary conjugates **110**–**112** self-assembled into micelle-like fluorescence organic nanoparticles. The formation of such micelle decreased thermal relaxation of the excited state of **109**, increasing the efficiency of energy transfer to PS **108**. The generation of $^1\text{O}_2$ was detected by oxidation of 1,3-diphenylisobenzofuran (DPBF) (Figure 70). The oxidation rates of DPBF were similar upon direct irradiation of tetraphenylporphyrin in micelles of **110**, **111**, and **112** under identical condition, since the concentration of tetraphenylpor-

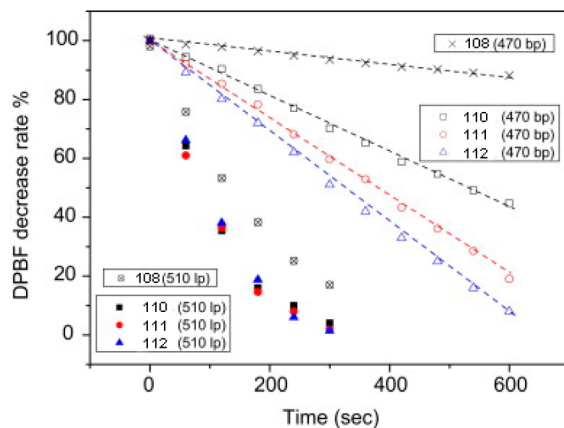


Figure 70. Oxidation rates of DPBF by $^1\text{O}_2$ generated by free PS or by binary conjugates after irradiation with a xenon lamp (output optical power densities were $50 \mu\text{W cm}^{-2}$ through 470 nm band pass and 33 mW cm^{-2} through 510 nm long pass). Adapted with permission from ref 172. Copyright 2011 Elsevier.

phyrin is the same in the three micelle systems. However, under excitation of energy donor, the oxidation of DPBF becomes more apparent in the micelles of binary conjugates containing more donor substituents, indicating the important role of FRET for $^1\text{O}_2$ generation. In addition, all binary conjugates oxidized DPBF faster than the free tetraphenylporphyrin under identical conditions, probably because the nanoparticles prevented aggregation of hydrophobic porphyrins. In subsequent work by Chang et al., PDT behavior using two-photon absorption of **109** under a 900 nm light source¹⁷³ was comparable to the above nanoparticles under one-photon excitation of energy donor.

5.2. Photodynamic Therapy Based on Multiphoton Excitation

The main absorption bands of porphyrin derivatives are usually in the UV and visible regions of the spectrum, wavelengths that are also strongly absorbed and scattered by the human tissue. To circumvent this problem, studies on electronic excitation of PSs by multiphoton absorption came up because it allows the use of near-IR radiation, to which tissues are transparent and hence have deeper penetration than UV-vis light. Two-photon absorbing (TPA) chromophores and lanthanide-doped upconversion nanoparticles (UCNP) have attracted increasing interest in PDT.

5.2.1. Photodynamic Therapy Based on Two-Photon Excitation.

Photosensitizers can either be designed specifically to have large TPA cross sections or be combined with nonphotosensitizing chromophores with large TPA cross-section which then transfer energy to the PS. The latter strategy is often more flexible by permitting various donor chromophores to be combined with existing photosensitizers, such as porphyrins, without interfering with the photophysical properties of these PSs. For example, in 2004 Prasad and co-workers demonstrated the generation of singlet oxygen by two-photon excitation of donors followed by FRET to the PS.¹⁷⁴ They grafted eight two-photon chromophores **113** as donors to a porphyrin **114** to obtain dendrimer **115** (Figure 71). The donors transferred excited-state energy to the porphyrin with 97% efficiency. When **115** and porphyrin **114** were excited at 780 nm at identical condition, the emission of **115** was 17 times stronger than that of **114**, indicating the utility of TPA chromophores for generating electronically excited PS. The

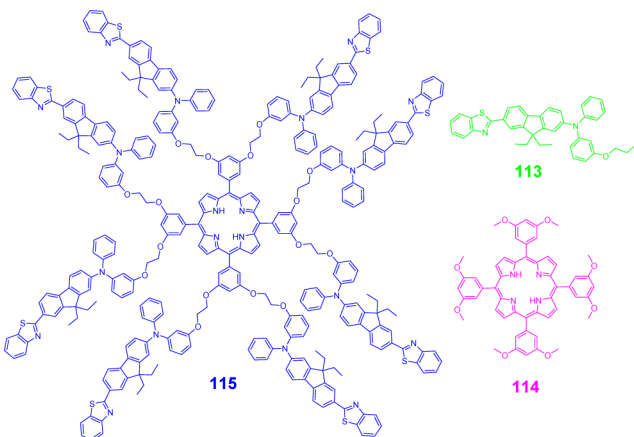


Figure 71. Chemical structures of chromophore **113**, porphyrin **114**, and dendrimer **115**.

generation of ${}^1\text{O}_2$ was also confirmed by the characteristic luminescence of ${}^1\text{O}_2$ at 1270 nm.

Prasad et al. prepared silica nanoparticles encapsulating PSs and fluorescent TPA dyes (Figure 72).¹⁷⁵ In this work 9,10-

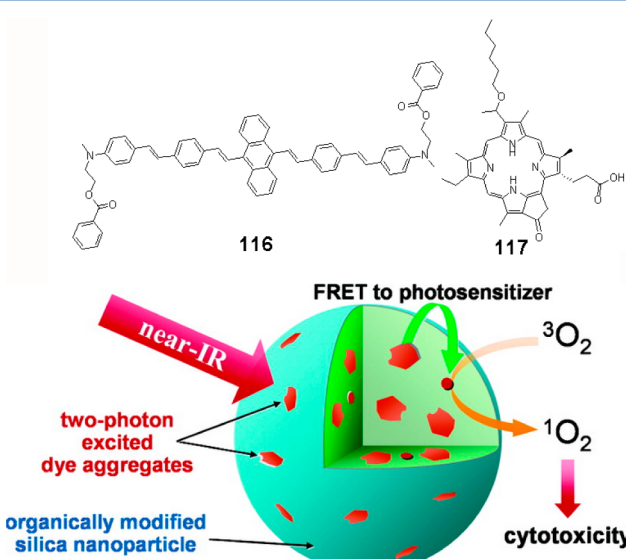


Figure 72. Schematic representation of silica nanoparticles with encapsulated 9,10-bis [4'-(4"-aminostyryl) styryl]anthracene (**116**) and 2-devinyl-2-(1-hexyloxyethyl)pyropheophorbide (**117**) for ${}^1\text{O}_2$ generation. Reprinted with permission from ref 175. Copyright 2007 American Chemical Society.

bis[4'-(4"-aminostyryl) styryl]anthracene (**116**) was used as a TPA energy donor. The photosensitizing energy acceptor was a porphyrinoid macrocycle **117**, which is energy matched with **116** for FRET. The one-photon excited fluorescence spectra of water-dispersible nanoparticles containing **116** (20 wt %) and **117** (1.1 wt %) showed 5-fold amplified **117** emission compared with nanoparticles encapsulating **117** only. This result verified the energy-harvesting capacity of **116** in silica nanoparticles. Pronounced energy harvesting with \sim 30-fold amplification of **117** emission in nanoparticles was observed under two-photon excitation (850 nm) due to the large difference in the two-photon absorptivities between **117** and **116** at the excitation wavelength. An emission peak at 1270 nm attributing to ${}^1\text{O}_2$ luminescence and photobleaching of ADPA

proved that silica matrix was permeable to oxygen, and hence, the particles were useful for PDT. The combination of biocompatibility and enhanced ${}^1\text{O}_2$ generation ability of the nanoparticle resulted in its effective photocytotoxicity to HeLa cells.

Jen's group employed amphiphilic TPA–chromophore-containing block copolymer **118** to form micelles for encapsulation of hydrophobic porphyrin photosensitizer **119** (Figure 73).¹⁷⁶ Under irradiation at 800 nm, the FRET efficiency of micelles with TPA chromophores reached 96% and bleaching of ADPA was 2.6 times faster than **120** formed micelles.

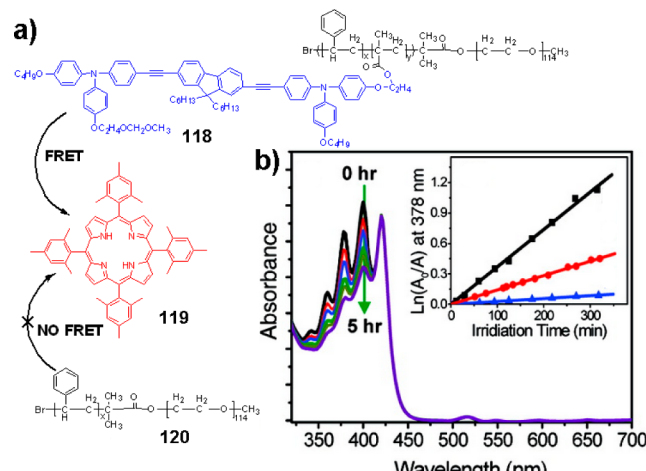


Figure 73. (a) Chemical structures of TPA-chromophore-containing block copolymer **118**, porphyrin photosensitizer **119**, and polymer **120**. (b) Photobleaching process of ADPA in **119/118** system ($\lambda_{\text{ex}} = 800 \text{ nm}$); (inset) bleaching of ADPA vs irradiation time in **119/118** (black), **119/120** (red), and **118** (blue). Adapted with permission from ref 176. Copyright 2007 American Chemical Society.

Photosensitizer-doped conjugated polymer nanoparticles (CPNs) have also been developed as PDT agents due to their large one-photon and two-photon excitation cross sections as well as efficient energy transfer between the polymer and the photosensitizer. Xu and co-workers fabricated **107**-doped **121** CPNs for enhanced two-photon singlet oxygen generation (Figure 74)¹⁷⁷ and studied them under irradiation by laser pulses at 800 nm. The photo-oxidation rate constants of ADPA with **107**-doped **121** CPNs was 15.9-fold faster than that with undoped **121** nanoparticles and 6.5-fold faster than that with **107** aggregates in water.

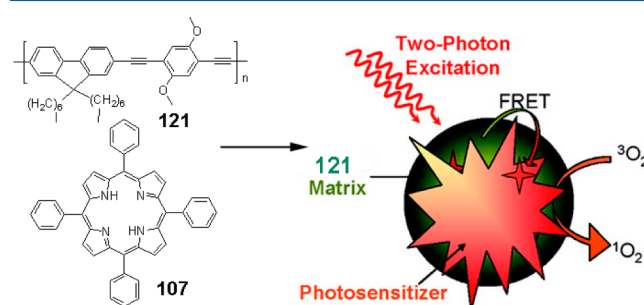


Figure 74. Enhanced two-photon singlet oxygen generation by porphyrin-doped CPNs. Adapted with permission from ref 177. Copyright 2011 American Chemical Society.

The same group also reported an electrostatic assembly of a cationic polyelectrolyte **122** with negatively charged porphyrin **123** to achieve efficient FRET from both one- and two-photon excited polymers to enhance emission of PSs (Figure 75).¹⁷⁸ The FRET from one- or two-photon excited **122** to **123** improved the **123** emission 9-fold and 30-fold, respectively. These results hold promise for developing effective PDT systems.

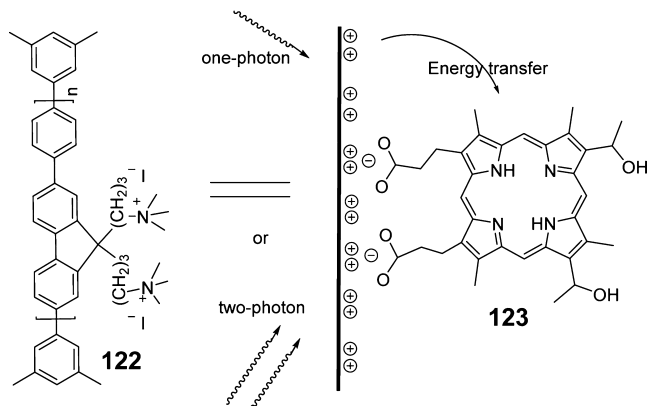


Figure 75. Chemical structures of **122** and **123**, and schematic representation of the **122/123** assembly. Adapted with permission from ref 178. Copyright 2009 Wiley-VCH Verlag GmbH & Co. KGaA, Weinheim.

McNeill et al. prepared CPNs by trapping hydrophobic *meso*-tetraphenyl porphyrin **107** as the photosensitizer during the collapse of polymer chains of **124**, **125**, or **126** for one- and two-photon excitation (Figure 76)¹⁷⁹ in water. Under one-

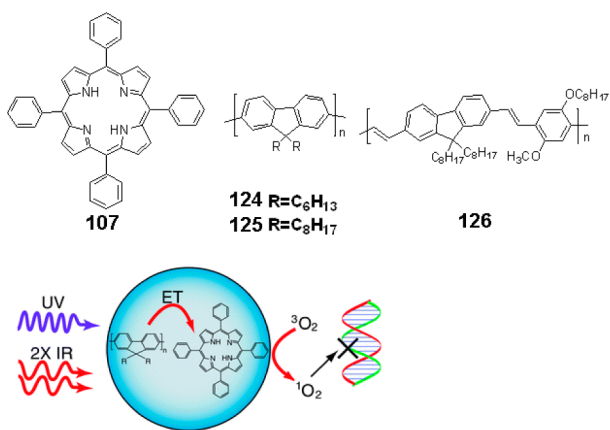


Figure 76. Chemical structures of porphyrin **107** and conjugated polymers **124**–**126**. Photosensitizer-doped conjugated polymer nanoparticles were constructed for $^1\text{O}_2$ generation. Reprinted with permission from ref 179. Copyright 2011 Royal Society of Chemistry.

photon excitation of polymers, the energy-transfer efficiency was estimated to be 95% for all three host polymers. The $^1\text{O}_2$ quantum yield of **107**-doped **124** CPNs was 50%, compared to 10% for undoped **124** nanoparticles, indicating that the efficient energy transfer and high yield of triplet porphyrin **107** improved $^1\text{O}_2$ generation. The gel electrophoresis measurement demonstrated that under irradiation most DNA was damaged by the reactive oxygen species generated by **107**-doped **124** nanoparticles. In their study, the two-photon excitation cross-

section of **107**-doped **126** nanoparticles at 800 nm for the generation of $^1\text{O}_2$ was estimated to be $\sim 10^6$ GM, which is both extraordinarily large compared to that of porphyrins (1–50 GM) and larger than the suggested threshold for clinical viability of PDT based on multiphoton excitation.

5.2.2. Photodynamic Therapy Based on Upconversion Nanoparticles.

Upconversion nanoparticles (UCNPs) are lanthanide-doped nanocrystals that emit visible light upon multiphoton excitation by NIR light.^{142a} In addition to chromophores with large two-photon absorption cross sections, UCNPs have become a promising energy donor in photodynamic therapy due to their high photostability. Zhang et al. were first to demonstrate the application of UCNPs for PDT.¹⁸⁰ Their UCNPs were coated with a porous, thin layer of silica which trapped a certain amount of photosensitizers (Figure 77). When the UCNPs were irradiated by a near-infrared source,

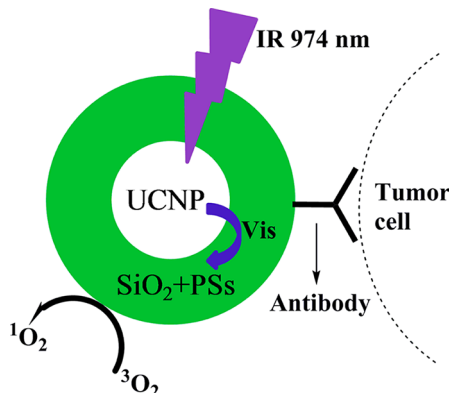


Figure 77. Schematic representation of the design of a versatile photosensitizer based on UCNPs. Adapted with permission from ref 180. Copyright 2007 American Chemical Society.

the resulting upconverted emission was absorbed by photosensitizers. The excited photosensitizers transferred energy to O_2 by triplet–triplet energy transfer to generate $^1\text{O}_2$. In 2010, Liu's group reviewed progress in the applications of UCNPs as energy donors for cancer therapy.¹⁸¹ Therefore, we will only cover work reported since that review.

Prud'homme and Ju et al. prepared PEGylated composite nanoparticles containing UCNPs and *meso*-tetraphenyl porphyrin (**107**).¹⁸² The overlap between emission of UCNPs and absorption of **107** ensures energy transfer from UCNPs to **107**, which generates singlet oxygen. Nanoprecipitation of poly(ethylene glycol-lactic acid) block copolymers (PEG-*b*-PLA), UCNPs, and **107** produced nanoparticles with a hydrophobic core of PLA blocks, UCNPs, and TPP and a hydrophilic shell of PEG blocks, ensuring stability of the particles in water, PBS buffer, and culture medium. In PDT experiment, 75% of the HeLa cancer cells were killed when they were incubated with the composite nanoparticles for 45 min and irradiated at 978 nm.

Similarly, Liu and co-workers fabricated PEGylated UCNPs by hydrophobic interactions of oleic acid layer on the surface of UCNPs and the PEG derivative (Figure 78).¹⁸³ Further, the Chlorin e6 (Ce6) photosensitizer was loaded into the hydrophobic layer of the PEGylated UCNPs. While plain UCNPs gave two strong upconversion emissions at 550 and 660 nm, Ce6 quenched the 660 nm emission by FRET. This UCNP–Ce6 supramolecular complex manifested highly efficient NIR-induced PDT of tumors. Although free Ce6

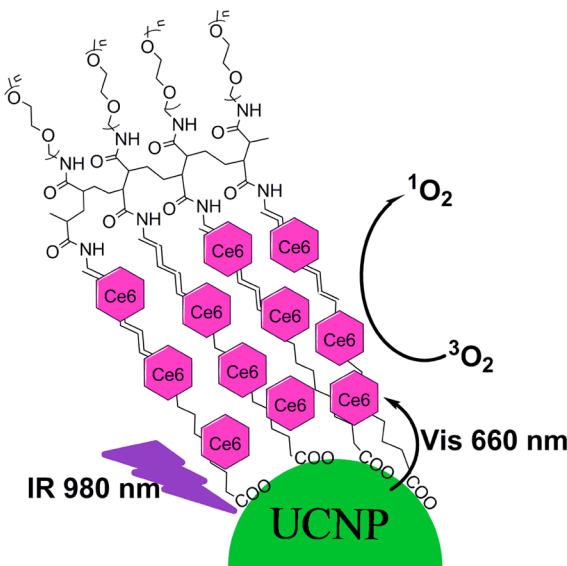


Figure 78. Schematic representation of UCNP–Ce6 supramolecular complex for ${}^1\text{O}_2$ generation. Adapted with permission from ref 183. Copyright 2011 Elsevier.

under 660 nm irradiation generated much more ${}^1\text{O}_2$ than UCNP–Ce6 directly exposed to 980 nm, as quantified by bleaching of *p*-nitroso-*N,N'*-dimethylaniline, ${}^1\text{O}_2$ generation by Ce6 decreased by ~80% when a 3 mm thick sample of pork tissue was placed between the light source and the Ce6 solution. Under the same conditions, ${}^1\text{O}_2$ generation by UCNP–Ce6 only decreased by ~5%. Furthermore, tumors growing on the skin of mice were inhibited by the NIR light-induced PDT even when tumors were hidden by an 8 mm thick pork slice for mimicking the treatment of internal tumors. These results highlight the promise of UCNPs for treatment of internal and deep tumors.

To improve the tumor-targeting capacity, Gu et al. coated the surface of oleic acid-capped UCNPs (OA–UCNPs) with folate-modified amphiphilic chitosan (**127**) by exploiting hydrophobic interaction between the octadecyl groups of the oleic acid and the octyl groups of **127** (Figure 79).¹⁸⁴ The photosensitizer zinc(II) phthalocyanine (**128**) was anchored in beneath the **127** layer of **127**–UCNPs through hydrophobic interactions. These nanoparticles demonstrated enhanced targeting of folate-overexpressed tumors. The absorption of **128** overlapped with the red emission of UCNPs at 660 nm, which ensured the activation of **128** by FRET from irradiation of UCNPs at NIR. The tumor inhibition reached 50% for the deep tumor model covered with 1 cm tissue versus 18% for visible-light induced treatment.

As the above-mentioned studies illustrate, the penetration depth is a key parameter for improving the effectiveness of PDT. By using TPA dyes or upconversion nanoconstructs as energy donor, PDT can utilize NIR excitation which is minimally absorbed or scattered by the tissue. To potentially simplify the treatment further, Wang et al. reported activation of PDT by *in situ* bioluminescence of luminol instead of by an external light source (Figure 80).¹⁸⁵ In their studies, a cationic oligo(*p*-phenylenevinylene) (OPV) was selected as the photosensitizer. In the presence of an oxidizing agent and horseradish peroxidase (HRP), luminol was oxidized to a negatively charged 3-aminophthalate which intensely emits at 425 nm. The spectral overlap between emission of the excited 3-

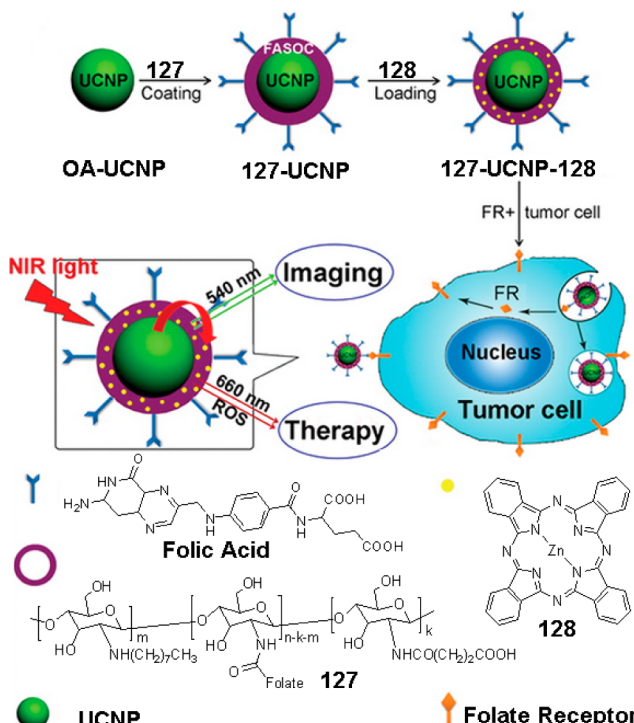


Figure 79. Schematic representation of the synthesis of multifunctional nanoconstruct and their folate-mediated binding to tumor cells with folate receptor overexpression. Adapted with permission from ref 184. Copyright 2013 American Chemical Society.

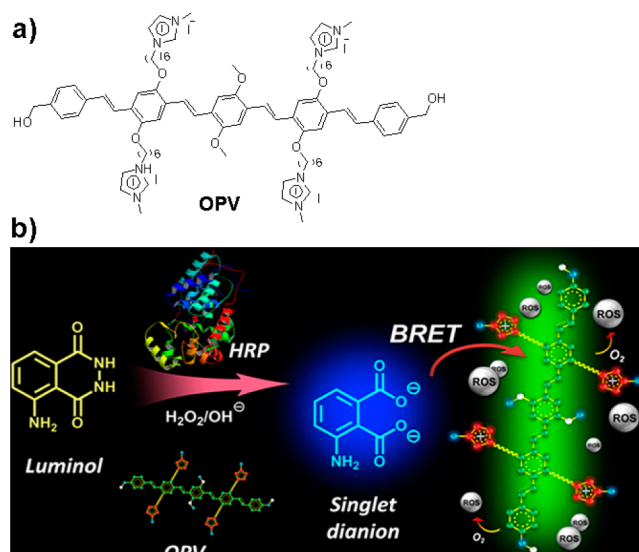


Figure 80. (a) Chemical structures of OPV as a photosensitizer. (b) Schematic representation of the BRET system for PDT. Reprinted with permission from ref 185. Copyright 2012 American Chemical Society.

aminophthalate and the absorption of OPV enabled bioluminescence resonance energy transfer (BRET), facilitated by electrostatic attraction between 3-aminophthalate and OPV. The triplet excited state of OPV was generated by intersystem crossing of singlet excited OPV. The triplet excited OPV then sensitized oxygen molecules in the surroundings for killing cancer cells and pathogenic microbes.

6. CONCLUSION

The development of supramolecular chemistry has provided tools for the preparation of self-assembled systems with high energy-transfer efficiency. Such assemblies have yielded successful mimics of the biological light-harvesting systems, which continue to advance our understanding of photosynthesis. Self-assembly of fluorophores has yielded fluorescent nanomaterials, with photophysical properties tuned by exploiting energy transfer to make them suitable for diverse applications in bioimaging and, upon introduction of recognition units, in biosensing. The assemblies containing triplet photosensitizers have been shown to efficiently generate singlet oxygen by triplet–triplet energy transfer and are now being used in photodynamic therapy, a noninvasive technique for cancer treatments.

Despite impressive progress, many challenges remain. It remains difficult to achieve high local densities of dyes without undesired intermolecular interactions, which self-quench fluorescence and decrease energy-transfer efficiency. Fixing dyes within organic–inorganic hybrid materials (e.g., functionalized clay) could offer a strategy to eliminate self-quenching and undesired aggregation,^{80a} but materials offering well-arranged sites for binding chromophores are rare. One approach that appears promising was recently reported by Klymchenko et al., who demonstrated self-assembly of polymers and cationic dyes with bulky tetrahedral counterions into brightly fluorescent nanoparticles.^{3b} Meanwhile, several groups have been using macrocyclic hosts as bulky “non-covalent building blocks” to suppress fluorescence quenching of guest chromophores.^{83,186} An alternative to preventing aggregation is to employ fluorophores that emit only when aggregated (so-called aggregation-induced emitters).¹⁸⁷ These three strategies are complementary and should be developed contemporaneously.

Looking forward, we speculate that the continued progress in using excitation energy transfer in biological applications is predicated on learning how to exploit more efficiently and more creatively than currently possible various noncovalent interactions to fabricate new supramolecular assemblies displaying tunable energy-transfer properties. As described in this review, so far such assemblies have been built primarily with hydrophobic and electrostatic interactions, whereas many examples of supramolecular constructs exploiting other weak interactions have been reported in other areas of supramolecular chemistry. In this way, by using various weak interactions, supramolecular assemblies containing multiple types of chromophores with well-controlled excitation energy transfer may be prepared and applied toward mimicking the whole circle of photosynthesis and producing high-resolution imaging, highly sensitive biosensing, and highly effective biomedical materials.

AUTHOR INFORMATION

Corresponding Authors

*E-mail: chtung@mail.ipc.ac.cn.

*E-mail: qzyang@mail.ipc.ac.cn.

Notes

The authors declare no competing financial interest.

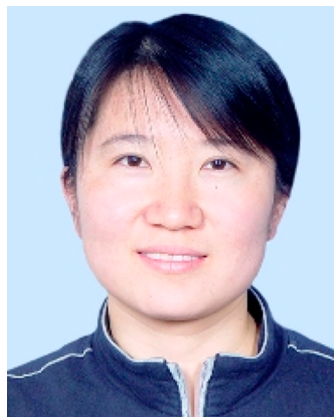
Biographies



Hui-Qing Peng received her B.Sc. degree in Chemistry from QiLu University of Technology (2009) and M.Sc. degree in Chemistry from Shantou University (2012). During her M.Sc. work she moved to the Technical Institute of Physics and Chemistry (TIPC), Chinese Academy of Sciences (CAS) in 2010 and continued toward her Ph.D. under the supervision of Prof. Qing-Zheng Yang. Her research interests focus on the design and synthesis of novel self-assembled systems for artificial light harvesting, cell imaging, and biosensors.



Li-Ya Niu received her B.Sc. degree in 2007 and M.Sc. degree in Material Science and Technology in 2010, both from Beihang University (BUAA). After she received her Ph.D. degree in Organic Chemistry in 2013 from the TIPC, CAS under the supervision of Prof. Qing-Zheng Yang, she joined Qing-Zheng Yang's group as an assistant professor. Her research is focused on fluorescent chemosensors and their biological applications.



Yu-Zhe Chen obtained her Ph.D. degree from TIPC, CAS under the guidance of Prof. Chen-Ho Tung and Li-Zhu Wu in 2006. She then

worked as a postdoctoral fellow in the group of Prof. Richard G. Weiss at Georgetown University from 2007 to 2009. She is currently an associate professor in TIPC. Her current research interests are focused on photochemistry and photophysics in supramolecular systems and optical sensors.



Li-Zhu Wu received her B.S. degree in Chemistry from Lanzhou University in 1990 and Ph.D. degree from the Institute of Photographic Chemistry, CAS, under the supervision of Professor Chen-Ho Tung in 1995. From 1995 to 1998, she worked at the Institute of Photographic Chemistry as an associate professor. After a postdoctoral stay (1997–1998) at the University of Hong Kong working with Professor Chi-Ming Che, she returned to the TIPC, CAS, as a full professor. Her research interests are focused on photochemical conversion, including artificial photosynthesis, visible light catalysis for organic transformation, and photoinduced electron-transfer, energy-transfer, and chemical reactions in supramolecular systems.



Chen-Ho Tung graduated from the Polymer Chemistry Department of the University of Science and Technology of China in 1963 and was awarded his Ph.D. degree in 1983 from Columbia University in New York under the supervision of Professor Nicholas J. Turro. He joined the Institute of Photographic Chemistry, CAS, and is currently a full professor at the TIPC and a member of the CAS. His research interests include photochemical reactions, photoinduced electron transfer, and energy transfer in supramolecular systems.



Qing-Zheng Yang received his Ph.D. degree in 2003 from the TIPC, CAS. After completing postdoctoral research at the University Louis Pasteur and the University of Illinois, Urbana, he joined the faculty at TIPC and then moved to Beijing Normal University in 2014, where he is currently a Professor of Chemistry. His research interests cover the photochemistry of supramolecular assemblies and fluorescent probes for bioimaging.

ACKNOWLEDGMENTS

We acknowledge the financial support received from the 973 Program (2013CB933800, 2013CB834505) and the National Natural Science Foundation of China (21222210, 21472202, 21402216).

REFERENCES

- (1) (a) Vredenberg, W. J.; Duygens, L. N. M. Transfer of Energy from Bacteriochlorophyll to a Reaction Center during Bacterial Photosynthesis. *Nature* **1963**, *197*, 355–357. (b) Vangronvelle, R.; Dekker, J. P.; Gillbro, T.; Sundstrom, V. Energy-Transfer and Trapping in Photosynthesis. *Biochim. Biophys. Acta, Bioenerg.* **1994**, *1187*, 1–65. (c) Kuhlbrandt, W.; Wang, D. N.; Fujiyoshi, Y. Atomic Model of Plant Light-Harvesting Complex by Electron Crystallography. *Nature* **1994**, *367*, 614–621. (d) Gust, D.; Moore, T. A.; Moore, A. L. Mimicking Photosynthetic Solar Energy Transduction. *Acc. Chem. Res.* **2000**, *34*, 40–48. (e) Gust, D.; Moore, T. A.; Moore, A. L. Solar Fuels via Artificial Photosynthesis. *Acc. Chem. Res.* **2009**, *42*, 1890–1898. (f) Şener, M.; Strümpfer, J.; Hsin, J.; Chandler, D.; Scheuring, S.; Hunter, C. N.; Schulten, K. Förster Energy Transfer Theory as Reflected in the Structures of Photosynthetic Light-Harvesting Systems. *ChemPhysChem* **2011**, *12*, 518–531. (g) Frischmann, P. D.; Mahata, K.; Würthner, F. Powering the Future of Molecular Artificial Photosynthesis with Light-Harvesting Metall-supramolecular Dye Assemblies. *Chem. Soc. Rev.* **2013**, *42*, 1847–1870.
- (2) (a) McDermott, G.; Prince, S. M.; Freer, A. A.; Hawthornthwaite-Lawless, A. M.; Papiz, M. Z.; Cogdell, R. J.; Isaacs, N. W. Crystal-Structure of an Integral Membrane Light-Harvesting Complex from Photosynthetic Bacteria. *Nature* **1995**, *374*, 517–521. (b) Pullerits, T.; Sundström, V. Photosynthetic Light-Harvesting Pigment–Protein Complexes: Toward Understanding How and Why. *Acc. Chem. Res.* **1996**, *29*, 381–389. (c) Hu, X. C.; Damjanovic, A.; Ritz, T.; Schulten, K. Architecture and Mechanism of the Light-Harvesting Apparatus of Purple Bacteria. *Proc. Natl. Acad. Sci. U.S.A.* **1998**, *95*, 5935–5941. (d) Polívka, T. S.; Frank, H. A. Molecular Factors Controlling Photosynthetic Light Harvesting by Carotenoids. *Acc. Chem. Res.* **2010**, *43*, 1125–1134. (e) Scholes, G. D.; Fleming, G. R.; Olaya-Castro, A.; van Grondelle, R. Lessons from Nature about Solar Light Harvesting. *Nat. Chem.* **2011**, *3*, 763–774.
- (3) (a) Rao, K. V.; Jain, A.; George, S. J. Organic-Inorganic Light-Harvesting Scaffolds for Luminescent Hybrids. *J. Mater. Chem. C* **2014**, *2*, 3055–3064. (b) Reisch, A.; Didier, P.; Richert, L.; Oncul, S.; Arntz,

- Y.; Mely, Y.; Klymchenko, A. S. Collective Fluorescence Switching of Counterion-Assembled Dyes in Polymer Nanoparticles. *Nat. Commun.* **2014**, *5*.
- (4) Reineke, S.; Lindner, F.; Schwartz, G.; Seidler, N.; Walzer, K.; Lussem, B.; Leo, K. White Organic Light-Emitting Diodes with Fluorescent Tube Efficiency. *Nature* **2009**, *459*, 234–238.
- (5) (a) Fan, J.; Hu, M.; Zhan, P.; Peng, X. Energy Transfer Cassettes Based on Organic Fluorophores: Construction and Applications in Ratiometric Sensing. *Chem. Soc. Rev.* **2013**, *42*, 29–43. (b) Chen, G.; Song, F.; Xiong, X.; Peng, X. Fluorescent Nanosensors Based on Fluorescence Resonance Energy Transfer (FRET). *Ind. Eng. Chem. Res.* **2013**, *52*, 11228–11245. (c) Genovese, D.; Rampazzo, E.; Bonacchi, S.; Montalti, M.; Zaccheroni, N.; Prodi, L. Energy Transfer Processes in Dye-Doped Nanostructures Yield Cooperative and Versatile Fluorescent Probes. *Nanoscale* **2014**, *6*, 3022–3036.
- (6) (a) Miyasaka, T. Toward Printable Sensitized Mesoscopic Solar Cells: Light-Harvesting Management with Thin TiO₂ Films. *J. Phys. Chem. Lett.* **2011**, *2*, 262–269. (b) Panda, D. K.; Goodson, F. S.; Ray, S.; Saha, S. Dye-Sensitized Solar Cells Based on Multichromophoric Supramolecular Light-Harvesting Materials. *Chem. Commun.* **2014**, *50*, 5358–5360.
- (7) (a) Lakowicz, J. R. *Principles of Fluorescence Spectroscopy*; Kluwer Academic/Plenum Publishers: New York, 1999. (b) Turro, N. J. *Modern Molecular Photochemistry*; University Science Books: Sausalito, CA, 1991.
- (8) (a) Förster, T. Zwischenmolekulare Energiewanderung und Fluoreszenz. *Ann. Phys.* **1948**, *437*, 55–75. (b) Förster, T. Transfer Mechanisms of Electronic Excitation. *Discuss. Faraday Soc.* **1959**, *27*, 7–17.
- (9) Deniz, A. A.; Laurence, T. A.; Beligere, G. S.; Dahan, M.; Martin, A. B.; Chemla, D. S.; Dawson, P. E.; Schultz, P. G.; Weiss, S. Single-Molecule Protein Folding: Diffusion Fluorescence Resonance Energy Transfer Studies of the Denaturation of Chymotrypsin Inhibitor 2. *Proc. Natl. Acad. Sci. U.S.A.* **2000**, *97*, 5179–5184.
- (10) (a) Montali, A.; Harms, G.; Renn, A.; Weder, C.; Smith, P.; P. Wild, U. Time-Resolved Fluorescence Study on the Mechanism of Polarizing Energy Transfer in Uniaxially Oriented Polymer Blends. *Phys. Chem. Chem. Phys.* **1999**, *1*, 5697–5702. (b) Sapsford, K. E.; Berti, L.; Medintz, I. L. Materials for Fluorescence Resonance Energy Transfer Analysis: Beyond Traditional Donor–Acceptor Combinations. *Angew. Chem., Int. Ed.* **2006**, *45*, 4562–4589. (c) Sahoo, H. Förster Resonance Energy Transfer – A Spectroscopic Nanoruler: Principle and Applications. *J. Photochem. Photobiol. C: Photochem. Rev.* **2011**, *12*, 20–30.
- (11) Dexter, D. L. A Theory of Sensitized Luminescence in Solids. *J. Chem. Phys.* **1953**, *21*, 836–850.
- (12) Somsen, O. J. G.; Vanmourik, F.; Vangrondelle, R.; Valkunas, L. Energy Migration and Trapping in a Spectrally and Spatially Inhomogeneous Light-Harvesting Antenna. *Biophys. J.* **1994**, *66*, 1580–1596.
- (13) Holden, D. A.; Guillet, J. E. Studies of the Antenna Effect in Polymer Molecules. 3. Role of Singlet Electronic Energy Migration in Naphthalene Polymer Photophysics. *Macromolecules* **1982**, *15*, 1475–1480.
- (14) Devadoss, C.; Bharathi, P.; Moore, J. S. Energy Transfer in Dendritic Macromolecules: Molecular Size Effects and the Role of an Energy Gradient. *J. Am. Chem. Soc.* **1996**, *118*, 9635–9644.
- (15) (a) McQuade, D. T.; Hegedus, A. H.; Swager, T. M. Signal Amplification of a “Turn-On” Sensor: Harvesting the Light Captured by a Conjugated Polymer. *J. Am. Chem. Soc.* **2000**, *122*, 12389–12390. (b) Thomas, S. W.; Joly, G. D.; Swager, T. M. Chemical Sensors Based on Amplifying Fluorescent Conjugated Polymers. *Chem. Rev.* **2007**, *107*, 1339–1386.
- (16) (a) Stewart, G. M.; Fox, M. A. Chromophore-Labeled Dendrons as Light Harvesting Antennae. *J. Am. Chem. Soc.* **1996**, *118*, 4354–4360. (b) Shortreed, M. R.; Swallen, S. F.; Shi, Z.-Y.; Tan, W.; Xu, Z.; Devadoss, C.; Moore, J. S.; Kopelman, R. Directed Energy Transfer Funnels in Dendrimeric Antenna Supermolecules. *J. Phys. Chem. B* **1997**, *101*, 6318–6322. (c) Jiang, D.-L.; Aida, T. Photoisomerization in Dendrimers by Harvesting of Low-Energy Photons. *Nature* **1997**, *388*, 454–456.
- (17) (a) Hoeben, F. J. M.; Herz, L. M.; Daniel, C.; Jonkheijm, P.; Schenning, A. P. H. J.; Silva, C.; Meskers, S. C. J.; Beljon, D.; Phillips, R. T.; Friend, R. H.; Meijer, E. W. Efficient Energy Transfer in Mixed Columnar Stacks of Hydrogen-Bonded Oligo(p-phenylene vinylene)s in Solution. *Angew. Chem., Int. Ed.* **2004**, *43*, 1976–1979. (b) Praveen, V. K.; Ranjith, C.; Bandini, E.; Ajayaghosh, A.; Armaroli, N. Oligo(phenylenevinylene) Hybrids and Self-Assemblies: Versatile Materials for Excitation Energy Transfer. *Chem. Soc. Rev.* **2014**, *43*, 4222–4242.
- (18) (a) Lehn, J.-M. Supramolecular Chemistry. *Science* **1993**, *260*, 1762–1763. (b) Brunsved, L.; Folmer, B. J. B.; Meijer, E. W.; Sijbesma, R. P. Supramolecular Polymers. *Chem. Rev.* **2001**, *101*, 4071–4098. (c) Gan, Q.; Ferrand, Y.; Bao, C.; Kauffmann, B.; Gréard, A.; Jiang, H.; Huc, I. Helix-Rod Host-Guest Complexes with Shutting Rates Much Faster than Disassembly. *Science* **2011**, *331*, 1172–1175. (d) Zheng, B.; Wang, F.; Dong, S.; Huang, F. Supramolecular Polymers Constructed by Crown Ether-Based Molecular Recognition. *Chem. Soc. Rev.* **2012**, *41*, 1621–1636. (e) Wang, M.-X. Nitrogen and Oxygen Bridged Calixaromatics: Synthesis, Structure, Functionalization, and Molecular Recognition. *Acc. Chem. Res.* **2012**, *45*, 182–195. (f) Karakostas, N.; Mavridis, I. M.; Seintis, K.; Fakis, M.; Koini, E. N.; Petsalakis, I. D.; Pistolis, G. Highly Efficient and Unidirectional Energy Transfer within a Tightly Self-Assembled Host-Guest Multichromophoric Array. *Chem. Commun.* **2014**, *50*, 1362–1365. (g) Guo, D.-S.; Liu, Y. Supramolecular Chemistry of p-Sulfonatocalix[n]arenes and Its Biological Applications. *Acc. Chem. Res.* **2014**, *47*, 1925–1934. (h) Han, Y.; Meng, Z.; Ma, Y.-X.; Chen, C.-F. Iptycene-Derived Crown Ether Hosts for Molecular Recognition and Self-Assembly. *Acc. Chem. Res.* **2014**, *47*, 2026–2040. (i) Tian, J.; Zhou, T.-Y.; Zhang, S.-C.; Aloni, S.; Altoe, M. V.; Xie, S.-H.; Wang, H.; Zhang, D.-W.; Zhao, X.; Liu, Y.; Li, Z.-T. Three-Dimensional Periodic Supramolecular Organic Framework Ion Sponge in Water and Microcrystals. *Nat. Commun.* **2014**, *5*.
- (19) (a) Crick, F. H. C.; Watson, J. D. The Complementary Structure of Deoxyribonucleic Acid. *Proc. R. Soc. London A* **1954**, *223*, 80–96. (b) Watson, J. D.; Crick, F. H. Molecular Structure of Nucleic Acids—A Structure for Deoxyribose Nucleic Acid. *Nature* **1953**, *171*, 737–738.
- (20) (a) Barbieri, A.; Ventura, B.; Ziessel, R. Photoinduced Energy-Transfer Dynamics in Multichromophoric Arrays Containing Transition Metal Complexes and Organic Modules. *Coord. Chem. Rev.* **2012**, *256*, 1732–1741. (b) Wong, K.-T.; Bassani, D. M. Energy Transfer in Supramolecular Materials for New Applications in Photonics and Electronics. *NPG Asia Mater.* **2014**, *6*, e116. (c) Yang, D.; Zou, R.; Zhu, Y.; Liu, B.; Yao, D.; Jiang, J.; Wu, J.; Tian, H. Magainin II Modified Polydiacetylene Micelles for Cancer Therapy. *Nanoscale* **2014**, *6*, 14772–14783.
- (21) (a) Abbel, R.; Grenier, C.; Pouderoijen, M. J.; Stoudam, J. W.; Leclère, P. E. L. G.; Sijbesma, R. P.; Meijer, E. W.; Schenning, A. P. H. J. White-Light Emitting Hydrogen-Bonded Supramolecular Copolymers Based on π -Conjugated Oligomers. *J. Am. Chem. Soc.* **2008**, *131*, 833–843. (b) Vijayakumar, C.; Praveen, V. K.; Ajayaghosh, A. RGB Emission Through Controlled Donor Self-Assembly and Modulation of Excitation Energy Transfer: A Novel Strategy to White-Light-Emitting Organogels. *Adv. Mater.* **2009**, *21*, 2059–2063. (c) Ner, Y.; Grote, J. G.; Stuart, J. A.; Sotzing, G. A. White Luminescence from Multiple-Dye-Doped Electrospun DNA Nanofibers by Fluorescence Resonance Energy Transfer. *Angew. Chem., Int. Ed.* **2009**, *48*, 5134–5138. (d) Praveen, V. K.; Ranjith, C.; Armaroli, N. White-Light-Emitting Supramolecular Gels. *Angew. Chem., Int. Ed.* **2014**, *53*, 365–368.
- (22) (a) Fischer, I.; Petkau-Milroy, K.; Dorland, Y. L.; Schenning, A. P. H. J.; Brunsved, L. Self-Assembled Fluorescent Organic Nanoparticles for Live-Cell Imaging. *Chem.—Eur. J.* **2013**, *19*, 16646–16650. (b) Chen, Y.-Z.; Chen, P.-Z.; Peng, H.-Q.; Zhao, Y.; Ding, H.-Y.; Wu, L.-Z.; Tung, C.-H.; Yang, Q.-Z. Water-Soluble, Membrane-Permeable Organic Fluorescent Nanoparticles with Large Tunability in Emission Wavelengths and Stokes Shifts. *Chem. Commun.* **2013**, *49*,

- 5877–5879. (c) Feng, L.; Liu, L.; Lv, F.; Bazan, G. C.; Wang, S. Preparation and Biofunctionalization of Multicolor Conjugated Polymer Nanoparticles for Imaging and Detection of Tumor Cells. *Adv. Mater.* **2014**, *26*, 3926–3930.
- (23) (a) Choi, M.-S.; Yamazaki, T.; Yamazaki, I.; Aida, T. Bioinspired Molecular Design of Light-Harvesting Multiporphyrin Arrays. *Angew. Chem., Int. Ed.* **2004**, *43*, 150–158. (b) Zhang, X.; Zeng, Y.; Yu, T.; Chen, J.; Yang, G.; Li, Y. Advances in Photofunctional Dendrimers for Solar Energy Conversion. *J. Phys. Chem. Lett.* **2014**, *5*, 2340–2350.
- (24) (a) Bandy, T. J.; Brewer, A.; Burns, J. R.; Marth, G.; Nguyen, T.; Stulz, E. DNA as Supramolecular Scaffold for Functional Molecules: Progress in DNA Nanotechnology. *Chem. Soc. Rev.* **2011**, *40*, 138–148. (b) Ruiz-Carretero, A.; Janssen, P. G. A.; Kaeser, A.; Schenning, A. P. H. J. DNA-Templated Assembly of Dyes and Extended π -Conjugated Systems. *Chem. Commun.* **2011**, *47*, 4340–4347.
- (25) Ward, M. D. Photo-Induced Electron and Energy Transfer in Non-covalently Bonded Supramolecular Assemblies. *Chem. Soc. Rev.* **1997**, *26*, 365–375.
- (26) Li, W.-S.; Aida, T. Dendrimer Porphyrins and Phthalocyanines. *Chem. Rev.* **2009**, *109*, 6047–6076.
- (27) Ajayaghosh, A.; Praveen, V. K.; Vijayakumar, C. Organogels as Scaffolds for Excitation Energy Transfer and Light Harvesting. *Chem. Soc. Rev.* **2008**, *37*, 109–122.
- (28) (a) Michel, H.; Epp, O.; Deisenhofer, J. Pigment Protein Interactions in the Photosynthetic Reaction Center from Rhodopseudomonas-Viridis. *EMBO J.* **1986**, *5*, 2445–2451. (b) Wasielewski, M. R. Photoinduced Electron Transfer in Supramolecular Systems for Artificial Photosynthesis. *Chem. Rev.* **1992**, *92*, 435–461.
- (29) (a) Wasielewski, M. R. Self-Assembly Strategies for Integrating Light Harvesting and Charge Separation in Artificial Photosynthetic Systems. *Acc. Chem. Res.* **2009**, *42*, 1910–1921. (b) Croce, R.; van Amerongen, H. Natural Strategies for Photosynthetic Light Harvesting. *Nat. Chem. Biol.* **2014**, *10*, 492–501.
- (30) (a) Miller, R. A.; Presley, A. D.; Francis, M. B. Self-Assembling Light-Harvesting Systems from Synthetically Modified Tobacco Mosaic Virus Coat Proteins. *J. Am. Chem. Soc.* **2007**, *129*, 3104–3109. (b) Dutta, P. K.; Varghese, R.; Nangreave, J.; Lin, S.; Yan, H.; Liu, Y. DNA-Directed Artificial Light-Harvesting Antenna. *J. Am. Chem. Soc.* **2011**, *133*, 11985–11993. (c) Peng, H.-Q.; Xu, J.-F.; Chen, Y.-Z.; Wu, L.-Z.; Tung, C.-H.; Yang, Q.-Z. Water-Dispersible Nanospheres of Hydrogen-Bonded Supramolecular Polymers and Their Application for Mimicking Light-Harvesting Systems. *Chem. Commun.* **2014**, *50*, 1334–1337.
- (31) Brousmiche, D. W.; Serin, J. M.; Fréchet, J. M. J.; He, G. S.; Lin, T.-C.; Chung, S.-J.; Prasad, P. N.; Kannan, R.; Tan, L.-S. Fluorescence Resonance Energy Transfer in Novel Multiphoton Absorbing Dendritic Structures. *J. Phys. Chem. B* **2004**, *108*, 8592–8600.
- (32) Kuhlbrandt, W. Many Wheels Make Light Work. *Nature* **1995**, *374*, 497–498.
- (33) (a) Prathapan, S.; Johnson, T. E.; Lindsey, J. S. Building-Block Synthesis of Porphyrin Light-Harvesting Arrays. *J. Am. Chem. Soc.* **1993**, *115*, 7519–7520. (b) Balaban, Teodor S.; Eichhöfer, A.; Lehn, J.-M. Self-Assembly by Hydrogen Bonding and π – π Interactions in the Crystal of a Porphyrin – Attempts to Mimic Bacteriochlorophyll c. *Eur. J. Org. Chem.* **2000**, *2000*, 4047–4057. (c) Balaban, T. S. Tailoring Porphyrins and Chlorins for Self-Assembly in Biomimetic Artificial Antenna Systems. *Acc. Chem. Res.* **2005**, *38*, 612–623.
- (34) Terazono, Y.; Kodis, G.; Bhushan, K.; Zaks, J.; Madden, C.; Moore, A. L.; Moore, T. A.; Fleming, G. R.; Gust, D. Mimicking the Role of the Antenna in Photosynthetic Photoprotection. *J. Am. Chem. Soc.* **2011**, *133*, 2916–2922.
- (35) Tomizaki, K.-y.; Loewe, R. S.; Kirmaier, C.; Schwartz, J. K.; Retsek, J. L.; Bocian, D. F.; Holten, D.; Lindsey, J. S. Synthesis and Photophysical Properties of Light-Harvesting Arrays Comprised of a Porphyrin Bearing Multiple Perylene-Monoimide Accessory Pigments. *J. Org. Chem.* **2002**, *67*, 6519–6534.
- (36) Balaban, T. S.; Goddard, R.; Linke-Schaetzel, M.; Lehn, J.-M. 2-Aminopyrimidine Directed Self-Assembly of Zinc Porphyrins Containing Bulky 3,5-Di-tert-butylphenyl Groups. *J. Am. Chem. Soc.* **2003**, *125*, 4233–4239.
- (37) Yong, C.-K.; Parkinson, P.; Kondratuk, D. V.; Chen, W.-H.; Stannard, A.; Summerfield, A.; Sprafke, J. K.; O'Sullivan, M. C.; Beton, P. H.; Anderson, H. L.; Herz, L. M. Ultrafast Delocalization of Excitation in Synthetic Light-Harvesting Nanorings. *Chem. Sci.* **2015**, *6*, 181–189.
- (38) (a) Nakamura, Y.; Aratani, N.; Osuka, A. Cyclic Porphyrin Arrays as Artificial Photosynthetic Antenna: Synthesis and Excitation Energy Transfer. *Chem. Soc. Rev.* **2007**, *36*, 831–845. (b) Aratani, N.; Kim, D.; Osuka, A. Discrete Cyclic Porphyrin Arrays as Artificial Light-Harvesting Antenna. *Acc. Chem. Res.* **2009**, *42*, 1922–1934. (c) Yang, J.; Yoon, M.-C.; Yoo, H.; Kim, P.; Kim, D. Excitation Energy Transfer in Multiporphyrin Arrays with Cyclic Architectures: Towards Artificial Light-Harvesting Antenna Complexes. *Chem. Soc. Rev.* **2012**, *41*, 4808–4826.
- (39) Takahashi, R.; Kobuke, Y. Hexameric Macroring of Gable-Porphyrins as a Light-Harvesting Antenna Mimic. *J. Am. Chem. Soc.* **2003**, *125*, 2372–2373.
- (40) Hwang, I.-W.; Kamada, T.; Ahn, T. K.; Ko, D. M.; Nakamura, T.; Tsuda, A.; Osuka, A.; Kim, D. Porphyrin Boxes Constructed by Homochiral Self-Sorting Assembly: Optical Separation, Exciton Coupling, and Efficient Excitation Energy Migration. *J. Am. Chem. Soc.* **2004**, *126*, 16187–16198.
- (41) Parkinson, P.; Knappke, C. E. I.; Kamonsutthipajit, N.; Sirithip, K.; Matichak, J. D.; Anderson, H. L.; Herz, L. M. Ultrafast Energy Transfer in Biomimetic Multistrand Nanorings. *J. Am. Chem. Soc.* **2014**, *136*, 8217–8220.
- (42) (a) Beck, J. B.; Rowan, S. J. Multistimuli, Multiresponsive Metallo-Supramolecular Polymers. *J. Am. Chem. Soc.* **2003**, *125*, 13922–13923. (b) Sugiyasu, K.; Fujita, N.; Takeuchi, M.; Yamada, S.; Shinkai, S. Proton-Sensitive Fluorescent Organogels. *Org. Biomol. Chem.* **2003**, *1*, 895–899. (c) Montalti, M.; Dolci, L. S.; Prodi, L.; Zaccheroni, N.; Stuart, M. C. A.; van Bommel, K. J. C.; Friggeri, A. Energy Transfer from a Fluorescent Hydrogel to a Hosted Fluorophore. *Langmuir* **2006**, *22*, 2299–2303.
- (43) Babu, S. S.; Kartha, K. K.; Ajayaghosh, A. Excited State Processes in Linear π -System-Based Organogels. *J. Phys. Chem. Lett.* **2010**, *1*, 3413–3424.
- (44) (a) Chen, L.; Revel, S.; Morris, K.; Adams, D. J. Energy Transfer in Self-Assembled Dipeptide Hydrogels. *Chem. Commun.* **2010**, *46*, 4267–4269. (b) Raeburn, J.; Zamith Cardoso, A.; Adams, D. J. The Importance of the Self-Assembly Process to Control Mechanical Properties of Low Molecular Weight Hydrogels. *Chem. Soc. Rev.* **2013**, *42*, 5143–5156.
- (45) Ajayaghosh, A.; Praveen, V. K. π -Organogels of Self-Assembled p-Phenylenevinylenes: Soft Materials with Distinct Size, Shape, and Functions. *Acc. Chem. Res.* **2007**, *40*, 644–656.
- (46) Ajayaghosh, A.; George, S. J.; Praveen, V. K. Gelation-Assisted Light Harvesting by Selective Energy Transfer from an Oligo(p-phenylenevinylene)-Based Self-Assembly to an Organic Dye. *Angew. Chem., Int. Ed.* **2003**, *42*, 332–335.
- (47) Ajayaghosh, A.; Vijayakumar, C.; Praveen, V. K.; Babu, S. S.; Varghese, R. Self-Location of Acceptors as “Isolated” or “Stacked” Energy Traps in a Supramolecular Donor Self-Assembly: A Strategy to Wavelength Tunable FRET Emission. *J. Am. Chem. Soc.* **2006**, *128*, 7174–7175.
- (48) Ajayaghosh, A.; Praveen, V. K.; Vijayakumar, C.; George, S. J. Molecular Wire Encapsulated into π Organogels: Efficient Supramolecular Light-Harvesting Antennae with Color-Tunable Emission. *Angew. Chem., Int. Ed.* **2007**, *46*, 6260–6265.
- (49) (a) Placine, F.; Desvergne, J.-P.; Belin, C.; Buffeteau, T.; Desbat, B.; Ducasse, L.; Lassègues, J.-C. Molecular Arrangement in the Gel Fibers of 2,3-Didecyloxyanthracene (DDOA): A Spectroscopic and Theoretical Approach. *Langmuir* **2003**, *19*, 4563–4572. (b) Desvergne, J.-P.; Brotin, T.; Meerschaut, D.; Clavier, G.; Placine, F.; Pozzo, J.-L.; Bouas-Laurent, H. Spectroscopic Properties and Gelling Ability of a Set of Rod-Like 2,3-disubstituted Anthracenes. *New J. Chem.* **2004**, *28*, 234–243.

- (50) Del Guerzo, A.; Olive, A. G. L.; Reichwagen, J.; Hopf, H.; Desvergne, J.-P. Energy Transfer in Self-Assembled [n]-Acene Fibers Involving ≥ 100 Donors Per Acceptor. *J. Am. Chem. Soc.* **2005**, *127*, 17984–17985.
- (51) Sugiyasu, K.; Fujita, N.; Shinkai, S. Visible-Light-Harvesting Organogel Composed of Cholesterol-Based Perylene Derivatives. *Angew. Chem., Int. Ed.* **2004**, *43*, 1229–1233.
- (52) Rehm, T. H.; Schmuck, C. Ion-Pair Induced Self-Assembly in Aqueous Solvents. *Chem. Soc. Rev.* **2010**, *39*, 3597–3611.
- (53) Nakashima, T.; Kimizuka, N. Light-Harvesting Supramolecular Hydrogels Assembled from Short-Legged Cationic L-Glutamate Derivatives and Anionic Fluorophores. *Adv. Mater.* **2002**, *14*, 1113–1116.
- (54) Bairi, P.; Roy, B.; Nandi, A. K. A Light Harvesting Bi-component Hydrogel with a Riboflavin Acceptor. *Chem. Commun.* **2012**, *48*, 10850–10852.
- (55) (a) Malinovskii, V. L.; Samain, F.; Häner, R. Helical Arrangement of Interstrand Stacked Pyrenes in a DNA Framework. *Angew. Chem., Int. Ed.* **2007**, *46*, 4464–4467. (b) Hannestad, J. K.; Sandin, P.; Albinsson, B. Self-Assembled DNA Photonic Wire for Long-Range Energy Transfer. *J. Am. Chem. Soc.* **2008**, *130*, 15889–15895. (c) Fry, H. C.; Garcia, J. M.; Medina, M. J.; Rico, U. M.; Gosztola, D. J.; Nikiforov, M. P.; Palmer, L. C.; Stupp, S. I. Self-Assembly of Highly Ordered Peptide Amphiphile Metalloporphyrin Arrays. *J. Am. Chem. Soc.* **2012**, *134*, 14646–14649.
- (56) Spillmann, C. M.; Medintz, I. L. Use of Biomolecular Scaffolds for Assembling Multistep Light Harvesting and Energy Transfer Devices. *J. Photochem. Photobiol. C: Photochem. Rev.* **2015**, *23*, 1–24.
- (57) Ma, Y.-Z.; Miller, R. A.; Fleming, G. R.; Francis, M. B. Energy Transfer Dynamics in Light-Harvesting Assemblies Templated by the Tobacco Mosaic Virus Coat Protein. *J. Phys. Chem. B* **2008**, *112*, 6887–6892.
- (58) Miller, R. A.; Stephanopoulos, N.; McFarland, J. M.; Rosko, A. S.; Geissler, P. L.; Francis, M. B. Impact of Assembly State on the Defect Tolerance of TMV-Based Light Harvesting Arrays. *J. Am. Chem. Soc.* **2010**, *132*, 6068–6074.
- (59) Endo, M.; Fujitsuka, M.; Majima, T. Porphyrin Light-Harvesting Arrays Constructed in the Recombinant Tobacco Mosaic Virus Scaffold. *Chem.—Eur. J.* **2007**, *13*, 8660–8666.
- (60) Nam, Y. S.; Shin, T.; Park, H.; Magyar, A. P.; Choi, K.; Fantner, G.; Nelson, K. A.; Belcher, A. M. Virus-Templated Assembly of Porphyrins into Light-Harvesting Nanoantennae. *J. Am. Chem. Soc.* **2010**, *132*, 1462–1463.
- (61) Fudickar, W.; Zimmermann, J.; Ruhmann, L.; Schneider, J.; Röder, B.; Siggen, U.; Fuhrhop, J.-H. Fluorescence Quenching and Size Selective Heterodimerization of a Porphyrin Adsorbed to Gold and Embedded in Rigid Membrane Gaps. *J. Am. Chem. Soc.* **1999**, *121*, 9539–9545.
- (62) Scolaro, L. M.; Castricano, M. A.; Romeo, A.; Micali, N.; Angelini, N.; Lo Passo, C.; Felici, F. Supramolecular Binding of Cationic Porphyrins on a Filamentous Bacteriophage Template: Toward a Noncovalent Antenna System. *J. Am. Chem. Soc.* **2006**, *128*, 7446–7447.
- (63) Chiti, F.; Dobson, C. M. In *Annual Review of Biochemistry*; Annual Reviews: Palo Alto, 2006; Vol. 75.
- (64) Kumar, R. J.; MacDonald, J. M.; Singh, T. B.; Waddington, L. J.; Holmes, A. B. Hierarchical Self-Assembly of Semiconductor Functionalized Peptide α -Helices and Optoelectronic Properties. *J. Am. Chem. Soc.* **2011**, *133*, 8564–8573.
- (65) Channon, K. J.; Devlin, G. L.; MacPhee, C. E. Efficient Energy Transfer within Self-Assembling Peptide Fibers: A Route to Light-Harvesting Nanomaterials. *J. Am. Chem. Soc.* **2009**, *131*, 12520–12521.
- (66) Stein, I. H.; Steinhauer, C.; Tinnefeld, P. Single-Molecule Four-Color FRET Visualizes Energy-Transfer Paths on DNA Origami. *J. Am. Chem. Soc.* **2011**, *133*, 4193–4195.
- (67) Kumar, C. V.; Duff, M. R. DNA-Based Supramolecular Artificial Light Harvesting Complexes. *J. Am. Chem. Soc.* **2009**, *131*, 16024–16026.
- (68) Woller, J. G.; Hannestad, J. K.; Albinsson, B. Self-Assembled Nanoscale DNA–Porphyrin Complex for Artificial Light Harvesting. *J. Am. Chem. Soc.* **2013**, *135*, 2759–2768.
- (69) Garo, F.; Häner, R. A DNA-Based Light-Harvesting Antenna. *Angew. Chem., Int. Ed.* **2012**, *51*, 916–919.
- (70) Janssen, P. G. A.; Vandenberghe, J.; van Dongen, J. L. J.; Meijer, E. W.; Schenning, A. P. H. J. ssDNA Templatized Self-Assembly of Chromophores. *J. Am. Chem. Soc.* **2007**, *129*, 6078–6079.
- (71) Ruiz-Carretero, A.; Janssen, P. G. A.; Stevens, A. L.; Surin, M.; Herz, L. M.; Schenning, A. P. H. J. Directing Energy Transfer in Discrete One-Dimensional Oligonucleotide-Templated Assemblies. *Chem. Commun.* **2011**, *47*, 884–886.
- (72) Pu, F.; Wu, L.; Ju, E.; Ran, X.; Ren, J.; Qu, X. Artificial Light-Harvesting Material Based on Self-Assembly of Coordination Polymer Nanoparticles. *Adv. Funct. Mater.* **2014**, *24*, 4549–4555.
- (73) Pu, F.; Wu, L.; Ran, X.; Ren, J.; Qu, X. G-Quartet-Based Nanostructure for Mimicking Light-Harvesting Antenna. *Angew. Chem., Int. Ed.* **2015**, *54*, 892–896.
- (74) Avinash, M. B.; Govindaraju, T. Nanoarchitectonics of Biomolecular Assemblies for Functional Applications. *Nanoscale* **2014**, *6*, 13348–13369.
- (75) Inagaki, S.; Ohtani, O.; Goto, Y.; Okamoto, K.; Ikai, M.; Yamanaka, K.-i.; Tani, T.; Okada, T. Light Harvesting by a Periodic Mesoporous Organosilica Chromophore. *Angew. Chem., Int. Ed.* **2009**, *48*, 4042–4046.
- (76) Takeda, H.; Goto, Y.; Maegawa, Y.; Ohsuna, T.; Tani, T.; Matsumoto, K.; Shimada, T.; Inagaki, S. Visible-Light-Harvesting Periodic Mesoporous Organosilica. *Chem. Commun.* **2009**, 6032–6034.
- (77) Waki, M.; Mizoshita, N.; Maegawa, Y.; Hasegawa, T.; Tani, T.; Shimada, T.; Inagaki, S. Enhanced Fluorescence Detection of Metal Ions Using Light-Harvesting Mesoporous Organosilica. *Chem.—Eur. J.* **2012**, *18*, 1992–1998.
- (78) Rao, K. V.; Datta, K. K. R.; Eswaramoorthy, M.; George, S. J. Light-Harvesting Hybrid Hydrogels: Energy-Transfer-Induced Amplified Fluorescence in Noncovalently Assembled Chromophore–Organoclay Composites. *Angew. Chem., Int. Ed.* **2011**, *50*, 1179–1184.
- (79) Ishida, Y.; Shimada, T.; Masui, D.; Tachibana, H.; Inoue, H.; Takagi, S. Efficient Excited Energy Transfer Reaction in Clay/Porphyrin Complex toward an Artificial Light-Harvesting System. *J. Am. Chem. Soc.* **2011**, *133*, 14280–14286.
- (80) (a) Takagi, S.; Shimada, T.; Eguchi, M.; Yui, T.; Yoshida, H.; Tryk, D. A.; Inoue, H. High-Density Adsorption of Cationic Porphyrins on Clay Layer Surfaces without Aggregation: The Size-Matching Effect. *Langmuir* **2002**, *18*, 2265–2272. (b) Egawa, T.; Watanabe, H.; Fujimura, T.; Ishida, Y.; Yamato, M.; Masui, D.; Shimada, T.; Tachibana, H.; Yoshida, H.; Inoue, H.; Takagi, S. Novel Methodology to Control the Adsorption Structure of Cationic Porphyrins on the Clay Surface Using the “Size-Matching Rule”. *Langmuir* **2011**, *27*, 10722–10729. (c) Ishida, Y.; Masui, D.; Shimada, T.; Tachibana, H.; Inoue, H.; Takagi, S. The Mechanism of the Porphyrin Spectral Shift on Inorganic Nanosheets: The Molecular Flattening Induced by the Strong Host–Guest Interaction due to the “Size-Matching Rule”. *J. Phys. Chem. C* **2012**, *116*, 7879–7885.
- (81) Nabiev, I.; Rakovich, A.; Sukhanova, A.; Lukashev, E.; Zagidullin, V.; Pachenko, V.; Rakovich, Y. P.; Donegan, J. F.; Rubin, A. B.; Govorov, A. O. Fluorescent Quantum Dots as Artificial Antennas for Enhanced Light Harvesting and Energy Transfer to Photosynthetic Reaction Centers. *Angew. Chem., Int. Ed.* **2010**, *49*, 7217–7221.
- (82) (a) Adronov, A.; Gilat, S. L.; Fréchet, J. M. J.; Ohta, K.; Neuwahl, F. V. R.; Fleming, G. R. Light Harvesting and Energy Transfer in Laser–Dye-Labeled Poly(aryl ether) Dendrimers. *J. Am. Chem. Soc.* **2000**, *122*, 1175–1185. (b) Zeng, Y.; Li, Y.-Y.; Chen, J.; Yang, G.; Li, Y. Dendrimers: A Mimic Natural Light-Harvesting System. *Chem.—Asian J.* **2010**, *5*, 992–1005. (c) Ziessl, R.; Ulrich, G.; Haefele, A.; Harriman, A. An Artificial Light-Harvesting Array Constructed from Multiple Bodipy Dyes. *J. Am. Chem. Soc.* **2013**, *135*, 11330–11344.

- (83) Zeng, Y.; Li, Y.; Li, M.; Yang, G.; Li, Y. Enhancement of Energy Utilization in Light-Harvesting Dendrimers by the Pseudorotaxane Formation at Periphery. *J. Am. Chem. Soc.* **2009**, *131*, 9100–9106.
- (84) Peng, H.-Q.; Chen, Y.-Z.; Zhao, Y.; Yang, Q.-Z.; Wu, L.-Z.; Tung, C.-H.; Zhang, L.-P.; Tong, Q.-X. Artificial Light-Harvesting System Based on Multifunctional Surface-Cross-Linked Micelles. *Angew. Chem., Int. Ed.* **2012**, *S1*, 2088–2092.
- (85) (a) Zhang, S.; Zhao, Y. Facile Synthesis of Multivalent Water-Soluble Organic Nanoparticles via “Surface Clicking” of Alkynylated Surfactant Micelles. *Macromolecules* **2010**, *43*, 4020–4022. (b) Zhang, S.; Zhao, Y. Rapid Release of Entrapped Contents from Multi-Functionalizable, Surface Cross-Linked Micelles upon Different Stimulation. *J. Am. Chem. Soc.* **2010**, *132*, 10642–10644.
- (86) (a) Sijbesma, R. P.; Beijer, F. H.; Brunsved, L.; Folmer, B. J. B.; Hirschberg, J. H. K. K.; Lange, R. F. M.; Lowe, J. K. L.; Meijer, E. W. Reversible Polymers Formed from Self-Complementary Monomers Using Quadruple Hydrogen Bonding. *Science* **1997**, *278*, 1601–1604. (b) Neuteboom, E. E.; Beckers, E. H. A.; Meskers, S. C. J.; Meijer, E. W.; Janssen, R. A. J. Singlet-Energy Transfer in Quadruple Hydrogen-Bonded Oligo(p-phenylenevinylene)perylene-diimide Dyads. *Org. Biomol. Chem.* **2003**, *1*, 198–203. (c) Dudek, S. P.; Pouderoijen, M.; Abbel, R.; Schenning, A. P. H. J.; Meijer, E. W. Synthesis and Energy-Transfer Properties of Hydrogen-Bonded Oligofluorenes. *J. Am. Chem. Soc.* **2005**, *127*, 11763–11768. (d) Wang, S.-M.; Yu, M.-L.; Ding, J.; Tung, C.-H.; Wu, L.-Z. Photoinduced Triplet-Triplet Energy Transfer via the 2-Ureido-4[1H]-pyrimidinone Self-Complementary Quadruple Hydrogen-Bonded Module. *J. Phys. Chem. A* **2008**, *112*, 3865–3869. (e) Li, S.-L.; Xiao, T.; Xia, W.; Ding, X.; Yu, Y.; Jiang, J.; Wang, L. New Light on the Ring—Chain Equilibrium of a Hydrogen-Bonded Supramolecular Polymer Based on a Photochromic Dithienylethene Unit and Its Energy-Transfer Properties as a Storage Material. *Chem.—Eur. J.* **2011**, *17*, 10716–10723.
- (87) Schmid, S. A.; Abbel, R.; Schenning, A. P. H. J.; Meijer, E. W.; Herz, L. M. Energy Transfer Processes along a Supramolecular Chain of π -Conjugated Molecules. *Philos. Trans. R. Soc. A* **2012**, *370*, 3787–3801.
- (88) Winiger, C. B.; Li, S.; Kumar, G. R.; Langenegger, S. M.; Häner, R. Long-Distance Electronic Energy Transfer in Light-Harvesting Supramolecular Polymers. *Angew. Chem., Int. Ed.* **2014**, *53*, 13609–13613.
- (89) Strümpfer, J.; Şener, M.; Schulten, K. How Quantum Coherence Assists Photosynthetic Light-Harvesting. *J. Phys. Chem. Lett.* **2012**, *3*, 536–542.
- (90) (a) Stephens, D. J.; Allan, V. J. Light Microscopy Techniques for Live Cell Imaging. *Science* **2003**, *300*, 82–86. (b) Lichtman, J. W.; Conchello, J.-A. Fluorescence Microscopy. *Nat. Methods* **2005**, *2*, 910–919.
- (91) (a) Rosi, N. L.; Mirkin, C. A. Nanostructures in Biodiagnostics. *Chem. Rev.* **2005**, *105*, 1547–1562. (b) Wu, X.; Chang, S.; Sun, X.; Guo, Z.; Li, Y.; Tang, J.; Shen, Y.; Shi, J.; Tian, H.; Zhu, W. Constructing NIR Silica-Cyanine Hybrid Nanocomposite for Bioimaging in Vivo: A Breakthrough in Photo-Stability and Bright Fluorescence with Large Stokes Shift. *Chem. Sci.* **2013**, *4*, 1221–1228.
- (92) Yuan, L.; Lin, W.; Zheng, K.; Zhu, S. FRET-Based Small-Molecule Fluorescent Probes: Rational Design and Bioimaging Applications. *Acc. Chem. Res.* **2013**, *46*, 1462–1473.
- (93) Li, C.; Hu, J.; Liu, S. Engineering FRET Processes within Synthetic Polymers, Polymeric Assemblies and Nanoparticles via Modulating Spatial Distribution of Fluorescent Donors and Acceptors. *Soft Matter* **2012**, *8*, 7096–7102.
- (94) Wang, L.; Tan, W. Multicolor FRET Silica Nanoparticles by Single Wavelength Excitation. *Nano Lett.* **2005**, *6*, 84–88.
- (95) Wagh, A.; Jyoti, F.; Mallik, S.; Qian, S.; Leclerc, E.; Law, B. Polymeric Nanoparticles with Sequential and Multiple FRET Cascade Mechanisms for Multicolor and Multiplexed Imaging. *Small* **2013**, *9*, 2129–2139.
- (96) Zhu, C.; Liu, L.; Yang, Q.; Lv, F.; Wang, S. Water-Soluble Conjugated Polymers for Imaging, Diagnosis, and Therapy. *Chem. Rev.* **2012**, *112*, 4687–4735.
- (97) Kaeser, A.; Schenning, A. P. H. J. Fluorescent Nanoparticles Based on Self-Assembled π -Conjugated Systems. *Adv. Mater.* **2010**, *22*, 2985–2997.
- (98) Abbel, R.; van der Weegen, R.; Meijer, E. W.; Schenning, A. P. H. J. Multicolour Self-Assembled Particles of Fluorene-Based Bolaamphiphiles. *Chem. Commun. (Camb.)* **2009**, 1697–1699.
- (99) Petkau, K.; Kaeser, A.; Fischer, I.; Brunsved, L.; Schenning, A. P. H. J. Pre- and Postfunctionalized Self-Assembled π -Conjugated Fluorescent Organic Nanoparticles for Dual Targeting. *J. Am. Chem. Soc.* **2011**, *133*, 17063–17071.
- (100) Rong, Y.; Wu, C.; Yu, J.; Zhang, X.; Ye, F.; Zeigler, M.; Gallina, M. E.; Wu, I. C.; Zhang, Y.; Chan, Y.-H.; Sun, W.; Uvdal, K.; Chiu, D. T. Multicolor Fluorescent Semiconducting Polymer Dots with Narrow Emissions and High Brightness. *ACS Nano* **2013**, *7*, 376–384.
- (101) Feng, X.; Yang, G.; Liu, L.; Lv, F.; Yang, Q.; Wang, S.; Zhu, D. A Convenient Preparation of Multi-Spectral Microparticles by Bacteria-Mediated Assemblies of Conjugated Polymer Nanoparticles for Cell Imaging and Barcoding. *Adv. Mater.* **2012**, *24*, 637–641.
- (102) Wang, F.; Liu, Z.; Wang, B.; Feng, L.; Liu, L.; Lv, F.; Wang, Y.; Wang, S. Multi-Colored Fibers by Self-Assembly of DNA, Histone Proteins, and Cationic Conjugated Polymers. *Angew. Chem., Int. Ed.* **2014**, *S3*, 424–428.
- (103) (a) Kobayashi, H.; Ogawa, M.; Alford, R.; Choyke, P. L.; Urano, Y. New Strategies for Fluorescent Probe Design in Medical Diagnostic Imaging. *Chem. Rev.* **2009**, *110*, 2620–2640. (b) Chang, S.; Wu, X.; Li, Y.; Niu, D.; Gao, Y.; Ma, Z.; Gu, J.; Zhao, W.; Zhu, W.; Tian, H.; Shi, J. A pH-Responsive Hybrid Fluorescent Nanoprober for Real Time Cell Labeling and Endocytosis Tracking. *Biomaterials* **2013**, *34*, 10182–10190. (c) Wu, X.; Sun, X.; Guo, Z.; Tang, J.; Shen, Y.; James, T. D.; Tian, H.; Zhu, W. In Vivo and *In Situ* Tracking Cancer Chemotherapy by Highly Photostable NIR Fluorescent Theranostic Prodrug. *J. Am. Chem. Soc.* **2014**, *136*, 3579–3588.
- (104) (a) Sun, W.; Yu, J.; Deng, R.; Rong, Y.; Fujimoto, B.; Wu, C.; Zhang, H.; Chiu, D. T. Semiconducting Polymer Dots Doped with Europium Complexes Showing Ultranarrow Emission and Long Luminescence Lifetime for Time-Gated Cellular Imaging. *Angew. Chem., Int. Ed.* **2013**, *S2*, 11294–11297. (b) Sun, W.; Hayden, S.; Jin, Y.; Rong, Y.; Yu, J.; Ye, F.; Chan, Y.-H.; Zeigler, M.; Wu, C.; Chiu, D. T. A Versatile Method for Generating Semiconducting Polymer Dot Nanocomposites. *Nanoscale* **2012**, *4*, 7246–7249.
- (105) Jin, Y.; Ye, F.; Zeigler, M.; Wu, C.; Chiu, D. T. Near-Infrared Fluorescent Dye-Doped Semiconducting Polymer Dots. *ACS Nano* **2011**, *5*, 1468–1475.
- (106) Zhang, X.; Yu, J.; Rong, Y.; Ye, F.; Chiu, D. T.; Uvdal, K. High-Intensity Near-IR Fluorescence in Semiconducting Polymer Dots Achieved by Cascade FRET Strategy. *Chem. Sci.* **2013**, *4*, 2143–2151.
- (107) So, M.-K.; Xu, C.; Loening, A. M.; Gambhir, S. S.; Rao, J. Self-Illuminating Quantum Dot Conjugates for *In Vivo* Imaging. *Nat. Biotechnol.* **2006**, *24*, 339–343.
- (108) Xiong, L.; Shuhendler, A. J.; Rao, J. Self-Luminescing BRET-FRET Near-Infrared Dots for *In Vivo* Lymph-Node Mapping and Tumour Imaging. *Nat. Commun.* **2012**, *3*.
- (109) (a) Jiang, Y.; Wang, Y.; Hua, J.; Tang, J.; Li, B.; Qian, S.; Tian, H. Multibranched Triarylamine End-Capped Triazines with Aggregation-Induced Emission and Large Two-Photon Absorption Cross-Sections. *Chem. Commun.* **2010**, *46*, 4689–4691. (b) Shao, A.; Guo, Z.; Zhu, S.; Zhu, S.; Shi, P.; Tian, H.; Zhu, W. Insight into Aggregation-Induced Emission Characteristics of Red-Emissive Quinoline-Malononitrile by Cell Tracking and Real-Time Trypsin Detection. *Chem. Sci.* **2014**, *5*, 1383–1389.
- (110) (a) Yuan, W. Z.; Lu, P.; Chen, S.; Lam, J. W. Y.; Wang, Z.; Liu, Y.; Kwok, H. S.; Ma, Y.; Tang, B. Z. Changing the Behavior of Chromophores from Aggregation-Caused Quenching to Aggregation-Induced Emission: Development of Highly Efficient Light Emitters in the Solid State. *Adv. Mater.* **2010**, *22*, 2159–2163. (b) Zhao, Z.; Chen, S.; Lam, J. W. Y.; Lu, P.; Zhong, Y.; Wong, K. S.; Kwok, H. S.; Tang, B. Z. Creation of Highly Efficient Solid Emitter by Decorating Pyrene Core with AIE-Active Tetraphenylethene Peripheries. *Chem. Commun. (Camb.)* **2010**, *46*, 2221–2223. (c) Zhao, Z.; Lu, P.; Lam, J. W. Y.;

- Wang, Z.; Chan, C. Y. K.; Sung, H. H. Y.; Williams, I. D.; Ma, Y.; Tang, B. Z. Molecular Anchors in the Solid State: Restriction of Intramolecular Rotation Boosts Emission Efficiency of Luminogen Aggregates to Unity. *Chem. Sci.* **2011**, *2*, 672–675. (d) Qin, W.; Ding, D.; Liu, J.; Yuan, W. Z.; Hu, Y.; Liu, B.; Tang, B. Z. Biocompatible Nanoparticles with Aggregation-Induced Emission Characteristics as Far-Red/Near-Infrared Fluorescent Bioprobes for in Vitro and in Vivo Imaging Applications. *Adv. Funct. Mater.* **2012**, *22*, 771–779.
- (111) Wu, W.-C.; Chen, C.-Y.; Tian, Y.; Jang, S.-H.; Hong, Y.; Liu, Y.; Hu, R.; Tang, B. Z.; Lee, Y.-T.; Chen, C.-T.; Chen, W.-C.; Jen, A. K. Y. Enhancement of Aggregation-Induced Emission in Dye-Encapsulating Polymeric Micelles for Bioimaging. *Adv. Funct. Mater.* **2010**, *20*, 1413–1423.
- (112) Escobedo, J. O.; Rusin, O.; Lim, S.; Strongin, R. M. NIR Dyes for Bioimaging Applications. *Curr. Opin. Chem. Biol.* **2010**, *14*, 64–70.
- (113) Ding, D.; Li, K.; Qin, W.; Zhan, R.; Hu, Y.; Liu, J.; Tang, B. Z.; Liu, B. Conjugated Polymer Amplified Far-Red/Near-Infrared Fluorescence from Nanoparticles with Aggregation-Induced Emission Characteristics for Targeted in Vivo Imaging. *Adv. Healthcare Mater.* **2013**, *2*, 500–507.
- (114) Geng, J.; Zhu, Z.; Qin, W.; Ma, L.; Hu, Y.; Gurzadyan, G. G.; Tang, B. Z.; Liu, B. Near-Infrared Fluorescence Amplified Organic Nanoparticles with Aggregation-Induced Emission Characteristics for in Vivo Imaging. *Nanoscale* **2014**, *6*, 939–945.
- (115) Li, C.; Liu, S. Polymeric Assemblies and Nanoparticles with Stimuli-Responsive Fluorescence Emission Characteristics. *Chem. Commun.* **2012**, *48*, 3262–3278.
- (116) (a) Asanuma, H.; Liang, X.; Nishioka, H.; Matsunaga, D.; Liu, M.; Komiyama, M. Synthesis of Azobenzene-Tethered DNA for Reversible Photo-Regulation of DNA Functions: Hybridization and Transcription. *Nat. Protoc.* **2007**, *2*, 203–212. (b) Angelos, S.; Yang, Y.-W.; Khashab, N. M.; Stoddart, J. F.; Zink, J. I. Dual-Controlled Nanoparticles Exhibiting AND Logic. *J. Am. Chem. Soc.* **2009**, *131*, 11344–11346. (c) Beharry, A. A.; Wong, L.; Tropepe, V.; Woolley, G. A. Fluorescence Imaging of Azobenzene Photoswitching in Vivo. *Angew. Chem., Int. Ed.* **2011**, *50*, 1325–1327. (d) Ying, Y.-L.; Zhang, J.; Meng, F.-N.; Cao, C.; Yao, X.; Willner, I.; Tian, H.; Long, Y.-T. A Stimuli-Responsive Nanopore Based on a Photoresponsive Host-Guest System. *Sci. Rep.* **2013**, *3*.
- (117) (a) Aznar, E.; Casasús, R.; García-Acosta, B.; Marcos, M. D.; Martínez-Máñez, R.; Sancenón, F.; Soto, J.; Amorós, P. Photochemical and Chemical Two-Channel Control of Functional Nanogated Hybrid Architectures. *Adv. Mater.* **2007**, *19*, 2228–2231. (b) Davis, D. A.; Hamilton, A.; Yang, J.; Cremar, L. D.; Van Gough, D.; Potisek, S. L.; Ong, M. T.; Braun, P. V.; Martinez, T. J.; White, S. R.; Moore, J. S.; Sottos, N. R. Force-Induced Activation of Covalent Bonds in Mechanoresponsive Polymeric Materials. *Nature* **2009**, *459*, 68–72. (c) Liu, D.; Chen, W.; Sun, K.; Deng, K.; Zhang, W.; Wang, Z.; Jiang, X. Resettable, Multi-Readout Logic Gates Based on Controllably Reversible Aggregation of Gold Nanoparticles. *Angew. Chem., Int. Ed.* **2011**, *50*, 4103–4107.
- (118) (a) Riskin, M.; Gutkin, V.; Felner, I.; Willner, I. Photochemical and Electrochemical Encoding of Erasable Magnetic Patterns. *Angew. Chem., Int. Ed.* **2008**, *47*, 4416–4420. (b) Li, H.; Wang, J.; Lin, H.; Xu, L.; Xu, W.; Wang, R.; Song, Y.; Zhu, D. Amplification of Fluorescent Contrast by Photonic Crystals in Optical Storage. *Adv. Mater.* **2010**, *22*, 1237–1241. (c) Yao, X.; Li, T.; Wang, S.; Ma, X.; Tian, H. A Photochromic Supramolecular Polymer Based on Bis-p-sulfonatocalix[4]arene Recognition in Aqueous Solution. *Chem. Commun.* **2014**, *50*, 7166–7168.
- (119) (a) Brieke, C.; Rohrbach, F.; Gottschalk, A.; Mayer, G.; Heckel, A. Light-Controlled Tools. *Angew. Chem., Int. Ed.* **2012**, *51*, 8446–8476. (b) Zhang, J.; Zou, Q.; Tian, H. Photochromic Materials: More Than Meets The Eye. *Adv. Mater.* **2013**, *25*, 378–399. (c) Zhang, J.; Wang, J.; Tian, H. Taking Orders from Light: Progress in Photochromic Bio-materials. *Mater. Horiz.* **2014**, *1*, 169–184. (d) Ma, X.; Tian, H. Stimuli-Responsive Supramolecular Polymers in Aqueous Solution. *Acc. Chem. Res.* **2014**, *47*, 1971–1981.
- (120) Giordano, L.; Jovin, T. M.; Irie, M.; Jares-Erijman, E. A. Diheteroarylethenes as Thermally Stable Photoswitchable Acceptors in Photochromic Fluorescence Resonance Energy Transfer (pcFRET). *J. Am. Chem. Soc.* **2002**, *124*, 7481–7489.
- (121) Yıldız, I.; Deniz, E.; Raymo, F. M. Fluorescence Modulation with Photochromic Switches in Nanostructured Constructs. *Chem. Soc. Rev.* **2009**, *38*, 1859–1867.
- (122) Zhu, L.; Wu, W.; Zhu, M.-Q.; Han, J. J.; Hurst, J. K.; Li, A. D. Q. Reversibly Photoswitchable Dual-Color Fluorescent Nanoparticles as New Tools for Live-Cell Imaging. *J. Am. Chem. Soc.* **2007**, *129*, 3524–3526.
- (123) Yıldız, I.; Impellizzeri, S.; Deniz, E.; McCaughan, B.; Callan, J. F.; Raymo, F. M. Supramolecular Strategies to Construct Biocompatible and Photoswitchable Fluorescent Assemblies. *J. Am. Chem. Soc.* **2010**, *133*, 871–879.
- (124) Tomasulo, M.; Deniz, E.; Alvarado, R. J.; Raymo, F. M. Photoswitchable Fluorescent Assemblies Based on Hydrophilic BODIPY-Spiropyran Conjugates. *J. Phys. Chem. C* **2008**, *112*, 8038–8045.
- (125) Kim, Y.; Jung, H.-y.; Choe, Y. H.; Lee, C.; Ko, S.-K.; Koun, S.; Choi, Y.; Chung, B. H.; Park, B. C.; Huh, T.-L.; Shin, I.; Kim, E. High-Contrast Reversible Fluorescence Photoswitching of Dye-Crosslinked Dendritic Nanoclusters in Living Vertebrates. *Angew. Chem., Int. Ed.* **2012**, *51*, 2878–2882.
- (126) Jung, H.-y.; You, S.; Lee, C.; You, S.; Kim, Y. One-Pot Synthesis of Monodispersed Silica Nanoparticles for Diarylethene-Based Reversible Fluorescence Photoswitching in Living Cells. *Chem. Commun.* **2013**, *49*, 7528–7530.
- (127) Jeong, K.; Park, S.; Lee, Y.-D.; Lim, C.-K.; Kim, J.; Chung, B. H.; Kwon, I. C.; Park, C. R.; Kim, S. Conjugated Polymer/Photochromophore Binary Nanococktails: Bistable Photoswitching of Near-Infrared Fluorescence for in Vivo Imaging. *Adv. Mater.* **2013**, *25*, 5574–5580.
- (128) Medintz, I. L.; Uyeda, H. T.; Goldman, E. R.; Mattoussi, H. Quantum Dot Bioconjugates for Imaging, Labelling and Sensing. *Nat. Mater.* **2005**, *4*, 435–446.
- (129) Algar, W. R.; Tavares, A. J.; Krull, U. J. Beyond Labels: A Review of the Application of Quantum Dots as Integrated Components of Assays, Bioprobes, and Biosensors Utilizing Optical Transduction. *Anal. Chim. Acta* **2010**, *673*, 1–25.
- (130) Pellegrino, T.; Manna, L.; Kudera, S.; Liedl, T.; Koktysh, D.; Rogach, A. L.; Keller, S.; Rädler, J.; Natile, G.; Parak, W. J. Hydrophobic Nanocrystals Coated with an Amphiphilic Polymer Shell: A General Route to Water Soluble Nanocrystals. *Nano Lett.* **2004**, *4*, 703–707.
- (131) Díaz, S. A.; Menéndez, G. O.; Etchehon, M. H.; Giordano, L.; Jovin, T. M.; Jares-Erijman, E. A. Photoswitchable Water-Soluble Quantum Dots: pcFRET Based on Amphiphilic Photochromic Polymer Coating. *ACS Nano* **2011**, *5*, 2795–2805.
- (132) Díaz, S. A.; Giordano, L.; Jovin, T. M.; Jares-Erijman, E. A. Modulation of a Photoswitchable Dual-Color Quantum Dot Containing a Photochromic FRET Acceptor and an Internal Standard. *Nano Lett.* **2012**, *12*, 3537–3544.
- (133) Díaz, S. A.; Giordano, L.; Azcárate, J. C.; Jovin, T. M.; Jares-Erijman, E. A. Quantum Dots as Templates for Self-Assembly of Photoswitchable Polymers: Small, Dual-Color Nanoparticles Capable of Facile Photomodulation. *J. Am. Chem. Soc.* **2013**, *135*, 3208–3217.
- (134) Wu, T.; Wilson, D.; Branda, N. R. Fluorescent Quenching of Lanthanide-Doped Upconverting Nanoparticles by Photoresponsive Polymer Shells. *Chem. Mater.* **2014**, *26*, 4313–4320.
- (135) Zhou, K.; Wang, Y.; Huang, X.; Luby-Phelps, K.; Sumer, B. D.; Gao, J. Tunable, Ultrasensitive pH-Responsive Nanoparticles Targeting Specific Endocytic Organelles in Living Cells. *Angew. Chem., Int. Ed.* **2011**, *50*, 6109–6114.
- (136) Zhou, K.; Liu, H.; Zhang, S.; Huang, X.; Wang, Y.; Huang, G.; Sumer, B. D.; Gao, J. Multicolored pH-Tunable and Activatable Fluorescence Nanoplatform Responsive to Physiologic pH Stimuli. *J. Am. Chem. Soc.* **2012**, *134*, 7803–7811.

- (137) Zhang, X.; Chen, Z.; Würthner, F. Morphology Control of Fluorescent Nanoaggregates by Co-Self-Assembly of Wedge- and Dumbbell-Shaped Amphiphilic Perylene Bisimides. *J. Am. Chem. Soc.* **2007**, *129*, 4886–4887.
- (138) Zhang, X.; Rehm, S.; Safont-Sempere, M. M.; Würthner, F. Vesicular Perylene Dye Nanocapsules as Supramolecular Fluorescent pH Sensor Systems. *Nat. Chem.* **2009**, *1*, 623–629.
- (139) Li, C.; Zhang, Y.; Hu, J.; Cheng, J.; Liu, S. Reversible Three-State Switching of Multicolor Fluorescence Emission by Multiple Stimuli Modulated FRET Processes within Thermoresponsive Polymeric Micelles. *Angew. Chem., Int. Ed.* **2010**, *49*, 5120–5124.
- (140) Liu, Q.; Feng, W.; Li, F. Water-Soluble Lanthanide Upconversion Nanophosphors: Synthesis and Bioimaging Applications in Vivo. *Coord. Chem. Rev.* **2014**, *273–274*, 100–110.
- (141) Feng, W.; Han, C.; Li, F. Upconversion-Nanophosphor-Based Functional Nanocomposites. *Adv. Mater.* **2013**, *25*, 5287–5303.
- (142) (a) Zhou, J.; Liu, Z.; Li, F. Upconversion Nanophosphors for Small-Animal Imaging. *Chem. Soc. Rev.* **2012**, *41*, 1323–1349. (b) Chen, G.; Qiu, H.; Prasad, P. N.; Chen, X. Upconversion Nanoparticles: Design, Nanochemistry, and Applications in Theranostics. *Chem. Rev.* **2014**, *114*, 5161–5214. (c) Sun, L.-D.; Wang, Y.-F.; Yan, C.-H. Paradigms and Challenges for Bioapplication of Rare Earth Upconversion Luminescent Nanoparticles: Small Size and Tunable Emission/Excitation Spectra. *Acc. Chem. Res.* **2014**, *47*, 1001–1009.
- (143) (a) Islangulov, R. R.; Lott, J.; Weder, C.; Castellano, F. N. Noncoherent Low-Power Upconversion in Solid Polymer Films. *J. Am. Chem. Soc.* **2007**, *129*, 12652–12653. (b) Singh-Rachford, T. N.; Haefele, A.; Ziessel, R.; Castellano, F. N. Boron Dipyrromethene Chromophores: Next Generation Triplet Acceptors/Annihilators for Low Power Upconversion Schemes. *J. Am. Chem. Soc.* **2008**, *130*, 16164–16165. (c) Singh-Rachford, T. N.; Castellano, F. N. Triplet Sensitized Red-to-Blue Photon Upconversion. *J. Phys. Chem. Lett.* **2009**, *1*, 195–200. (d) Ji, S.; Wu, W.; Wu, W.; Guo, H.; Zhao, J. Ruthenium(II) Polyimine Complexes with a Long-Lived ^3IL Excited State or a $^3\text{MLCT}/^3\text{IL}$ Equilibrium: Efficient Triplet Sensitizers for Low-Power Upconversion. *Angew. Chem., Int. Ed.* **2011**, *50*, 1626–1629. (e) Duan, P.; Yanai, N.; Kimizuka, N. Photon Upconverting Liquids: Matrix-Free Molecular Upconversion Systems Functioning in Air. *J. Am. Chem. Soc.* **2013**, *135*, 19056–19059.
- (144) Liu, Q.; Yang, T.; Feng, W.; Li, F. Blue-Emissive Upconversion Nanoparticles for Low-Power-Excited Bioimaging in Vivo. *J. Am. Chem. Soc.* **2012**, *134*, 5390–5397.
- (145) Liu, Q.; Yin, B.; Yang, T.; Yang, Y.; Shen, Z.; Yao, P.; Li, F. A General Strategy for Biocompatible, High-Effective Upconversion Nanocapsules Based on Triplet–Triplet Annihilation. *J. Am. Chem. Soc.* **2013**, *135*, 5029–5037.
- (146) Kurishita, Y.; Kohira, T.; Ojida, A.; Hamachi, I. Rational Design of FRET-Based Ratiometric Chemosensors for in Vitro and in Cell Fluorescence Analyses of Nucleoside Polyphosphates. *J. Am. Chem. Soc.* **2010**, *132*, 13290–13299.
- (147) Peng, H.-s.; Stolwijk, J. A.; Sun, L.-N.; Wegener, J.; Wolfbeis, O. S. A Nanogel for Ratiometric Fluorescent Sensing of Intracellular pH Values. *Angew. Chem., Int. Ed.* **2010**, *49*, 4246–4249.
- (148) Wu, C.; Bull, B.; Christensen, K.; McNeill, J. Ratiometric Single-Nanoparticle Oxygen Sensors for Biological Imaging. *Angew. Chem., Int. Ed.* **2009**, *48*, 2741–2745.
- (149) Pu, K.; Shuhendler, A. J.; Rao, J. Semiconducting Polymer Nanoprobe for in Vivo Imaging of Reactive Oxygen and Nitrogen Species. *Angew. Chem., Int. Ed.* **2013**, *52*, 10325–10329.
- (150) Ma, C.; Zeng, F.; Huang, L.; Wu, S. FRET-Based Ratiometric Detection System for Mercury Ions in Water with Polymeric Particles as Scaffolds. *J. Phys. Chem. B* **2011**, *115*, 874–882.
- (151) Ye, F.; Wu, C.; Jin, Y.; Chan, Y.-H.; Zhang, X.; Chiu, D. T. Ratiometric Temperature Sensing with Semiconducting Polymer Dots. *J. Am. Chem. Soc.* **2011**, *133*, 8146–8149.
- (152) Zhou, J.; Liu, Q.; Feng, W.; Sun, Y.; Li, F. Upconversion Luminescent Materials: Advances and Applications. *Chem. Rev.* **2015**, *115*, 395–465.
- (153) Liu, J.; Liu, Y.; Liu, Q.; Li, C.; Sun, L.; Li, F. Iridium(III) Complex-Coated Nanosystem for Ratiometric Upconversion Luminescence Bioimaging of Cyanide Anions. *J. Am. Chem. Soc.* **2011**, *133*, 15276–15279.
- (154) Liu, Y.; Chen, M.; Cao, T.; Sun, Y.; Li, C.; Liu, Q.; Yang, T.; Yao, L.; Feng, W.; Li, F. A Cyanine-Modified Nanosystem for in Vivo Upconversion Luminescence Bioimaging of Methylmercury. *J. Am. Chem. Soc.* **2013**, *135*, 9869–9876.
- (155) Cen, Y.; Wu, Y.-M.; Kong, X.-J.; Wu, S.; Yu, R.-Q.; Chu, X. Phospholipid-Modified Upconversion Nanoprobe for Ratiometric Fluorescence Detection and Imaging of Phospholipase D in Cell Lysate and in Living Cells. *Anal. Chem.* **2014**, *86*, 7119–7127.
- (156) Ding, Y.; Zhu, H.; Zhang, X.; Zhu, J.-J.; Burda, C. Rhodamine B Derivative-Functionalized Upconversion Nanoparticles for FRET-Based Fe^{3+} -Sensing. *Chem. Commun.* **2013**, *49*, 7797–7799.
- (157) Zhou, Q.; Swager, T. M. Method for Enhancing the Sensitivity of Fluorescent Chemosensors: Energy Migration in Conjugated Polymers. *J. Am. Chem. Soc.* **1995**, *117*, 7017–7018.
- (158) McQuade, D. T.; Pullen, A. E.; Swager, T. M. Conjugated Polymer-Based Chemical Sensors. *Chem. Rev.* **2000**, *100*, 2537–2574.
- (159) (a) Jeong, J.-E.; Woo, S.-J.; Le, V. S.; Choi, H.; Woo, H. Y. Combination of Conjugated Polyelectrolytes and Biomolecules: A New Optical Platform for Highly Sensitive and Selective Chemo- and Biosensors. *Macromol. Res.* **2014**, *22*, 461–473. (b) Feng, L.; Zhu, C.; Yuan, H.; Liu, L.; Lv, F.; Wang, S. Conjugated Polymer Nanoparticles: Preparation, Properties, Functionalization and Biological Applications. *Chem. Soc. Rev.* **2013**, *42*, 6620–6633. (c) Liang, J.; Li, K.; Liu, B. Visual Sensing with Conjugated Polyelectrolytes. *Chem. Sci.* **2013**, *4*, 1377–1394. (d) Achyuthan, K. E.; Bergstedt, T. S.; Chen, L.; Jones, R. M.; Kumaraswamy, S.; Kushon, S. A.; Ley, K. D.; Lu, L.; McBranch, D.; Mukundan, H.; Rininsland, F.; Shi, X.; Xia, W.; Whitten, D. G. Fluorescence Superquenching of Conjugated Polyelectrolytes: Applications for Biosensing and Drug Discovery. *J. Mater. Chem.* **2005**, *15*, 2648–2656.
- (160) (a) Vögtle, F.; Gestermann, S.; Kauffmann, C.; Ceroni, P.; Vicinelli, V.; Balzani, V. Coordination of Co^{2+} Ions in the Interior of Poly(propylene amine) Dendrimers Containing Fluorescent Dansyl Units in the Periphery. *J. Am. Chem. Soc.* **2000**, *122*, 10398–10404. (b) Xu, M. H.; Lin, J.; Hu, Q. S.; Pu, L. Fluorescent Sensors for the Enantioselective Recognition of Mandelic Acid: Signal Amplification by Dendritic Branching. *J. Am. Chem. Soc.* **2002**, *124*, 14239–14246.
- (161) (a) Meallet-Renault, R.; Pansu, R.; Amigoni-Gerbier, S.; Larpent, C. Metal-Chelating Nanoparticles as Selective Fluorescent Sensor for Cu^{2+} . *Chem. Commun. (Camb.)* **2004**, 2344–2345. (b) Trau, D.; Yang, W. J.; Seydack, M.; Caruso, F.; Yu, N. T.; Renneberg, R. Nanoencapsulated Microcrystalline Particles for Superamplified Biochemical Assays. *Anal. Chem.* **2002**, *74*, 5480–5486.
- (162) Montalti, M.; Prodi, L.; Zaccheroni, N. Fluorescence Quenching Amplification in Silica Nanosensors for Metal Ions. *J. Mater. Chem.* **2005**, *15*, 2810–2814.
- (163) Bonacchi, S.; Rampazzo, E.; Montalti, M.; Prodi, L.; Zaccheroni, N.; Mancin, F.; Teolato, P. Amplified Fluorescence Response of Chemosensors Grafted onto Silica Nanoparticles. *Langmuir* **2008**, *24*, 8387–8392.
- (164) Frigoli, M.; Ouadahi, K.; Larpent, C. A Cascade FRET-Mediated Ratiometric Sensor for Cu^{2+} Ions Based on Dual Fluorescent Ligand-Coated Polymer Nanoparticles. *Chem.—Eur. J.* **2009**, *15*, 8319–8330.
- (165) Rampazzo, E.; Bonacchi, S.; Genovese, D.; Juris, R.; Sgarzi, M.; Montalti, M.; Prodi, L.; Zaccheroni, N.; Tomaselli, G.; Gentile, S.; Satriano, C.; Rizzarelli, E. A Versatile Strategy for Signal Amplification Based on Core/Shell Silica Nanoparticles. *Chem.—Eur. J.* **2011**, *17*, 13429–13432.
- (166) Bazzicalupi, C.; Caltagirone, C.; Cao, Z.; Chen, Q.; Di Natale, C.; Garau, A.; Lippolis, V.; Lvova, L.; Liu, H.; Lundström, I.; Mostallino, M. C.; Nieddu, M.; Paolesse, R.; Prodi, L.; Sgarzi, M.; Zaccheroni, N. Multimodal Use of New Coumarin-Based Fluorescent

- Chemosensors: Towards Highly Selective Optical Sensors for Hg²⁺ Probing. *Chem.—Eur. J.* **2013**, *19*, 14639–14653.
- (167) Cheng, L.; Wang, C.; Feng, L.; Yang, K.; Liu, Z. Functional Nanomaterials for Phototherapies of Cancer. *Chem. Rev.* **2014**, *114*, 10869–10939.
- (168) Xing, C.; Xu, Q.; Tang, H.; Liu, L.; Wang, S. Conjugated Polymer/Porphyrin Complexes for Efficient Energy Transfer and Improving Light-Activated Antibacterial Activity. *J. Am. Chem. Soc.* **2009**, *131*, 13117–13124.
- (169) Xing, C.; Liu, L.; Tang, H.; Feng, X.; Yang, Q.; Wang, S.; Bazan, G. C. Design Guidelines for Conjugated Polymers with Light-Activated Anticancer Activity. *Adv. Funct. Mater.* **2011**, *21*, 4058–4067.
- (170) Liu, K.; Liu, Y.; Yao, Y.; Yuan, H.; Wang, S.; Wang, Z.; Zhang, X. Supramolecular Photosensitizers with Enhanced Antibacterial Efficiency. *Angew. Chem., Int. Ed.* **2013**, *52*, 8285–8289.
- (171) Zhang, J.; An, F.; Li, Y.; Zheng, C.; Yang, Y.; Zhang, X.; Zhang, X. Simultaneous Enhanced Diagnosis and Photodynamic Therapy of Photosensitizer-Doped Perylene Nanoparticles via Doping, Fluorescence Resonance Energy Transfer, and Antenna Effect. *Chem. Commun.* **2013**, *49*, 8072–8074.
- (172) Chang, C.-C.; Hsieh, M.-C.; Lin, J.-C.; Chang, T.-C. Selective Photodynamic Therapy Based on Aggregation-Induced Emission Enhancement of Fluorescent Organic Nanoparticles. *Biomaterials* **2012**, *33*, 897–906.
- (173) Hsieh, M.-C.; Chien, C.-H.; Chang, C.-C.; Chang, T.-C. Aggregation Induced Photodynamic Therapy Enhancement Based on Linear and Nonlinear Excited FRET of Fluorescent Organic Nanoparticles. *J. Mater. Chem. B* **2013**, *1*, 2350–2357.
- (174) Dichtel, W. R.; Serin, J. M.; Edder, C.; Fréchet, J. M. J.; Matuszewski, M.; Tan, L.-S.; Ohulchanskyy, T. Y.; Prasad, P. N. Singlet Oxygen Generation via Two-Photon Excited FRET. *J. Am. Chem. Soc.* **2004**, *126*, 5380–5381.
- (175) Kim, S.; Ohulchanskyy, T. Y.; Pudavar, H. E.; Pandey, R. K.; Prasad, P. N. Organically Modified Silica Nanoparticles Co-encapsulating Photosensitizing Drug and Aggregation-Enhanced Two-Photon Absorbing Fluorescent Dye Aggregates for Two-Photon Photodynamic Therapy. *J. Am. Chem. Soc.* **2007**, *129*, 2669–2675.
- (176) Chen, C.-Y.; Tian, Y.; Cheng, Y.-J.; Young, A. C.; Ka, J.-W.; Jen, A. K. Y. Two-Photon Absorbing Block Copolymer as a Nanocarrier for Porphyrin: Energy Transfer and Singlet Oxygen Generation in Micellar Aqueous Solution. *J. Am. Chem. Soc.* **2007**, *129*, 7220–7221.
- (177) Shen, X.; He, F.; Wu, J.; Xu, G. Q.; Yao, S. Q.; Xu, Q.-H. Enhanced Two-Photon Singlet Oxygen Generation by Photosensitizer-Doped Conjugated Polymer Nanoparticles. *Langmuir* **2011**, *27*, 1739–1744.
- (178) Wu, C.; Xu, Q.-H. Enhanced One- and Two-Photon Excitation Emission of a Porphyrin Photosensitizer by FRET from a Conjugated Polyelectrolyte. *Macromol. Rapid Commun.* **2009**, *30*, 504–508.
- (179) Grimland, J. L.; Wu, C.; Ramoutar, R. R.; Brumaghim, J. L.; McNeill, J. Photosensitizer-Doped Conjugated Polymer Nanoparticles with High Cross-Sections for One- and Two-Photon Excitation. *Nanoscale* **2011**, *3*, 1451–1455.
- (180) Zhang, P.; Steelant, W.; Kumar, M.; Scholfield, M. Versatile Photosensitizers for Photodynamic Therapy at Infrared Excitation. *J. Am. Chem. Soc.* **2007**, *129*, 4526–4527.
- (181) Wang, F.; Banerjee, D.; Liu, Y.; Chen, X.; Liu, X. Upconversion Nanoparticles in Biological Labeling, Imaging, and Therapy. *Analyst* **2010**, *135*, 1839–1854.
- (182) Shan, J.; Budijono, S. J.; Hu, G.; Yao, N.; Kang, Y.; Ju, Y.; Prud'homme, R. K. Pegylated Composite Nanoparticles Containing Upconverting Phosphors and meso-Tetraphenyl Porphine (TPP) for Photodynamic Therapy. *Adv. Funct. Mater.* **2011**, *21*, 2488–2495.
- (183) Wang, C.; Tao, H.; Cheng, L.; Liu, Z. Near-Infrared Light Induced in Vivo Photodynamic Therapy of Cancer Based on Upconversion Nanoparticles. *Biomaterials* **2011**, *32*, 6145–6154.
- (184) Cui, S.; Yin, D.; Chen, Y.; Di, Y.; Chen, H.; Ma, Y.; Achilefu, S.; Gu, Y. In Vivo Targeted Deep-Tissue Photodynamic Therapy Based on Near-Infrared Light Triggered Upconversion Nanoconstruct. *ACS Nano* **2012**, *7*, 676–688.
- (185) Yuan, H.; Chong, H.; Wang, B.; Zhu, C.; Liu, L.; Yang, Q.; Lv, F.; Wang, S. Chemical Molecule-Induced Light-Activated System for Anticancer and Antifungal Activities. *J. Am. Chem. Soc.* **2012**, *134*, 13184–13187.
- (186) (a) Liu, K.; Yao, Y.; Kang, Y.; Liu, Y.; Han, Y.; Wang, Y.; Li, Z.; Zhang, X. Supramolecular Approach to Fabricate Highly Emissive Smart Materials. *Sci. Rep.* **2013**, *3*. (b) Ryan, S. T. J.; Del Barrio, J.; Ghosh, I.; Biedermann, F.; Lazar, A. I.; Lan, Y.; Coulston, R. J.; Nau, W. M.; Scherman, O. A. Efficient Host–Guest Energy Transfer in Polycationic Cyclophane–Perylene Diimide Complexes in Water. *J. Am. Chem. Soc.* **2014**, *136*, 9053–9060.
- (187) (a) Hong, Y.; Lam, J. W. Y.; Tang, B. Z. Aggregation-Induced Emission: Phenomenon, Mechanism and Applications. *Chem. Commun.* **2009**, *45*, 4332–4353. (b) Huang, W.; Wang, H.; Sun, L.; Li, B.; Su, J.; Tian, H. Propeller-Like D-π-A Architectures: Bright Solid Emitters with AIEE Activity and Large Two-Photon Absorption. *J. Mater. Chem. C* **2014**, *2*, 6843–6849.